UNIVERSITÀ
DEGLI STUDI
DI BRESCIA

DOTTORATO DI RICERCA IN TECHNOLOGY FOR HEALTH

ING-INF/06 BIOINGEGNERIA ELETTRONICA E INFORMATICA

XXXV CICLO

Inertial sensors for movement analysis of upper limbs: application on normal-weight and obese individuals

DOTTORANDO

Riccardo Monfrini
Matricola: 730274

SUPERVISORE

Prof. Nicola Francesco Lopomo
Università degli Studi di Brescia

CO-SUPERVISORE

Prof.ssa Veronica Cimolin
Politecnico di Milano

Anno Accademico 2021/22

To all the people who encouraged

and supported me during my studies.

SOMMARIO

Introduzione

L'analisi quantitativa del movimento umano fornisce una misura accurata della postura e dei gesti, consentendo l'identificazione di alterazioni dovute a patologie o agli effetti di trattamenti riabilitativi. Lo stato dell'arte è fondato sull'utilizzo di sistemi optoelettronici stereofotogrammetrici solitamente integrati con pedane di forza ed implementati in laboratori appositamente dedicati. Le moderne tecnologie "wearable" hanno permesso di realizzare applicazioni "su campo", mantenendo la naturalità del gesto, indirizzate a patologie valutabili fuori del contesto ospedaliero.

Obiettivo

L'obiettivo di questo studio è la validazione di un sistema basato su sensori inerziali (IMU) rispetto a uno optoelettronico stereofotogrammetrico, considerato il "gold standard", per l'analisi del movimento degli arti superiori di soggetti obesi.

Metodi

Sono stati acquisiti ed analizzati gesti caratteristici delle attività quotidiane, come la flessione e il raggiungimento di un target. Per i soggetti normopeso la fase sperimentale è stata realizzata presso il laboratorio "Luigi Divieti" del Politecnico di Milano, mentre le acquisizioni sui soggetti obesi (BMI >30 kg/m^2) all'ospedale San Giuseppe, Istituto Auxologico Italiano di Piancavallo (VB). Includendo soggetti ambosessi non affetti da patologie dell'apparato locomotore o neurologico, patologie genetiche - come le sindromi di Down o Prader-Willi – sono stati reclutati per il gruppo dei soggetti normopeso 15 uomini e 15 donne (età media = 23 anni, BMI medio = 22,2 kg/m^2), mentre per il gruppo dei pazienti obesi sono stati inseriti nella sperimentazione 17 donne e 6 uomini, con età media di 46 anni e BMI medio di 41,6 kg/m^2.

Al fine di validare l'approccio "wearable", sono stati utilizzati due sistemi optoelettronici (Smart DX400, BTSBioengineering a Milano, e VICON 460, Oxford Metrics Ltd a Piancavallo), implementando il marker set "plug-in gait" modificato per un'analisi full-

body, che ha costituito il riferimento per la cinematica. Come tecnologia indossabile è stato invece utilizzato un sistema basato su unità di misura inerziali (Awinda, Xsens, NL) con protocollo full-body e software per l'analisi biomeccanica. Al fine di ottenere informazioni coerenti, sono state realizzate opportune fasi di calibrazione anatomico-funzionale dei diversi sistemi e modelli. I dati acquisiti sono stati poi analizzati usando un codice dedicato (Matlab, The Mathworks, US) così da poter confrontare gli angoli articolari stimati con i diversi sistemi di acquisizione, secondo precise metriche di similarità, quali *linear fit*, coefficienti di correlazione multipla (CMC), RMSD e *Mean Absolute Variability* (MAV); le variazioni sono state analizzate anche in maniera puntuale attraverso un approccio *Statistical Parametric Mapping* (SPM) e i range of motion sono stati confrontati mediante l'analisi di Bland-Altman.

Risultati

L'analisi di Bland-Altman evidenzia concordanza fra le misure dei range of motion ottenute mediante i due sistemi adottati considerando sia individui normopeso che obesi. I bias dell'articolazione della spalla (circa 100°) risultano rilevanti, la situazione migliora per le altre articolazioni. Le deviazioni standard associate a spalla e gomito dei normopeso sono rispettivamente 10% e 42%. $R^2 > 0,5$. Le somme degli errori quadratici sono dell'ordine di 10^4. Circa i soggetti obesi, la deviazione standard associata alla spalla è 30%. In questo caso, $R^2 < 0,5$. Le somme degli errori quadratici sono dell'ordine di 10^5. Considerando l'articolazione della spalla, in entrambi i gruppi CMC > 0,8 nel piano principale di ogni movimento. Lo scarto quadratico fra le misure e la variazione media assoluta risultano fra 20° e 60°.

I coefficienti angolari ricavati mediante regressione lineare, per i soggetti normopeso si avvicinano a 1. Questi risultati peggiorano per i soggetti obesi aumentando. In entrambi i gruppi i termini dell'intercetta sono rilevanti. D'altra parte, i valori di R^2 si avvicinano a 1 per gli angoli più rappresentativi di ogni gesto.

La media e la deviazione standard degli angoli articolari sono state calcolate puntualmente. Sia Per i soggetti normopeso che per gli obesi l'approccio *Statistical Parametric Mapping* ha restituito valori significativi ($p < 0,001$).

Conclusione

Questo lavoro di tesi ha implementato e validato un metodo di analisi del movimento degli arti superiori di soggetti obesi basato su IMU, utilizzando sistemi optoelettronici stereofotogrammetrici come "gold standard". Sono stati considerati possibili scenari di valutazione dei gesti nel mondo reale.

I risultati hanno permesso una valutazione quantitativa della cinematica, evidenziando aspetti di similarità nelle misure realizzate con entrambi i sistemi. Sono state riscontrate differenze in termini di *range of motion* e circa gli angoli articolari fuori dal piano di movimento. Queste possono essere dovute alla complessità delle articolazioni e ai differenti modelli implementati nei sistemi. Alcune discrepanze sono legate alla definizione dei punti di repere che dovranno essere compensate. Con soggetti obesi, le criticità sono acuite da artefatti da tessuto molle e cross-talking.

ABSTRACT

Introduction

Quantitative human movement analysis provides accurate measures of postures and motion patterns and allows the recognition of their alterations due to pathologies or of the effects of rehabilitative treatments. The state of the art is based on marker-based optoelectronic stereophotogrammetric systems, usually integrated with force platforms and set up in dedicated laboratories. On the other hand, modern wearable technologies allow to perform assessments on the field, which ensure the naturality of the gestures, concerning pathologies, that can be examined in outpatient context and out of the clinical environment.

Objective

The objective of this research consists in the validation of a system based on inertial measurement units (IMUs) with respect to an optoelectronic marker-based stereophotogrammetric system, which is considered the gold standard, as a reliable solution for the assessment of obese subjects' upper limb movements.

Methods

Movements typical of daily activities, such as abduction, flexion and reaching of a target, were assessed. Normal-weight people's experimental evaluation was carried out in "Luigi Divieti" laboratory at Politecnico di Milano, whereas obese patients' (BMI > 30 kg/m^2) acquisitions took place at ospedale San Giuseppe, Istituto Auxologico Italiano di Piancavallo (VB). Both female and male subjects were included. They were not affected with musculoskeletal or neurological pathologies, genetic pathologies – such as Down or Prader-Willi syndromes. Normal-weight subjects' group consisted of 15 men and 15 women (average age = 23 years, average BMI = 22,2 kg/m^2), whereas for the obese subjects' group, 17 women and 6 men were involved into the trial (average age = 46 years, average BMI = 41,6 kg/m^2).

For the validation of the wearable approach, two optoelectronic systems were employed (Smart DX400, BTSBioengineering in Milan, and VICON 460, Oxford Metrics Ltd in Piancavallo) and a modified "plug-in gait" marker set was adopted for a full-body analysis, which constitutes the reference for the kinematics. As a wearable technology, an IMU-based system was used (Awinda, Xsens) with a full-body protocol and a software for biomechanical analysis (Analyze, Xsens). In order to get coherent information, adequate anatomical-functional calibrations of the systems and models were realized. The acquired data were analyzed by means of dedicated routines (Matlab, The Mathworks), in such a way to compare the joint angles estimated with the two acquisition systems. Similarity metrices were adopted, such as linear fit, coefficients of multiple correlation (CMC), RMSD and Mean Absolute Variability (MAV); variations were assessed also point by point with Statistical Parametric Mapping (SPM) and the range of motions were compared with Bland–Altman analysis.

Results

Bland-Altman analysis evidences good agreement between the measurements of the ranges of motions (ROMs) obtained by means of the two adopted systems considering both normal-weight and obese individuals. The biases of the shoulder joint (almost 100°) result relevant, the situation improves for the other joints. The standard deviations associated to normal-weight subjects' shoulder and the elbow are 10% and 42%, respectively. $R^2 > 0,5$. The sums of square errors are of the order of 10^4. As for obese people, the standard deviation associated to the shoulder is 30%. In this case, $R^2 < 0,5$. The sums of square errors are of the order of 10^5.

Considering the shoulder joint, in both groups CMC > 0,8 in the principal plane of each movement. The root mean square deviation between the measurements (RMS) and the mean absolute variation (MAV) are between 20° and 60°.

The angular coefficients found with the linear regression method for normal-weight subjects are near 1. These results are worse for obese subjects since they increased. In both groups the scalar addends are relevant. On the other hand, the R^2 values approach 1 for the most significant angles of each gesture.

The mean and the standard deviation of the joint angle were computed point by point. Both for normal weight and obese subjects, SPM vector field analyses generally found significance ($p < 0,001$).

Conclusion

An IMU-based methodology dedicated to obese subjects' upper limb motion analysis was implemented and validated with respect to optoelectronic stereophotogrammetric systems, the gold standard, and considering possible scenarios of evaluations of the gestures in real situations.

Similarities were highlighted between the measurements realized with the two system. Differences were noticed regarding the range of motion and the joint angles outside the plane of motion. They may be due to the complexity of the joints and to the kinematic models. Some discrepancies were connected to the position of the landmarks, which should be compensated. Critical issues increased with obese subjects because of soft tissue artefacts and cross-talking.

CONTENTS

1. INTRODUCTION

1.1 BRIEF DESCRIPTION OF THE PROJECT

Since obese subjects' excessive body mass represents a critical overloading condition that could damage their musculoskeletal apparatus during daily activities, it is important to find reliable ways to monitor their movement strategies, notice and correct any awkward posture and non-ergonomic gesture. The physical conditions of obese subjects do not allow them to undergo long and demanding clinical exams, required to assess their functional performance and identify any issue concerning the musculoskeletal system in term of performing movement.

For this reason, the aim of this research was to validate an approach for motion analysis based on inertial measurement units (IMUs), which are ubiquitous, non-invasive and versatile, with respect to a marker-based optoelectronic stereophotogrammetric system that is indeed accurate and reliable – thus representing the current state-of-the-art -, but can be employed only in a specialized laboratory and under controlled conditions. Without loss of generality, this work specifically focused on the analysis of upper limbs, which represents in fact a novelty for this kind of applications.

In this frame, this work defined a specifical validation protocol including both normal (i.e., non-obese) and obese subjects and identifying a specific marker set for the assessment and locations for the IMUs thus to obtain a complete and accurate analysis.

In a first phase focused on normal subject, the first experimental part of the research was held at the "Luigi Divieti" Posture and Movement Analysis Lab of Politecnico di Milano, Milano, Italy, where a marker-bases optoelectronic system (Smart DX400, BTS Bioengineering) was available; in that context, an IMU-based system (MVN Awinda, Xsens) with dedicated software for biomechanical analysis (MVN Analyze) was also introduce to test the reliability of this approach for upper limb movements. The abovementioned trial was performed on a control group composed of 30 volunteers. Eventually, the same procedure was carried out on a group of 23 obese patients at Istituto Auxologico Italiano, Ospedale San Giuseppe, Piancavallo, VB, Italy, where a

different marker-based system (Vicon 460, Vicon) was employed by using the same marker set previously used on the control group.

A dedicated workflow was implemented to process and analyze the data provided by both the marker-based optoelectronic system, in order to obtain joint angle; furthermore, a dedicated routine was used to maintain the coherence with the joint angle provided by the IMU-based system. Specific metrics and statistical analysis were implemented to compare the results obtained by the IMU-based system, with respect to the "gold standards".

1.2 THESIS STRUCTURE

First of all, it is useful to discuss the conditions characterizing obese subjects and to highlight the importance of the quantitative assessment of their movement. In this frame, the state of the art was analyzed through a systematic review, specifying which systems were on the market or used in research, the reasons why they are advantageous and widely used, but also their limitations.

Subsequently the thesis will get to the core of the project, where the pillars of this work are. In particular, a detailed description of the used methodologies and the main findings are reported, with specific focus on the comparison between the marker-based optoelectronic system and the IMU-based one.

1.3 BACKGROUND CONCERNING OBESE SUBJECTS

The quantitative human motion analysis provides accurate measurements of postures and movements, allowing the detection of their alterations due to pathologies and the effects of rehabilitative treatments. Conventionally, the assessment is performed by means of marker-based optoelectronic stereophotogrammetric systems integrated with force plates in specially designed laboratories. Nonetheless, the availability of wearable equipment has facilitated the "on field" examination, including outpatient settings; for instance, inertial measurement units (IMUs) have been widely proposed to allow for a quantitative analysis of human movement by fusing the information acquired by means of accelerometers, gyroscopes and magnetometers.

Human motion analysis can specifically be applied to a defined population to extract information about functional limitations; in this frame, obesity has been demonstrated to be a physical condition which heavily affects the possibility to realize daily activities, including not only walking [2–6] but also trunk [7] and upper limb movements [8]. In obese subjects (BMI > 30 kg/m^2) [9], the excessive mass could in fact limit/alter the capability of movement [1]. In this picture, quantitative analysis of human motion provides accurate measurements of both postures and movements [12,13], allowing to detect any biomechanical alterations due to overweight [10,11]. At present, this assessment is usually performed by means of marker-based optoelectronic systems. Although IMU performance has been highlighted in several applications related to human motion analysis [15–18], their use in obese subjects, and in particular for upper limb movements, is still under discussion.

2. TECHNOLOGICAL STATE OF THE ART

This chapter is a presentation of the technologies and the methodologies, which are employed nowadays for the quantitative evaluation of human movement; particular attention is given also to obese population. They are usually adopted to monitor lifestyle, for clinical assessment and to support rehabilitation.

In the last part of the chapter, an overall perspective on the analysis of the movement is introduced, underling that this is a science which investigates the kinematics of gestures such as walking, sit-to-stand and controlled movement of the upper limbs. The results of a systematic review of the literature are also included, which point out the characteristics of different systems and their limitation when they are adopted to assess obese subjects' motion characteristics.

2.1 WEARABLE AND OPTOELECTRONIC DEVICES

In the literature, many articles explain how different movement analysis techniques have been applied first to collect information about lifestyle, to identify bad habits and also to evaluate, in some cases, the "action" on the joints of the human body during different activities.

The section that follows is a report concerning several devices used for qualitative and quantitative description of human movement; they are currently on the market and widely used.

Before discussing them in detail, it is useful to classify these methodologies into two groups: the former is based on the use of "wearable" sensors (i.e., smart devices), the latter on marker-based optoelectronic systems, which represent the current state-of-the-art concerning the analysis of human movement.

2.1.1 SENSORS FOR MOVEMENT ANALYSIS

There are two different types of sensors, in one case they are embedded inside latest generation portable devices such as smartwatches, which can be used daily. This kind of technology measures physiological parameters, thus allowing quantitative evaluation of

the users' habits; in fact, they are above all technological solutions that are able to provide proper stimuli to maintain or adopt a healthy lifestyle.

In the second case, sensors are employed for clinical evaluation allowing a very thorough acquisition of several specific parameters. They can substitute systems, which require hospital laboratories or inpatient settings. Therefore, markers and infrared cameras are not needed, instead sensors – like the inertial measurement units (IMUs) are applied on the body segments involved in the motion analysis.

In both cases, the most commonly used instruments in these devices are pedometers, accelerometers, goniometers, gyroscopes, switches, actometers, systems for the evaluation of physical activity (i.e. type, intensity, frequency and duration)[1].

The most common systems and devices adopted in this field are cited and briefly describe:

- *Optical or magnetic systems* can be adopted for accurate estimations, but they are expensive and must be installed in specialized environments. By rigidly placing a magnetic sensor on a body segment, the position and orientation of the body segment relative to the field generator can be calculated. Optical systems consist of a set of standard cameras that record the scene where the subject is moving.
- *Video recording systems* can also be used for more precise measures but introduce ethical issues related to privacy; it is not possible to monitor patients during everyday activities with these solutions.
- *Pedometers* are instruments that measure the number of steps taken by a person. They work with a switching mechanism such as a spring-loaded mass designed to identify impacts generated by steps. By counting the steps, energy consumption and the covered distance can also be estimated. However, the main problems with pedometers are the inability to distinguish the intensity of movements and insensitivity to small movements or non-ambulatory activities.

[1] "System and WBAN for controlling obesity", Maali Said Mohammed et al., 2018, Hindawi Journal of Healthcare Engineering

Some studies have also shown that the reliability of these devices is reduced in obese subjects.

- A valid alternative is the *inertial pedometer* based on piezoelectric sensors, which can measure changes in applied forces and then estimate accelerations/angular velocity during movement; as drawback, inertial pedometers are ten times more expensive than spring lever pedometers.
- *Accelerometers* are inexpensive, easy to use, robust and non-invasive. They measure acceleration, so thanks to them it is possible to determine the duration, intensity of physical activity and the resulting energy expenditure. They consist of piezoelectric sensors, can be multiaxial, and estimate the components of accelerations in many directions. They can also be equipped with a memory and store the processed data before sending them to users' smartphones or web applications. These devices can assess physical activity via digital counters or algorithms. Their main disadvantage is their difficulty in accurately recognizing activities such as carrying something, lifting objects and riding a bicycle, and distinguishing between standing and sitting situations. Another problem is the lack of standardization: there is no commonly adopted metric and normalization factor in the literature across studies to recognize the outputs of the algorithms used in this device.
- *Gyroscopes* are sensors similar to accelerometers, but instead of measuring linear motion, they evaluate the rotational motion around a given axis.
- *Actometers* are devices that measure and record activity and rest. They are mainly based on accelerometers, but they can integrate also GPS systems; specifically, they evaluate movement in three dimensions, so as to provide an indication of physical activity and therefore of energy expended.

In addition to these physical elements, there exists also online platforms or applications for smartphones able to communicate with the sensors themselves, to save the acquired data in order to record the performed physical activity and any progress over time.

In particular, wearable sensors are easy to be used by obese patients themselves during their daily activities, in this way it is possible for them to directly notice the unhealthy

habits and, at the same time, this technology stimulates people to improve their lifestyle. By exploiting artificial intelligence techniques, they could also be used to immediately point out the motion strategies that could turn out to be dangerous. Their versatility gives the patients the possibility to obtain some information about their health conditions. Anyway, the strong drawback of these devices is that they are usually localized in a single area of the body, so they cannot give complete and meaningful information. Clinical examinations should provide a more complete view on the whole subject.

The following is a detailed description of how the sensors are used.

2.1.1.1 SMART DEVICES

Smart devices are watches, bracelets, harnesses, or patches that allow to monitor various parameters such as the heart rate, the blood oxygenation, the number of steps or calory consumption. They are commonly adopted for their versatility and ease-to-use in daily life activities.

These systems make it easy to examine the gestures of daily life and the individual physiological responses thanks to a continuous collection of data.

This type of analysis lends itself, not so much to a clinical and quantitative assessment of the patient, but more to a qualitative assessment that leads to health promotion in non-hospital settings and prevention of obesity, obesity-related diseases and pathologies related to an excessively sedentary lifestyle.

It is possible to observe in literature how these types of devices have been exploited to promote a healthy lifestyle.

For example, Cattivelli et al. suggested an Acceptance and Commitment Therapy (ACT)[2] combined with the adoption of wearable technology in order to, on one hand, reinforce healthy behavior in everyday life and, on the other hand, promote weight loss.

[2] "ACTonHEALTH study protocol: promoting psychological flexibility with activity tracker and mHealth tools to foster healthful lifestyle for obesity and other chronic health conditions", Cattivelli et al., 2018, Cattivelli et al. Trials

In fact, being conscious increases self-awareness and allows to take note of bad habits. In this way, the subject does not lose motivation, but finds a way to pursue his goal.

Another example is the meta-analysis conducted by Megan A. Kirk et al.[3] showing that adoption of wearable devices stimulates increased physical activity. This results in an average increase of 2592 steps/day and 30 minutes/day of additional walking time compared to the control condition. This may be due to the motivational support of the smart devices, which provide health coaching and counselling through alerts sent via an app.

On the other hand, Jakicic et al.[4] showed that wearable technology is less effective in the long run. They observed that a group of people, who had undergone a 24-month treatment with these devices, lost an average of 3.5 kg, while the control group lost 5.9 kg by adopting a standard treatment.

As can be seen from these articles taken from the literature, the systems are characterized by affordable prices and easy availability, making them usable by everyone; however, they are not as reliable as clinical tools.

Furthermore, the influence of wearable devices on patient behavior during daily life cannot be fully verified.

The following are the main monitoring devices on the market that balance cost, accuracy, and versatility.

[3] "Wearable Technology and Physical Activity Behavior Change in Adults With Chronic Cardiometabolic Disease: A Systematic Review and Meta-Analysis", Megan A. Kirk et al., 2019, American Journal of Health Promotion

[4] "Effect of Wearable Technology Combined With a Lifestyle Intervention on Long-term Weight Loss - The IDEA Randomized Clinical Trial", John M.Jakicic et al., 2016, Original Investigation

I. Fitbit

Fitbit Inc[5]. designs wearable sensors such as trackers or smartwatches, whose accuracy has been validated by several tests. These devices are capable of evaluating various parameters, in fact, they count steps, monitor the sleep process, calories consumption, heart rate and body temperature.

Thanks to wireless technology, it is possible to access data through the system itself, using the dedicated application or via the web. An example is the Fitbit Zip model (Figure 1), characterized by a triaxial accelerometer; it is able to estimate the time spent in the light and the intensity of physical activity performed, is easily transportable (35.6 x 28.9 x 9.6 mm) and its battery lasts 4-6 months.

Figure 1: Fitbit Zip

This device is inexpensive and doesn't require any specialized technical knowledge to use. Zip does not need any specialized computer to work. It works with software on the Web when an Internet connection is available; if that's not possible, it can be synchronized with a smartphone and show the data collected via the app[1].

[5] www.Fitbit.com

II. BodyMedia FIT

BodyMedia wristbands, which can be seen in Figure 2, are created by BodyMedia Inc[1]. They consist of multiple sensors that can provide real-time analysis. They include a three-dimensional accelerometer to track the movement of the user's upper arm and identify location, a heat sensor that records body heat consumption, a thermistor to measure skin and cuff temperature, and electrodes to estimate muscle activity. In fact, they can describe physiological activity in terms of the number of steps taken, forces applied, and calories burned. These systems are clock shaped. They can commonly store data for processing and send it to mobile apps via USB or wireless technologies. They have rechargeable batteries with a two-week battery life.

Figure 2: BodyMedia wristband

III. Nike Fuel Band

This device in Figure 3 is a sports monitoring bracelet, rechargeable with lithium-ion batteries or USB charger. It can be connected to a smartphone app, the Nike Band App to record and save sport performance[6].

Data of interest range from physical activity time, calorie consumption and steps taken. The algorithm that allows it to work is based on the kinetics of oxygen consumption.

[6] www.Nike.com

Based on the time spent and calories consumed, the iPhone program will provide a series of suggestions and motivations to the athlete.

Depending on the movement that is done and the activity that is performed, different Fuel Points are accumulated, which can then be used to improve the performance and to compare it with other peoples' ones.

This type of approach is based on the principle of "Gamification of fitness", i.e. training in the form of a game, to make it more attractive, fun and affordable for everyone that promotes a healthier lifestyle.

Figure 3: Nike fuelband

2.1.1.2 WEREABLE DEVICES FOR MOVEMENT ANALYSIS

This typology is based on the use of multiple IMU sensors to be placed on specific body segments, in order to provide a more global and detailed view of the subject during the realization of the movements.

They can be used in the clinical field as a replacement for the marker-based optoelectronic system, in order to study healthy or pathological subjects' kinematics and to evaluate, for instance, the evolution of a disease or the progress of a physiotherapy treatment.

Wearable IMUs can also be exploited for the development of exergames[7], video games with increasingly realistic movements, which stimulates training. The presence of accelerometers provides the game with information regarding motion. Besides entertaining the users, these programs encourage them to follow a physical activity program and acquire healthy habits.

As far as this project is concerned, the focus is on clinical applications. The kind of sensors to be validated in this work is discussed in detail below.

I. XSens

XSens MVN[8] is an inexpensive and easy-to-use IMU-based motion acquisition system that provides extensive information about the movement of the entire human body.

MVN is not only limited to a studio or a laboratory, but it is a totally portable system and therefore usable anywhere, in fact, there are no limitations in the volume of measurement (except for the wireless range). It is based both on wireless communications centered on advanced sensor fusion algorithms, through the use of biomechanical model assumptions, and on the latest generation of inertial sensors.

MVN is able to incorporate synchronized video data, as it is a full-body inertial kinematic measurement system. As an output, an instantaneous graph is obtained in which the angles of the joints can be observed. In addition, a C3D exporter has been developed that contains the segment information included in the Xsens MVN system, such as the center of mass.

There are many fields of applications. Some examples are listed below.

- *Sports, biomechanics, ergonomics, rehabilitation and human-machine interaction*. In this type of fields, the advanced calibration of the functional axes and the totally portable measurement system are exploited; therefore, there is no need to touch the anatomical landmarks to fix the markers. The calculation of internal

[7] "Near-Realistic Mobile Exergames With Wireless Wearable Sensors", Bobak Mortazavi et al., 2014, IEEE JOURNAL OF BIOMEDICAL AND HEALTH INFORMATICS

[8] "MVN User Manual", Revision Z 01/04/2021, Xsens

forces and moments is facilitated because there is a direct low-noise measurement of acceleration and angular velocity.

- *3D Animation*. It enjoys short setup times, lack of intrusive invalid data, and ease of use.
- *Simulation, training and virtual reality*. Ability to obtain low-latency fluid motion data through the advantageous portable system and affordable price.

In this project, as already anticipated, the system was exploited for biomechanical purposes in order to validate it for obese subjects' motion analysis.

Below are briefly reported the fundamental elements characterizing this system.

1. Motion tracker

Three types of motion detectors are available (Figure 4): three MTx-STRs in series, one MTx used as an end tracker and MTw.

Figure 4: XSens sensors:
left: MTx sensor, center: MTx-STRs sensor, right: MTw sensor

MTx, MTx-STR and MTw are miniature inertial measurement units and contain inside them:

- 3D linear accelerometers, which measure accelerations;
- 3D magnetometers, which measure the (Earth) magnetic field;
- 3D gyroscopes, which measure angular velocities;
- a barometer, capable of measuring atmospheric pressure.

These trackers are placed at specific points on the body and are useful for measuring the movements of each body segment. In this thesis the MTw trackers were used. It is important to place them exactly on the corresponding segment, specifically at the point

where the maximum range of motion and a minimum amount of skin artefacts occur. This is because each detector has its own ID that is used during motion acquisition.
Through Xsens algorithm development, drift-free 3D orientation can be provided. The MTw is designed to make sure that during time synchronization, the accuracy of single sensor readout on a multi-unit wireless network is not lost, therefore it provides reliable measures of the orientation of human body segments. This is crucial in order to obtain joint angles.
The MTw tracker has a LiPo battery, which can last up to a maximum of 6 hours and is able to maintain, in stand-by, a level of charge for approximately 90 hours. It recharges via a micro-USB connection located on the Awinda station in one hour. A LED has been placed at the top to check the status of the device. On the side of each MTw there is a label that indicates the corresponding segment.

2. Awinda station - Awinda dongle

The Awinda station (Figure 5) controls the reception of synchronized wireless data from all MTw connected wirelessly.

Figure 5: Awinda station

On the back of this element there are four ports, two of them have the task to send (sync out), two to receive (sync in) information for the synchronization of external devices. On the top instead there are 6 spaces, with micro-USB input that allows to recharge the sensors. In the lateral part instead, there is the antenna that allows the recognition and interaction of connected devices.

The Awinda dongle (Figure 6) controls the reception of synchronized wireless data from all MTw connected wirelessly, it has the same purpose as the previously described station, it allows data reception up to 32 sensors, it may have an antenna or not. In the second case the area it covers is smaller.

Figure 6: Awinda USB Dongle and Awinda Dongle ANT

3. Body Pack (BP) and battery

The Body Pack (BP), as can be seen in Figure 7, manages to synchronize the samples by retrieving their data and interconnecting MTx strings. This data is propagated through an optimized 2.4 GHz diffuse spectrum wireless connection.

The following are the connectors found in the body pack.

On the top of the Body Pack there are four connectors. With Xsens facing up, from left to right you have:

- the two central 5-pin connectors, which are to be connected to the tracker strings;
- the larger connector is a 5-pin connector that, instead, connects to the battery cable.

While at the bottom there are three connectors:

- A micro-USB connector, mostly supported for the purpose of configuring the BP in the future;
- A single battery pack powers the BP. This pack has intelligent lithium-ion charging and has a typical runtime of 9.5 hours;
- An Ethernet connector to be used for wired recording in case the system is connected directly to the recording PC instead of transferring data via wireless signal.

Figure 7: Body Pack

4. Software

Control of the MVN system is provided by the MVN Analyze/Animate software; this is a 64-bit application for Windows 10. Several plug-ins are included, such as MotionBuilder, Time Code and Remote Control; some of them are part of the MVN Analyze/Animate installer.

It is a very easy to use software and has the functionality of real-time viewing and recording. When offline, it is possible to make changes to the recorded sessions and analyze them.

5. BVH

BVH is an exporter type, the acronym stands for BioVision Hierarchical data. It embeds assimilated motion data into an ASCII format for later import into various applications.

BVH file consists of two parts, a header section which describes the hierarchy and initial pose of the skeleton; and a data section which contains the motion data.

Different sample rates are available, ranging from 60 Hz up to 240 Hz, and it can be selected in the motion section, where also the number of motion frames can be found.

As for the actual motion data, the spatial coordinates of the segments and the Euler angles of each one with respect to the adjacent one can be found in the rest of the file. Each row corresponds to a sample of motion data.

Note, however, that unfortunately the BVH format is restrictive and cannot compress all the information obtained with MVN, thus limiting the numerical resolution of BVH files. There can also be rounding problems with Euler angles, particularly in the conversion for some poses. Since all segments are connected, errors such as foot shift and soft tissue artefacts, are "projected" onto the feet.

6. MVNX

MVN files are provided in Open XML format and then transformed into MVNX files to be analyzed and opened in programs such as Microsoft Excel, Access, MATLAB, and C-Motion Visual 3D. By default, MVNX contains the 3D segment and position data.

Additional values can be exported such as:

3D position, angular and linear acceleration and velocity of all 23 segments;

3D joint angles of 22 joints;

Location of the body's center of mass;

Contact data indicating which contact point was detected as ground contact;

3D orientation, free acceleration, and magnetic field data of all 17 MTs.

To calculate kinematic data, such as orientation or position, MVN Fusion Engine can be used. This data is measured for each body segment relative to a fixed reference coordinate system on the ground.

These conventions are used to define the axes of the global reference system:

- X pointing to local magnetic north;
- Y points west;
- Z points upward.

When the character is in the T-pose, the axes of each body segment are perfectly in line with those of the global reference system.

In the following chapter it will be explained in detail how the axes of each body segment are exploited.

7. Suit

The system also has a Lycra suit on which motion trackers can be placed or on which detectors are mounted in a platform with an accompanying set of MVN straps (Figure 8). The latter are formed from non-latex composite material and are safe and hygienic, which is why they are frequently used by clinicians. In addition, they can be used to interchange configurations between subjects of different sizes.

The straps can be worn directly on the skin for close contact and are suitable for most of the adult population.

Figure 8: Suit

2.1.2 MARKER-BASED OPTOELECTRONIC STEREOPHOTOGRAMMETRIC SYSTEM

Marker-based optoelectronic stereophotogrammetric systems[9] are widely used for human motion evaluation and they are considered the gold standard in this field. This technology is versatile and can be used to assess various gestures accurately. It relies on

[9] "Tecniche per l'analisi del movimento", Carlo Albino Frigo, 2018, "Bioingegneria del sistema motorio"

the use of infrared cameras, reflective markers, small plastic spheres coated with reflective material and a computer to acquire and record the exam. In the Figure 9 there is a schematic representation of an optoelectronic system. There exist different protocols that define the positioning of these markers in the body segments next to the joint centers, which allows the standardization of analysis.

Through the use of a processor and several cameras, it is possible to reconstruct the 3D coordinates, in the reference system of the laboratory, of the marker under examination.

Figure 9: Representation of optoelectronic system

Since there are multiple cameras, the procedure for reconstructing these coordinates may include optimization algorithms, which exploit a redundancy of information given by the cameras, that can improve the accuracy of the coordinates.

Once a movement has been recorded, it is possible to observe a set of points corresponding to the reflective markers, which represent the subject performing a task. Through a subsequent modelling and classification process, it is possible to reconstruct the joint angles which describe the movement.

The optoelectronic system, as stated above, is the gold standard for motion analysis. However, in recent years researchers are trying to validate sensors for the same purpose in order to reduce the difficulty of the acquisition and speed up the analysis.

In the third chapter, the optoelectronic systems used during this project are described.

3. A SYSTEMATIC REVIEW OF TECHNOLOGY FOR HUMAN MOVEMENT ANALYSIS IN OBESE SUBJECTS

This chapter represents part of the content of the paper "Technological solutions for human movement analysis in obese subjects: a systematic review", Monfrini R, Rossetto G, Scalona E, Galli M, Cimolin V, Lopomo NF, published in the journal Sensors MDPI.

3.1 INTRODUCTION

Obesity represents one of the most prevalent pathologies in developed countries [1], and the global prevalence of obesity has increased by nearly 80% since the 1980s [2].

Obesity has been shown to be a condition that can affect the ability to perform daily-life activities, such as walking [3–6], lumbopelvic movements [7], standing up [8,9], and tasks involving upper limb movements [10], thus significantly impacting the overall quality of life. In obese individuals, excessive weight can limit and alter their overall capacity for movement, leading to a range of functional limitations [11].

Hence, it is important to quantify and monitor how the obese population carries out specific movements. This information can help to characterize their functional limitations, and prevent further issues impacting their musculoskeletal system, due—for instance—to high compressive forces on the anti-gravitational joints and the muscular fatigue [12]. Therefore, there is growing interest in developing tools that are able to monitor the physical activity and movement of the obese population, so as to evaluate the limitations affecting their daily life activities and quantify their clinical conditions.

In this context, it is essential to introduce technological and methodological approaches able to reliably and safely provide quantitative information about the movements of obese subjects. Indeed, the analysis of human motion is widely adopted in clinical and research fields to investigate pathological conditions, including obesity, and pursue an objective and integrated assessment [13]. Specifically, human movement analysis is used to assess the biomechanical features (including both kinematics and kinetics) of obese

subjects in order to better understand the most common problems affecting this population.

Currently, movement analysis—particularly motion tracking—is usually performed using marker-based stereophotogrammetric optoelectronic systems integrated with force platforms, and used within controlled experimental environments [13,14]. However, over the past decade, the availability of wearable equipment has made it possible to conduct examinations in more ecological and daily-life conditions [15–18]. For instance, magneto-inertial measurement units (MIMUs) can provide a quantitative evaluation of movement by integrating information from triaxial accelerometers, gyroscopes, and magnetometers; these solutions are, in general, non-invasive and easy-to-use, allowing for continuous monitoring and self-assessment to evaluate and prevent risk, even at home.

Unfortunately, the use of non-invasive technological solutions that are externally applied to the skin is highly susceptible to soft tissue artefacts (STA) [19], particularly when considering the obese population. This issue can be addressed by simultaneously monitoring the movement of skin markers/sensors and the underlying bone using imaging methods such as biplane radiography [20] and Magnetic Resonance Imaging (MRI) [21].

While numerous studies investigating the application of various technologies to movement analysis in the obese population are present in the literature, a systematic review is currently absent. Therefore, this study aimed to identify and summarize the existing literature, and highlight the different technological and methodological strategies used to evaluate movement analysis approaches within the obesity context, with a particular focus on gait and functional assessment. Based on the outcomes obtained from the reviewing process, this work also aimed to report any advantages or limitations regarding each technology, whenever available and discussed.

3.2 MATERIALS AND METHODS

Information Sources

This study was conducted and reported following the Preferred Reporting Items for Systematic Review and Meta-Analyses (PRISMA) 2020 [22]. A proper workflow was created following the PRISMA for systematic review protocols (PRISMA-P) [23] which was online, registered on Open Science Framework available at https://doi.org/10.17605/OSF.IO/72UAE (accessed on 5 March 2023). The search process was started in March 2022 by considering three different electronic databases, i.e., PubMed, Scopus, and Web of Science.

Three reviewers (M.R., R.G. and S.E.) were involved in the inclusion/exclusion process, following the eligibility criteria, as hereinafter reported; a fourth reviewer helped in case of discrepancy (L.N.F.).

Eligibility Criteria and Search Strategy

The research question was defined using the Patients-Intervention-Comparison-Outcome-Study (PICOS) approach [24]; in particular, papers were included if they were focused on observational studies reporting quantitative measurements (S); they were focused on obese population (P); they performed the assessment using specific human motion analysis techniques (I). Comparisons (C) and outcomes (O) were not defined.

The full search string was: (*"obesity" OR "obese") AND ("biomechanics" OR "movement analysis" OR "motion analysis" OR "wearable" OR "optoelectronic" OR "marker-based" OR "markerless" OR "inertial" OR "IMU").*

Study Selection

Studies were included if they met the following inclusion criteria:

- published from 2010 to 2022.
- written in the English language.
- conducted on adults (≥18 years old).
- conducted on subjects with Body Mass Index (BMI) > 30.

- reporting at least one measurement parameter/metric related to movement analysis (e.g., joint angles, joint moments, etc.).
- based on observational study design.

Otherwise, the exclusion criteria were:

- Systematic narrative and scoping reviews; letters to editors and commentaries; book or chapters; conference proceedings; case reports or case series.
- Studies including population not stratified among normal-weight, overweight, and obese subjects.
- Studies focused on pre-post intervention evaluation (e.g., arthroplasty, etc.).
- Studies involving patients affected by chronic pathologies and/or patients in pain.
- Studies reporting no information about the used systems/devices/instrumentations (e.g., model or manufacturer specification).
- Studies focused on posture and balance evaluation.

Data Items and Collection

Identified data were exported from electronic databases and imported into a web application for systematic reviews (Rayyan [25]). All the information concerning the studies was manually extracted from the included papers thanks to a full-text analysis, exported, and collected in a custom database, created according to the Cochrane guidelines [26].

As summarized in Table 1, the following data were included:

- Author and year of publication.
- Aim of the work.
- Characteristics of the study population.
- Tasks required of participants.
- Technology used for data acquisition.
- Sensors/marker placement/location.
- Outcomes/measurements.

Quality Assessment: Risk of Bias in Individual Studies

Included papers were assessed using the methodological index for non-randomized studies (MINORS) [27] in order to quantify the individual and overall risk of bias. The MINORS tool comprises a total of twelve items, with items from eight to twelve used only for comparative studies. The items are scored 0 when they are not reported, 1 if they are reported but inadequate, or 2 if reported and adequate. The ideal overall score is 16 for non-comparative studies and 24 for comparative studies. The data extracted from the included studies were summarized qualitatively, providing a narrative synthesis of the findings.

Authors (year)	Aim of the Work	Study Population	Task	Technology	Sensor Placement	Outcome Measures
Kim et al., 2022 (a) [28]	Investigate changes in whole-body angular momentum in a population with different BMI.	13 obese class 1 and 2 6M, 7 F BMI 34.1 ± 2.2 kg/m^2 11 obese class 3 5 M, 6 F BMI 47.1 ± 7.0 kg/m^2 14 normal weights 7M, 7 F BMI 22.0 ± 2.6 kg/m^2	Gait on treadmill	Optoelectronic system 10 cameras (Vicon Motion Systems Ltd, Oxford, UK). Split-belt treadmill with 2 force plates (Bertec Corporation, Columbus, OH, USA).	44 passive reflective markers: trunk, pelvis, thighs, shanks, and feet. Markers were placed bilaterally on the posterior heel, three metatarsal heads (1st, 2nd, and 5th), medial and lateral malleoli, medial and lateral femoral epicondyles, greater trochanter, anterior superior iliac spine, posterior superior iliac spinae, and acromion process. A single marker was placed on the xiphoid process, jugular notch, 7th cervical vertebra, and 10th thoracic vertebrae. Rigid clusters of four markers were attached to the shank and thigh bilaterally.	• Spatiotemporal gait parameters: walking speed (m/s), step width (m), step length (m), double support time (s). • Kinetics: external moment about the body's COM (Nm), vertical free moment (Nm), whole body angular momentum (Nm).
Kim et al., 2022 (b) [29]	Investigated changes in dynamic balance control in adults with different BMI scores.	14 obese 6M, 8 F BMI 44.3 ± 7.5 kg/m^2 14 normal weights 7M, 7 F BMI 21.9 ± 2.7 kg/m^2	Gait overground and on a treadmill	Optoelectronic system 10 cameras (Vicon Motion Systems Ltd, Oxford, UK). Split-belt treadmill with 2 force plates (Bertec Corporation, Columbus, OH, USA). 6.1 m long × 0.9 m wide pressure-sensitive gait carpet (Protokinetics LLC, Peekskill, NY, USA).	44 passive reflective markers: trunk, pelvis, thighs, shanks, and feet. Markers were placed bilaterally on the posterior heel, three metatarsal heads (1st, 2nd, and 5th), medial and lateral malleoli, medial and lateral femoral epicondyles, greater trochanter, anterior superior iliac spine, posterior superior iliac spinae, and acromion process. A single marker was placed on the xiphoid process, jugular notch, 7th cervical vertebra, and 10th thoracic vertebrae. Rigid clusters of four markers were attached to the shank and thigh bilaterally.	• Spatiotemporal gait parameters: step width (m), step length (m), double support time (s). • Kinetics: whole body angular momentum (Nm), ground reaction force (N), vertical ground reaction moment (Nm), external moment arms (Nm).
Vakula et al., 2022 [30]	Comparison of spatiotemporal parameters and kinetic patterns between young adults with and without obesity.	48 obese 24 M, 24 F BMI 33.0 (32.1–33.9) kg/m^2 48 normal weights 24 M, 24 F BMI 21.6 (20.7–22.5)	Gait overground	Optoelectronic system 9 cameras (Qualisys, Goteborg, Sweden). Two force platforms (AMTI, Watertown, MA, USA).	Calibration: 5 markers were placed on the heel counter, medial and lateral malleoli, and first and fifth meta-tarsals.	• Spatiotemporal gait parameters: stance time (s), double support time (s), double support to stance ratio (%), step width (% height), step length (% height), cadence (steps/min),

		kg/m^2				and gait stability ratio (GSR, step/m)). • Kinetics: total support moment (Nm), ankle extensor moment (%), knee extensor moment (%), hip extensor moment (%).
Capodaglio et al., 2021 [31]	Quantify the three-dimensional knee and ankle joint kinematics and kinetics in participants with obesity.	32 obese 15 M, 17 F BMI 38.0 ± 4.7 kg/m^2 16 normal weights 6 M, 10 F BMI 21.2 ± 2.0 kg/m^2	Gait overground	Optoelectronic system 6-cameras (460, Vicon Motion Systems Ltd, Oxford, UK) Two force platforms (Kistler Instruments Corp, Winterthur, CH).	Davis, 22 markers [32]	• Kinematics: knee and ankle flexion at initial contact (°), maximum ankle dorsiflexion and plantarflexion angles during the stance and swing phase (°), the dynamic range of motion of the knee in the sagittal plane during stance and swing phases (°), the dynamic range of motion for ankle dorsi-plantarflexion in the whole gait cycle (°). • Kinetics: maximum value of ankle plantarflexion moment in terminal stance (Nm/kg), the first peak of knee abduction moment and maximum value of knee extension moment (Nm/kg), minimum (W/kg) value in the first phase of stance and maximum (W/kg) ankle power during terminal stance.

Cimolin et al., 2021 [33]	Design and validation of obesity-specific shoes during the walking task with a single IMU.	23 obese 6 M, 17 F BMI > 30 kg/m^2	Gait overground with and without specific shoes	Single IMU (G-Sensor, BTS Bioengineering, Milan, Italy).	Lower back, approximately at the L4-L5 vertebrae position.	• Spatiotemporal gait parameters: walked distance (m), gait speed (m/s), step length (m), and cadence (step/min).
Garcia et al., 2021 [34]	Examine the influence of sex and obesity on sagittal and frontal plane knee mechanics during gait in young adults.	48 obese 24 M, 24 F BMI 33.0 kg/m^2 48 normal weights 24 M, 24 F BMI 21.6 kg/m^2	Gait overground	Optoelectronic system 9 cameras (Qualisys, Goteborg, Sweden). Two force platforms (AMTI, Germantown, MD, USA). Infrared timing gates (Tractronix, Belton, MO, USA).	Passive reflective markers were placed on the lateral aspect of the pelvis to represent the anterior surface of the palpated ASIS landmark. Rigid clusters of 4 non-collinear markers were firmly affixed on the sacrum, and bilaterally on the thigh, shank, and foot segments to minimize soft-tissue artefacts [35].	• Kinematics: knee flexion (°) knee varus velocity (°/s). • Kinetics: knee adduction moment (Nm), knee flexion moment (Nm).
Ghasemi et al., 2021 [7]	Measurement and comparison between obese and normal-weight subjects of the spine, trunk, pelvis kinematics, lumbopelvic coordination.	9 obese BMI 35.3 ± 2.6 kg/m^2 9 normal weights BMI 23.9 ± 1.3 kg/m^2	Loading handling activities	Opto-electronic system, 10 cameras (Vicon Motion Systems Ltd, Oxford, UK).	Plug in gait, 39 markers [32,36]	• Kinematics: trunk, lumbar, and pelvis ROM (°) in all anatomical planes, lumbopelvic ratio (lumbar to pelvis rotations at different trunk angles).
Kim et al., 2021 [37]	Determine the influences of arch height and obesity on gait mechanics in adults with obesity.	26 obese BMI 39.0 kg/m^2 21 normal weights BMI 22.7 kg/m^2	Gait overground and on a treadmill	Opto-electronic system 10 cameras (Vicon Motion Systems Ltd, Oxford, UK). Split-belt treadmill with 2 force plates (Bertec Corporation, Columbus, OH, USA). Pressure-sensitive gait carpet (Protokinetics LLC, Peekskill, NY, USA).	Passive reflective markers were placed bilaterally on the posterior heel, three metatarsal heads (1st, 2nd, and 5th), medial and lateral malleoli, medial and lateral femoral epicondyles, greater trochanter, anterior superior iliac spine, posterior superior iliac spinae, and acromion process. A single marker was placed on the xiphoid process, jugular notch, 7th cervical vertebra, and 10th thoracic vertebrae. Rigid clusters of four markers were attached to the shank and thigh bilaterally.	• Spatiotemporal parameters: step width (m), step length (m), double support time (s). • Kinematics: knee and ankle joint angle in three anatomical planes (°). • Kinetics: knee and ankle peak internal joint moments (Nm).
Law et al., 2021 [38]	Evaluate the difference in lower limbs kinematics and kinetics among 3	11 obese 3M, 8 F BMI 30.0–34.9 kg/m^2	Stair ascent and descent	Opto-electronic system 10 cameras (Vicon MX-13, Vicon Motion Systems Ltd, Oxford, UK).	Ottawa Motion Analysis Model (UOMAM) [39], 43 markers	• Kinematics: Peak and ROM (°) of hip, knee, and ankle angles in the

	groups (normal weight, overweight, and obese) during stair ascent and descent.	21 overweights 14 M, 7 F BMI 25.9–29.9 kg/m^2 20 normal weights 9M, 11 F BMI 18.5–24.9 kg/m^2		4 Force plates: two portable Kistler (Model 9286AA, Kistler Instruments Corp, Winterhur, CH) built into the staircase and two Bertec (Model FP 4060-08, Bertec Corporation, Cloumbus, OH, USA).		sagittal and frontal plane. • Kinetics: peak joint moments (Nm/kg) of hip, knee, and ankle in the sagittal and frontal plane.
Pau et al., 2021 [40]	Assessment of the possible alteration in lower limb joint kinematics in obese individuals during gait.	26 obese 11 M, 15 F BMI Median 39.0 (34.9–51.6) kg/m^2 26 normal weights 11 M, 15 F BMI Median 21.4 (17.0–26.5) kg/m^2	Gait overground	Optoelectronic system 6 cameras (Vicon Motion Systems Ltd, Oxford, UK). Two force platforms (Kistler Instruments Corp, Winterthur, CH).	Davis, 22 markers [32]	• Spatiotemporal gait parameters: speed (m/s), stride length (m), cadence (step/min), stance phase (% gait cycle), swing (%gait cycle), double support phase (% gait cycle). • Kinematics: range of motion (ROM, °) of hip, knee, and ankle joints in the sagittal plane observed during the gait cycle. • Symmetry parameters (Cyclograms): cyclogram area (°^{2}), cyclogram orientations (°), trend symmetry.
Maktouf et al., 2020 [41]	Investigate the influence of age and/or obesity on gait parameters, with a focus on ankle muscle activities.	80 obese BMI 37.2 kg/m^2 70 normal weights BMI 22.9 kg/m^2	Gait on treadmill	Gait analysis treadmill with force plates (Zebris; FDM-T, Zebris medical GmbH, Isny, Germany). Surface EMG Powerlab 16/35 system (Powerlab 16/35, ADInstruments, Dunedin, New Zealand).	Two unipodal surface electrodes (Uni-gel Single Electrode-T3425, Thought Technology Ltd., Montreal, Canada) were placed on three ankle joint muscles: the gastrocnemius medialis, the soleus, and the tibialis anterior of the dominant leg.	• Spatiotemporal gait parameters: step length (cm), step width (cm), stride length (cm), walking cycle (% gait cycle). • Kinetics: CoP length (mm), vertical ground reaction force (N/kg),

						• Root mean square of the gastrocnemius, soleus, and tibialis anterior on the gait cycle.
Sample et al., 2020 [42]	Effects of increased step-width on knee biomechanics during inclined and declined walking.	6 obese 6 M BMI 32.2 ± 2.6 kg/m^2 7 normal weights 1M, 6F BMI 23.3 ± 2.6 kg/m^2	Inclined walking	Opto-electronic system 12-cameras (Vicon Motion Systems Ltd, Oxford, UK). Two force platforms (AMTI, BP600600 and OR-6-7; AMTI, Watertown, MA, USA).	Retroreflective anatomical markers were placed on bony landmarks bilaterally on the acromion process, iliac crest, greater trochanter, medial femoral epicondyle, lateral femoral epicondyle, medial malleolus, lateral malleolus, and on the shoe above the first and fifth metatarsal heads and the second toe. For the tracking markers, 4 retroreflective markers, attached to thermoplastic plates, were placed on the posterior trunk, posterior aspect of the pelvis (2 marker clusters on each side), the lateral surface of thighs and shanks, and finally on the the heel of the shoe.	• Kinematics: the peak of knee extension/flexion and knee adduction angles (°) and ROM (°). • Kinetics: peak loading-response (N), knee extension, and knee abduction moments (Nm).
Badawy et al., 2019 [43]	Evaluation of changes in trunk angles and moments during the dominant side of one-handed carrying of various load.	10 obese M BMI 33.5 kg/m^2 10 normal weights M BMI 23.3 kg/m^2	Gait with different loads in the dominant hand	Opto-electronic system 10 cameras (Vicon Motion Systems Ltd, Oxford, UK). 2 ground force plates (AMTI BP400600, AMTI, Watertown, MA, USA).	Full-body obese specific kinematic marker set, 79 markers [44]	• Kinematics: trunk angles (°) in three anatomical planes. • Kinetics: the moment at the L4/L5 vertebral segment of the trunk (Nm) in three anatomical planes.
Cimolin et al., 2019 [45]	Validate Time Up and Go test measured by a wearable IMU in obese and normal-weight women.	44 F obese BMI 41.1 ± 7.9 kg/m^2 14 F normal weights, BMI 22.8 ± 3.5 kg/m^2	Time up and go	IMU, (G-Sensor, BTS Bioengineering, Milan, Italy).	Lower back, approximately at the L2 vertebrae position.	• Kinematics: trunk flexion/extension angle (°).
Dames et al., 2019 [46]	Comparison of kinematics and kinetics during gait	10 obese. 6M, 4F BMI 33.7 ± 2.9 kg/m^2	Gait on treadmill	Optoelectronic system (Vicon Motion Systems Ltd, Oxford, UK).	Plug in gait [32,36]	• Spatiotemporal gait parameters: stride length (m), duration of

	barefoot vs. shod of obese population.			Instrumented treadmill with two force plates (AMTI, Watertown, MA, USA).		the stance phase (s), duration of swing time (s), double support time (s). • Kinematics: ROM (°) of hip, knee and, ankle joint angles in sagittal plane. • Kinetics: joint moment peaks (Nm) of ankle, knee, and hip in sagittal plane.
Pamukoff et al., 2019 [47]	Comparison of femoral cartilage characteristics using ultrasound imaging in individuals with and without obesity.	48 obese 24 M, 24 F BMI (31.9–34.2) kg/m^2 48 normal weights, 24 M, 24 F BMI (21.1–22.1) kg/m^2	Gait overground	Logiq E ultrasound device (GE Healthcare, Fairfield CT, USA) and a 12-5 MHz linear array transducer. Isokinetic dynamometer (HUMAC NORM, Stroughton, MA, USA). Opto-electronic system 9 cameras (Qualisys, Göteborg, Sweden). Two force plates (AMTI, Watertown, MA, USA).	The ultrasound probe was placed anteriorly over the medial and lateral femoral condyles in the transverse plane and superior to the border of the patella. Markers were placed on the lateral side of the pelvis such that the marker represents the anterior surface of the palpated anterior superior iliac spine (ASIS) landmark [48]. Rigid clusters of four markers were affixed to the sacrum, and bilaterally to the thigh, shank, and foot.	• Kinetics: peak external knee adduction moment (% BW*ht).
Rosso et al., 2019 [49]	Comparison of gait characteristics of overweight/obese and normal-weight subjects.	10 obese BMI 31.1 ± 3.3 kg/m^2 12 normal weights, BMI 22.7 ± 1.2 kg/m^2	Gait overground	7 IMUs (H-gait, TSDN121, ATR Promotions, Kyoto, Japan).	The sensor on the pelvis was located posteriorly in the middle point between the iliac crests. The six sensors on the lower limbs were positioned on the lateral side of the thighs, on the anterior side of the tibia, and below the medial malleolus, bilaterally [50,51].	• Spatiotemporal gait parameters: step length (cm), step width (cm), stride length (cm), cycle time (s), stance time (% gait cycle), and cadence (stride/min). • Kinematics: ROM (°) during the gait cycle of the hip, knee, and ankle joint kinematics in the sagittal, frontal, and

						transversal planes; trajectories of knee and ankle joint center in the transversal plane.
Vakula et al., 2019 [35]	Compare quadriceps function and gait biomechanics in young adults with and without obesity.	48 obese 24 M, 24 F BMI 33.1 ± 4.1 kg/m^2 48 normal weights 24 M, 24 F BMI 21.6 ± 1.7 kg/m^2	Gait overground	Logiq E ultrasound device (GE Healthcare, Fairfield CT) and a 12-5 MHz linear array transducer. Isokinetic dynamometer (HUMAC NORM, Stroughton, MA, USA). Opto-electronic system 9 cameras (Qualisys, Göteborg, Sweden). Two force plates (AMTI, Watertown, MA, USA).	The ultrasound probe was placed anteriorly over the medial and lateral femoral condyles in the transverse plane, and superior to the border of the patella. Markers were placed on the lateral side of the pelvis such that the marker represents the anterior surface of the palpated anterior superior iliac spine (ASIS) landmark [48]. Rigid clusters of four markers were affixed to the sacrum, and bilaterally to the thigh, shank, and foot.	• Kinematics: knee flexion and abduction angle (°). • Kinetics: vertical ground reaction force (N), vertical loading response (N/s), the external moment of the knee (Nm), knee joint stiffness (Nm per degree).
Clément et al., 2018 [20]	Comparison of soft tissue artefact and its effects on knee kinematics between non-obese and obese subjects performing a squatting activity recorded using an exoskeleton.	8 obese 1 M, 7 F BMI 34.3 ± 2.7 kg/m^2 9 normal weights 4 M, 5 F BMI 24.8 ± 2.3 kg/m^2	Squatting activity wearing an exoskeleton	Exoskeleton (Emovi Inc., Laval, QC, Canada). Biplane radiographic imaging system EOS® system (EOS Imaging Inc., Paris, France).	The exoskeleton was fixed on one of the subjects' lower limbs and was calibrated to define the anatomical frames of the femur and tibia relative to the technical frames of the exoskeleton. The anatomical frames were built using the functional approach developed by [52].	• Kinematics: movement of the femoral harness and tibial plate relative to the femur and tibia; knee flexion angle (°).
Horsak et al., 2018 [48]	Investigate if the test-retest reliability for 3D gait kinematics in a young obese population is affected by using two different hip joint center localization approaches.	10 obese 8 M, 2 F BMI 34.2 ± 3.9 kg/m^2	Gait overground	Opto-electronic system 8 cameras motion capture system (MX-series, Vicon Motion Systems Ltd, Oxford, UK).	Cleveland Clinic Marker set: twenty-seven retro-reflective spherical markers, some of which were attached in a standardized way as a cluster of three on rigid base plates to the thigh and shank, and others to anatomical landmarks. To account for anterior soft tissue offset of the ASIS markers, the markers were placed on the lateral	• Kinematics: hip and knee joint angles (°).

					side of the pelvis, so that the marker center reflects the anterior surface of the palpated ASIS landmark.	
Milner et al., 2018 [53]	Determine how velocity adjustment and different step lengths affect knee joint loading.	10 obese 5M, 5F BMI 33.7 ± 3.8 kg/m^2 10 normal weights 5M, 5F BMI 22.2 ± 1.6 kg/m^2	Gait overground	Optoelectronic system 8 cameras (Vicon Motion Systems Ltd, Oxford, UK). Two force platforms (AMTI, Watertown, MA, USA).	Anatomical markers: greater trochanters, medial and lateral epicondyles, medial and lateral malleoli, posteroinferior calcaneus, and first and fifth metatarsal heads. Tracking markers: shells located on the posterior pelvis, proximolateral thigh, posterodistal shank, posterosuperior, lateral, and medial aspects of the calcaneus.	• Spatiotemporal gait parameters: step length (m) velocity (m/s). • Kinetics: peak tibiofemoral joint contact force (N/FFW), tibiofemoral joint impulse (Ns/FFW), peak knee adduction impulse (Nms/FFW*ht).
Yocum et al., 2018 [54]	Investigate self-selected step width and its effects on knee joint biomechanics of obese participants during stair negotiation.	10 obese BMI 32.8 ± 2.7 kg/m^2 14 normal weights BMI 22.5 ± 1.9 kg/m^2	Stair negotiation and walking level	Opto-electronic system 12 cameras (Vicon Motion Systems Ltd, Oxford, UK). Two force platforms (AMTI, BP600600 and OR-6-7, AMTI, Watertown, MA, USA). 3-step staircase (FP-stairs, AMTI, Watertown, MA, USA) bolted to the force platforms.	Retro-reflective anatomical markers were placed bilaterally on the 1st and 5th metatarsal heads, the distal end of 2nd toe, medial and lateral aspects of malleoli and femoral epicondyles, greater trochanters, iliac crests, and acromion processes. A semi-rigid thermoplastic shell with four reflective tracking markers was placed on postero-lateral aspects of the posterior trunk, shanks and thighs, and mid-dorsal aspect of shoes. Four tracking markers placed on two separate shells were placed on the left and right posterior-lateral aspects of the pelvis.	• Spatio-temporal parameters: stair ascent, descent, and level walking Step Widths (m) and Speeds (m/s). • Kinematics: knee extension and abduction angle (°). • Kinetics: vertical ground reaction force (N), knee extension, and knee abduction moments (Nm).
Agostini et al., 2017 [55]	Validation of inertial measurement system for the evaluation of gait parameters in obese and normal-weight population.	10 obese M BMI 31.1 ± 3.3 kg/m^2 12 normal weights M BMI 22.8 ± 1.1 kg/m^2	Gait overground	7 IMUs (H-gait system, TSDN121, ATR Promotions, Kyoto, Japan). Multiple system STEP32: Six footswitches and six electrogoniometers (Medical Technology, Torino, Italy).	Six STEP32 foot-switches were fixed under both barefoot soles (3 under each foot). Footswitches were positioned beneath the back portion of the heel, the first, and fifth metatarsal heads. Six STEP32 electrogoniometric sensors were fixed on the ankle, knee, and hip joints of each lower limb. H-Gait inertial sensors: two below the medial malleolus, two on the shanks in correspondence with the anterior side of the tibia bone, two on the lateral side	• Spatiotemporal gait parameters: cadence (strides/min), stance (%gait cycle), swing (%gait cycle), double support (%gait cycle). • Kinematics: ROM (°) during the gait cycle of hip, knee, and ankle joint angle in the sagittal plane.

					of the thighs, and one on the pelvis, in the posterior center point between the left and right iliac crest.	
Camomilla et al., 2017 [21]	Assessment of pelvis soft tissue artefact during walking.	1 obese M BMI 36.9 kg/m^2 1 overweight M BMI 28.4 kg/m^2 3 normal weights 1 M, 2 F BMI 22.3–23.9 kg/m^2	8 postures: mid-stance postures and star-arc postures	Optoelectronic system 8 cameras (VICON MX, Vicon Motion Systems Ltd, Oxford, UK). MRI (Master Philips Medical System, Best, The Netherlands).	UP-CAST approach matching the point identified on the specific-subject model with marker clusters; Iliac spines, the sacrum, and the right femur lateral and medial epicondyles, 7 markers on the pelvis, 4 markers on the anterior aspect of the thigh [56].	• Kinematics: pelvic orientation (°) and joint hip angles (°) in all anatomical planes.
Liu et al., 2017 [57]	Inspect how obesity affects dynamic gait stability among young adults.	23 obese F BMI 35.1 ± 3.9 kg/m^2 21 normal weights BMI 21.7 ± 2.4 kg/m^2	Gait on treadmill	Opto-electronic system 8 cameras (Vicon Motion Systems Ltd, Oxford, UK).	26 retro-reflective markers	• Spatio-temporal parameters: step length (m), cadence (step/min), step width (m), gait speed. • Kinematics: center of mass (COM), trunk angle (angle between the trunk segment and the vertical axis in the sagittal plane).
Meng et al., 2017 [58]	Assess gait features of normal weight, overweight, and obese adults.	10 obese BMI 35.3 ± 3.1 kg/m^2 10 overweight BMI 28.3 ± 1.5 kg/m^2 10 normal weights BMI 21.9 ± 1.2 kg/m^2	Gait overground	7 inertial measurement sensors (Xsens Technologies B.V. Enschede, Netherlands). 4.9m long GaitRite Portable Walkway System (CIR Systems Inc., Sparta, Netherlands).	Sensors are placed on the sacrum, on the front of bilateral thighs, shanks, and the dorsal surface of the feet.	• Spatio-temporal parameters: normalized step length, and normalized stride length. • Kinematics: hip and knee joint angle (°).
Singh et al., 2017 [59]	Assess the biomechanical gait changes in obese and normal-weight female adult subjects after a 30-min walking session.	10 obese F BMI 36.1 ± 4.2 kg/m^2	Gait overground	GaitRite Portable Walkway System (CIR Systems Inc., Sparta, Netherlands). Optotrak motion analysis system (Model 3020; Northern Digital Inc., Waterloo, Ontario, Canada).	Triads of infrared-emitting diodes were placed on the pelvis and trunk and bilaterally on the thighs, legs, and feet. Markers were affixed to the lateral aspect of the foot, the shaft of the tibia, and the lateral aspect of the thigh. Femoral epicondyle motion was tracked by two markers mounted on a custom femoral tracking device [60].	• Kinetics: hip extension and abduction moment (Nm/kg), knee extension and adduction moment (Nm/kg).

				Kistler force plate (Kistler Instruments Corp, Winterthur, CH).	Pelvic markers were affixed on the sacrum using a 5-cm extension. A similar extension was placed on the lower cervical vertebrae to track the trunk segment.	
Yang et al., 2017 [61]	Dynamic gait stability control during the slip differs between obese and normal-weight young adults.	23 obese 15 M, 8 F BMI 35.1 ± 3.9 kg/m^2 20 normal weights 6 M, 14 F BMI 21.6 ± 2.4 kg/m^2	Perturbed gait on a treadmill	ActiveStep treadmill (Simbex, Lebanon, NH, USA) was donned with a safety harness instrumented with a load cell. Opto-electronic system (Vicon Motion Systems Ltd, Oxford, UK).	26 retro-reflective markers	• Kinematics: trunk angle (°). • Kinetics: knee joint isometric strength capability in flexors and extensors (Nm/kg); COM stability, position, and velocity.
Pamukoff et al. 2016 [62]	Compare gait biomechanics between normal-weight and obese young adults.	15 obese BMI (30.2–36.7) kg/m^2 15 normal weights BMI (21.0–22.1) kg/m^2	Gait overground	Electromagnetic tracking sensors (Motion Star, Ascension Corp., Burlington, VT, USA) acquired by the Motion Monitor motion capture system (Innovative Sports Training, Chicago, IL, USA). Non-conductive force plate (Model 4060-NC, Bertec Corp., Columbus, OH, USA).	Sensors were positioned on the pelvis, thigh, shank, and foot of the dominant limb [63].	• Kinematics: the peak of knee flexion angle (°). • Kinetics: vertical ground reaction force (N/bw), knee internal and external moment (bw*ht)
Fu et al., 2015 [64]	Quantify the effect of obesity on soft tissue work during level walking at a constant velocity.	11 obese BMI 34.9 ± 4.1 kg/m^2 9 normal weights BMI 22.0 ± 1.0	Gait on treadmill	Opto-electronic system 7 cameras (Nexus, Vicon Motion Systems Ltd, Oxford, UK). Split-belt force-measuring treadmill (Bertec Corp, Columbus, OH, USA).	Passive reflective markers were placed over the seventh cervical vertebrae, acromion processes, right scapular inferior angle, sternoclavicular notch, xiphoid process, 10th thoracic vertebrae, posterior-superior iliac spines, medial/lateral femoral epicondyles, medial/lateral malleoli, calcanei, first metatarsal heads, second metatarsal heads, and proximal and distal heads of the fifth metatarsals. To account for adipose tis-	• Kinematics: sagittal component of hip, knee, and ankle angles (°). • Kinetics: the sagittal moment of hip, knee, and ankle (Nm/kg), power of hip, knee, and ankle (W/kg).

					sue around the pelvis, virtual markers were placed on the anterior superior iliac spines and iliac crests using a digitizing wand (C-Motion, Germantown, MD). Marker clusters were placed on the thighs, shanks, and sacrum to aid in 3D tracking [44].	
Singh et al. 2015 [65]	Analyze the biomechanics of obese and normal-weight females during squat and lunge exercises.	10 obese F BMI 39.2 ± 3.7 kg/m^2 10 normal weights F, BMI 21.6 ± 2.3 kg/m^2	Squat and lunge exercise	Triads of infrared emitting diodes (IREDs) Optotrak motion analysis system (Model 3020, Northern Digital Inc., Waterloo, ON, Canada). Kistler force plate (Kistler Instruments Corp, Winterthur, CH).	Markers were affixed to the lateral aspect of the foot, to the shaft of the tibia, and the lateral aspect of the thigh. Femoral epicondyle motion was tracked by two markers mounted on a custom femoral tracking device [66]. Pelvic and trunk marker triads were attached to 5 cm extensions with base plates affixed over the sacrum and lower cervical vertebrae.	• Kinematics: range of motion at the hip, knee, and ankle, and trunk segment flexion angles (°). • Kinetics: support moment (summation of the lower limb ankle, knee, and hip extensor moments, Nm/kg).
Glave et al., 2014 [67]	Examine how the classification of participants by body fat percentage resulted in a different change to select kinematic variables during gait in the female population.	12 obese F BMI 31.4 ± 7.0 kg/m^2 10 normal weights F, BMI 21.7 ± 2.1 kg/m^2	Gait overground	Peak motus motion analysis software (Vicon Motion Systems Ltd, Oxford, UK) 2 cameras (frontal and lateral perspective)	6 reflective markers for sagittal view: anterior superior iliac spine, the external border of the greater trochanter, the lateral epicondyle of the femur, the lateral malleolus, the base of the fifth toe, and the back of the heel. 3 markers for frontal view: 1 on the sacrum and on both heels.	• Spatiotemporal gait parameters: walking speed (m/s), stride length (m), step width (m). • Kinematics: knee angular displacement (°), ankle angular displacement (°), peak knee flexion velocity (°/s), peak knee extension velocity (°/s).
Haight et al., 2014 [68]	Examine how different walking conditions reduced tibiofemoral loading.	9 obese 1 M, 8 F BMI 35.0 ± 3.8 kg/m^2 10 normal weights 5 M, 5 F BMI 22.1 ± 1.0 kg/m^2	Walking at different speeds and inclinations on a treadmill	Optoelectronic system 10 cameras (Nexus, Vicon Motion Systems Ltd, Oxford, UK). Dual belt, inclinable, force-measuring treadmill (Fully instrumented treadmill; Bertec Corp, Columbus, OH, USA).	Obesity-specific marker set [44] EMG electrodes: soleus, lateral gastrocnemius, vastus lateralis, vastus medialis, biceps femoris long head, semimembranosus.	• Kinematics: the peak of hip, knee, and ankle flexion/extension angles (°). • Kinetics: the peak of hip extension, knee extension, internal abduction, ankle

				Surface EMG (Noraxon, Scottsdale, A, USA).		dorsiflexion moments; peak compressive tibiofemoral forces, and rates of tibiofemoral loading.
Lerner et al., 2014 (a) [69]	Evaluate the effect of different speeds on lower limb muscles.	9 obese 1 M, 8 F BMI 30-40 kg/m^2 10 normal weights 5 M, 5 F BMI < 25 kg/m^2	Walking at different speeds on a treadmill	Optoelectronic system 10 cameras (Nexus, Vicon Motion Systems Ltd, Oxford, UK). Dual belt, inclinable, force-measuring treadmill (Fully instrumented treadmill; Bertec Corp, Columbus, OH, USA). Surface EMG (Noraxon, Scottsdale, A, USA).	Obesity-specific marker set [44] EMG electrodes: soleus, lateral gastrocnemius, vastus lateralis, vastus medialis, biceps femoris long head, semimembranosus.	• Kinematics: the peak of the pelvis, hip, knee, and ankle flexion/extension angles (°). • Kinetics: individual muscle forces (from EMG data) and individual muscle contribution (ground reaction force).
Lerner et al., 2014 (b) [44]	Developed an obesity-specific marker set that accounted for subcutaneous adiposity.	9 obese 1 M, 8 F BMI 35.0 ± 3.8 kg/m^2 10 normal weights 5 M, 5 F BMI 22.1 ± 1.0 kg/m^2	Walking on treadmill	Optoelectronic system 10 cameras (Nexus, Vicon Motion Systems Ltd, Oxford, UK). Dual belt, inclinable, force-measuring treadmill (Fully instrumented treadmill; Bertec Corp, Columbus, OH, USA). Surface EMG (Noraxon, Scottsdale, A, USA).	Obesity-specific marker set which utilized digitized markers and marker clusters and a modified Helen Hayes marker set. EMG electrodes: soleus, lateral gastrocnemius, vastus lateralis, vastus medialis, biceps femoris long head, semimembranosus.	• Kinematics: sagittal plane joint angles of the pelvis, hip, and knee. • Kinetics: axial joint contact force of hip and knee; muscle force of vasti, hamstring, rectus femoris, and iliopsoas.
Mignardot et al., 2013 [70]	Identifying the role and contribution of some morphological characteristics and the physical activity lifestyle in the observed postural-kinetic deficits.	12 obese 5 M, 7 F BMI 36.6 ± 3.3 kg/m^2 8 normal weights 4 M, 4 F BMI 21.4 ± 2.0 kg/m^2	Gait overground	Optoelectronic system (optotrack 3020 H, NDI, Ontario, Canada). Force platform (OR6-7, AMTI, Watertown, MA, USA).	Ten active markers were placed on anatomical landmarks: eyes, ear (auditory meatus), shoulder (acromion), elbow (ulnar epicondyle), wrist (radial tuberosity), finger (head of the 5th metacarpal bone), hip (greater trochanter), knee (lateral femoral condyle), ankle (lateral malleolus), and foot (fifth metatarsal head).	• Kinematics: wrist mean speed (m/s), range of motion of elevation angle of the shank, thigh, pelvis, head, humerus, forearm, hand (°); intersegmental angle shift of ankle, knee, hip, neck, shoulder, elbow, and wrist (°). • Kinetics: center of mass (COM) and center of

						pressure (COP) in three anatomical directions.
Ranavolo et al. 2013 [71]	Evaluate how obesity affects coordination during locomotion using the CRP (continuous relative phase) method.	25 obese 8 M, 17 F BMI (33.8–44) kg/m^2 25 normal weights 8 M, 17 F BMI (19.0–27.8) kg/m^2	Gait overground	Opto-electronic system 8 cameras (SMART–E System, BTS Bioengineering, Milan, Italy).	Davis marker placement protocol [32].	• Spatio-temporal gait parameters: stride duration (s), mean speed (m/s), cadence (step/min), duration of the stance (%), duration of the swing (%), and double support phase (%). • Kinematics: range of motion of pelvic tilt, obliquity, and rotation; hip flexion/extension, abd/add, rot; knee flexion/extension, ankle dorsi/plantarflexion, foot progression, inter-joint coordination on the sagittal plane.
Roemer et al., 2013 [72]	Determine the effects of BMI on the biomechanics of ergometer rowing in the lower extremities.	10 obese BMI 35.5 ± 4.7 kg/m^2 10 overweights BMI 26.7 ± 1.3kg/m^2 10 normal weights BMI 21.8 ± 1.6 kg/m^2	Rowing	Opto-electronic system 6 cameras (Vicon Motion Systems Ltd, Oxford, UK). Concept II Model D ergometer equipped with two 3D AMTI force transducers (AMTI, Watertown, MA, USA).	48 passive reflective markers	• Kinematics: flexion/extension and ab-/adduction angles and torques in hip, knee, and ankle joint; internal/external rotation angles (°). • Kinetics: torques of hip and knee joint.
Russel et al., 2013 [73]	Determine if laterally wedged insoles could reduce the peak knee joint contact force and the peak medial location of the joint contact force.	14 obese F BMI 37.2 ± 6.1 kg/m^2 14 normal weights F BMI 22.4 ± 1.2 kg/m^2	Gait overground	Opto-electronic system 8 cameras (240 Hz; Oqus 300, Qualisys, Gothen-burg, Sweden). One force platform (AMTI, Watertown, MA, USA).	Spherical retro-reflective markers were placed on the pelvis including the iliac crests, greater trochanters, anterior superior iliac spines, and the space between the fifth lumbar and first sacral vertebrae. Posterior superior iliac spine markers were used to help	• Kinematics: hip, knee, and ankle 3D joint angles (°). • Kinetics: ground reaction forces, 3D hip moment, knee flexion/extension moment, and ankle subtalar and talocrural

	during walking in obese women.				track the motion of the pelvis in the obese group as markers on the anterior superior iliac spines can experience excessive movement in this population. Other markers were secured to the medial and lateral femoral epicondyles and malleoli. Locations on the foot were palpated through the shoe and included the first and fifth metatarsal heads and the distal toe. Rigid arrays of markers were secured to the lateral thigh, lateral leg, and posterior heel.	moment (Nm); Center of pressure lateral and medial (cm).
Silvernail et al., 2013 [74]	Influence of BMI and velocity on knee biomechanics in walking.	10 obese BMI 34.4 ± 3.9 kg/m^2 10 overweights BMI 26.9 ± 1.3 kg/m^2 10 normal weights BMI 22.4 ± 2.1 kg/m^2	Gait overground	Opto-electronic system 7 cameras (Vicon Motion Systems Ltd, Oxford, UK). Two force platforms (AMTI, Watertown, MA, USA).	Anatomical markers were placed bilaterally on the iliac crest, greater trochanter, medial and lateral epicondyles, medial and lateral malleoli, and the first and fifth metatarsal heads. Four non-collinear tracking markers were attached to moulded thermoplastic shells [75] on the pelvis, thighs, and shanks [30], and three separate non-collinear markers on the heels [76].	• Spatio-temporal parameters: walking velocity (m/s). • Kinematics: knee flexion excursion (°), peak knee flexion angle (°), knee adduction angle (°). • Kinetics: external knee adduction moment (Nm/ffw*ht), external knee flexion moment (Nm/ffw*ht).
Ehlen et al., 2011 [77]	Quantify the energetics and biomechanics of uphill versus level walking in moderately obese adults.	12 obese 5 M, 7 F BMI 33.4 ± 2.4 kg/m^2	Inclined and level walking on a treadmill	Three-dimensional motion capture system (Motus 9.2; Vicon Motion Systems Ltd, Oxford, UK). Dual-belt, inclinable, force-measuring treadmill (Fully Instrumented Treadmill; Bertec, Columbus, OH, USA).	Retro-reflective spheres following the modified Helen Hayes marker set to identify anatomical landmarks and delineate lower extremity segments [36]. Markers were placed on the sacrum and anterior superior iliac spine, mid-thigh (femoral wand), femoral epicondyle, mid-shank (tibial wand), lateral malleolus, second metatarsal head, and calcaneus of each leg.	• Kinematics: hip, knee, ankle sagittal joint angle (°). • Kinetics: ground reaction force (N), hip and knee extension, knee abduction, and ankle plantarflexion moment (Nm).
Russel et al., 2010 [78]	Metabolic cost and biomechanical risk	10 obese F BMI 33.1 ± 4.2 kg/m^2	Gait overground and on the treadmill	Opto-electronic system 8 cameras Qualisys Mo-	Marker locations included bilateral iliac crests, greater trochanters and	• Kinematics: peak impact shock during foot-

	factors for the knee in obese women.	10 normal weights F BMI 22.7 ± 0.9 kg/m^2		tion Capture System (Qualisys, Gothenburg, Sweden). Three-dimensional force platform (AMTI, Watertown, MA, USA).	anterior superior iliac spines. A sacral marker was placed on L5/S1. Other markers on the right leg only included medial and lateral femoral epicondyles, medial and lateral malleoli, first and fifth metatarsal heads, and the distal end of the first metatarsal. Rigid arrays of markers secured to the right lateral thigh, lower leg, and posterior heel tracked the motion of the segments.	ground contact (vertical deceleration m/s^2). • Kinetics: peak adduction moment of the knee (Nm) and knee adduction moment angular impulse (Nm).
Vismara et al., 2010 [79]	Proposal of a protocol to evaluate the functional mobility of the spine segment.	13 obese F BMI 39.2 ± 3.6 kg/m^2 13 obese with non-specific low back pain F BMI 41.9 ± 5.3 kg/m^2 11 normal weights F BMI 20.1 ± 1.2 kg/m^2	Forward flexion and lateral bending of the trunk	Optoelectronic system 6 cameras (Vicon 460, Vicon Motion Systems Ltd, Oxford, UK).	Five markers were placed along the spine: two on the thoracic (T1 and T6), two on the lumbar vertebrae (L1 and L3), and one on the sacrum (S1). Four markers on the pelvis: left and right anterior and left and right posterior iliac spines (LASIS, RASIS, LPSIS, RPSIS). Two markers on the acromion of the left and right shoulders.	• Kinematics: sagittal plane: forward trunk inclination, anterior pelvic tilt, angle related to lordosis, lumbar movement, angle related to kyphosis, thoracic movement. Frontal plane: lateral bending, lateral trunk inclination, pelvis obliquity, lumbar curve, lumbar movement, thoracic curve, thoracic movement, and shoulders. Symmetry index of lateral trunk inclination.

Table 1: Study characteristics

3.3 RESULTS

Study Selection

The initial search identified a total of 3720 papers; of these, 1281 were duplicates and were removed accordingly. The obtained 2439 studies were preliminary screened for eligibility criteria, and 2207 were eliminated. A total of 232 were then screened in full, and from the residual papers: thirty-two had full text not available; one had a different study design; thirty-seven had a population not stratified according to the inclusion criteria or with BMI < 30 kg/m^2; thirty-nine had a population with less than 18 years; twenty-three included a population affected by other pathologies or pain; nine were focused on the surgical intervention; two papers had no precise indication about the instrumentation; twenty-four papers were focused on posture or balance, or the analysis of plantar pressure; fifteen papers had other focuses; one paper was not written in English; six papers were different publication types from the inclusion criteria. Finally, a total of 43 papers were included in this review. The complete PRISMA flowchart is reported in Figure 10.

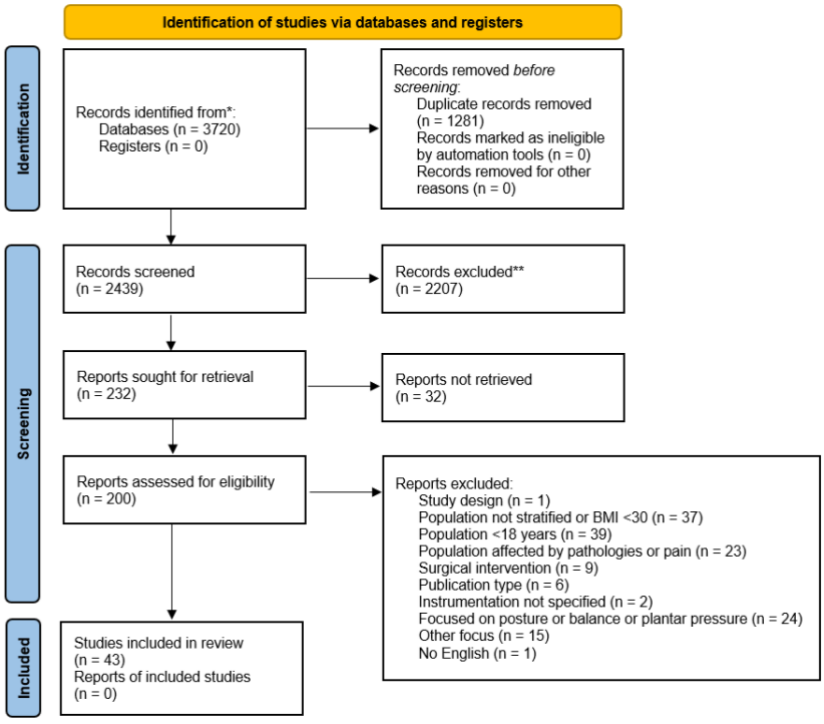

*Figure 10. PRISMA diagram. * PubMed=913; Scopus=1659; Web of Science=1148; **manually excluded*

Risk of Bias

Focusing on the evaluation of risk of bias, Table 2 shows the scores specifically associated with the included articles and estimated through the MINORS tool [37].

Items 1 (clearly stated aim), 3 (prospective collection of data), and 4 (endpoints appropriate to the aim of the study) were graded as two in all forty-three studies. Item 2 (inclusion of consecutive patients) represented a critical item since all studies were graded as one. Item 5 (unbiased assessment of the study endpoint) was also considered critical, and was graded as zero in all studies because no one mentioned strategies or methods to avoid bias concerning this issue. Items 6 and 7 were graded as zero in all forty-three studies because no studies had a follow-up evaluation in their study design.

A further critical item was represented by Item 8, where twenty-one papers were graded as zero, and one paper was graded as one. Item 9 (adequate control group) was graded as two when the control group was available, and the BMI stratification was used as a reference. Item 10 (contemporary groups) was graded as two in thirty-three studies, where subjects were collected for this study; this point was graded as one in five studies, where data were already available and derived from retrospective studies.

Furthermore, Item 11 (baseline equivalence of groups) was graded as two in twenty-nine studies, where samples were balanced between the study group and the control group; this item was graded as one in nine studies because the data were reported but considered not adequate. Finally, Item 12 (adequate statistical analysis), where twenty-three of thirty-eight papers were graded as one, and fifteen papers were graded as two.

Table 2: List of the included papers assessed using the methodological index (MINORS) tool, to quantify the individual and overall Risk of Bias. Legend of items 1: A clearly stated aim; 2: Inclusion of consecutive patients; 3: Prospective collection of data; 4: Endpoints appropriate to the aim of the study; 5: Unbiased assessment of the study endpoint; 6: Follow-up period appropriate to the aim of the study; 7: Loss to follow-up less than 5%; 8: Prospective calculation of the study size; 9: Adequate control group; 10: Contemporary groups; 11: Baseline equivalence of groups; 12: Adequate statistical analyses. The items are scored 0 (not reported), 1 (reported but inadequate), or 2 (reported and adequate). The global ideal score is 16 for non-comparative studies and 24 for comparative studies.

Author (year)	1	2	3	4	5	6	7	8	9	10	11	12	Tot. Score
Vakula et al., 2022 [30]	2	1	2	2	0	0	0	2	2	2	2	2	17 (24)
Kim et al., 2022 (b) [29]	2	1	2	2	0	0	0	2	2	2	2	1	16 (24)
Kim et al., 2022 (a) [28]	2	1	2	2	0	0	0	2	2	2	2	1	16 (24)
Pau et al., 2021 [40]	2	1	2	2	0	0	0	2	2	2	2	1	16 (24)
Law et al., 2021 [38]	2	1	2	2	0	0	0	0	2	2	2	1	14 (24)
Kim et al., 2021 [37]	2	1	2	2	0	0	0	2	2	2	2	1	16 (24)
Ghasemi et al., 2021 [7]	2	1	2	2	0	0	0	2	2	2	2	2	17 (24)
Garcia et al., 2021 [34]	2	1	2	2	0	0	0	0	2	2	2	2	15 (24)

Cimolin et al., 2021 [33]	2	1	2	2	0	0	0	2	-	-	-	-	9 (16)
Capodaglio et al., 2021 [31]	2	1	2	2	0	0	0	2	2	1	2	2	16 (24)
Sample et al., 2020 [42]	2	1	2	2	0	0	0	2	2	2	2	2	17 (24)
Maktouf et al., 2020 [41]	2	1	2	2	0	0	0	2	2	2	2	2	17 (24)
Vakula et al., 2019 [35]	2	1	2	2	0	0	0	2	2	2	2	2	17 (24)
Rosso et al., 2019 [49]	2	1	2	2	0	0	0	0	2	1	2	2	14 (24)
Pamukoff et al., 2019 [47]	2	1	2	2	0	0	0	2	2	2	2	2	17 (24)
Dames et al., 2019 [46]	2	1	2	2	0	0	0	2	-	-	-	-	9 (16)
Cimolin et al., 2019 [45]	2	1	2	2	0	0	0	0	2	2	1	2	14 (24)
Badaway et al., 2019 [43]	2	1	2	2	0	0	0	0	2	2	2	2	15 (24)
Yocum et al., 2018 [54]	2	1	2	2	0	0	0	0	2	2	2	1	14 (24)
Milner et al., 2018 [53]	2	1	2	2	0	0	0	2	2	2	2	2	17 (24)
Horsak et al., 2018 [48]	2	1	2	2	0	0	0	0	-	-	-	-	7 (16)
Clément et al., 2018 [20]	2	1	2	2	0	0	0	0	2	2	2	1	14 (24)
Yang et., al 2017 [61]	2	1	2	2	0	0	0	0	2	2	1	1	13 (24)
Sing et al., 2017 [59]	2	1	2	2	0	0	0	0	2	2	2	1	14 (24)
Meng et al., 2017 [58]	2	1	2	2	0	0	0	0	2	2	2	1	14 (24)
Liu et al., 2017 [57]	2	1	2	2	0	0	0	2	2	2	1	1	15 (24)
Camomilla et al., 2017 [21]	2	1	2	2	0	0	0	0	-	-	-	-	7 (16)
Agostini et al., 2017 [55]	2	1	2	2	0	0	0	0	2	2	2	1	14 (24)
Pamukoff et al., 2016 [62]	2	1	2	2	0	0	0	2	2	2	2	2	17 (24)
Sing et al., 2015 [65]	2	1	2	2	0	0	0	1	2	2	1	1	14 (24)
Fu et al., 2015 [64]	2	1	2	2	0	0	0	0	2	1	1	1	12 (24)
Lerner et al., 2014 (b) [44]	2	1	2	2	0	0	0	0	2	1	1	1	12 (24)
Lerner et al., 2014 (a) [69]	2	1	2	2	0	0	0	0	2	1	1	1	12 (24)
Haight et al., 2014 [68]	2	1	2	2	0	0	0	0	2	2	1	1	12 (24)
Glave et al., 2014 [67]	2	1	2	2	0	0	0	2	2	2	2	1	16 (24)
Silvernail et al., 2013 [74]	2	1	2	2	0	0	0	2	2	2	2	1	16 (24)
Russel et al., 2013 [73]	2	1	2	2	0	0	0	2	2	2	2	1	16 (24)
Roemer et al., 2013 [72]	2	1	2	2	0	0	0	2	2	2	2	2	17 (24)
Ranavolo et al., 2013 [71]	2	1	2	2	0	0	0	0	2	2	2	2	15 (24)
Mignardot et al., 2013 [70]	2	1	2	2	0	0	0	0	2	2	2	1	14 (24)
Ehlen et al., 2011 [77]	2	1	2	2	0	0	0	0	-	-	-	-	7 (16)
Vismara et al., 2010 [79]	2	1	2	2	0	0	0	0	2	2	1	2	14 (24)
Russel et al., 2010 [78]	2	1	2	2	0	0	0	2	2	2	2	1	16 (24)

Study Characteristics

Study characteristics are summarized and displayed in Table 1.

Considering the population involved, five of forty-three papers included only one group of obese subjects without a control group [33,46,48,59,77]; six studies included three groups, represented by obese, over-weight, and normal-weight subjects [21,38,58,72,74,79]. The remaining thirty-two papers involved two groups, i.e., obese and normal-weight subjects.

More than half of the papers focused on gait tasks: (i) gait overground [30,31,33–35,40,47–49,53,55,58,59,62,67,70,71,73,74]; (ii) gait on the treadmill [28,41,44,46,57,64]; and (iii) the comparison between the overground and treadmill [29,37,78]. Moreover, perturbed gait [61], inclined walking [42,68,77], and gaits with different loads in the dominant hand [43] were investigated. Only in a few papers were subjects asked to perform more functional movements: stair ascending and descending [38,54], spinal

monitoring during load handling activities [7], squatting activities [20,65], different pelvis postures such as mid stance postures, star arc postures, and other postures [21], time up and go [45], rowing [72], and forward flexion and lateral bending of the trunk [79].

The most adopted technology for movement analysis even in obese subjects resulted to be the marker-based optoelectronic stereophotogrammetric systems [7,21,48,57,71,79], usually integrated with two or more force platforms [28–31,34,35,37,38,40,42–44,46,47,53,54,57,59,64,65,68–70,72–74,77,78].

Passive refracting markers were usually located according to standard protocols, such as "Davis", "Plug-in Gait", or "Hellen Hayes" [31,40,46,77], while different custom marker sets were also proposed according to the different objectives. The relevant anatomical markers position for the gait assessment were iliac spines, greater trochanters, medial and lateral epicondyles, medial and lateral malleoli, lateral wands over the mid-femur and mid-tibia, medial and lateral knees, medial and lateral ankles, second metatarsal heads of the toes, and heels. Lerner et al., [44] proposed a market set specifically designed for assessing movement in obese population, which was also adopted in [43,68,69].

In this context, Camomilla et al., [21] quantified the soft tissue displacement of pelvic landmarks during hip movements integrating the data gathered from the optoelectronic system and MRI, while Clement et al., [20] evaluated the effects of STA on the estimated 3D knee kinematics using biplane radiography.

Concerning wearable technologies, in five papers, MIMUs were specifically adopted, focusing on a single sensor [33,45] or using a 7-sensors protocol for assessing only the lower limb kinematics [49,55,58]. Pamukoff et al., [62] used electromagnetic tracking sensors, while Clement et al., [20] used an exoskeleton to estimate the kinematics of the lower limbs.

Surface Electromyography (sEMG) was further adopted in [41,44,68,69] to quantify the muscle activity and estimate the residual lower-extremity muscle forces in the obese population.

In 17 papers spatiotemporal gait parameters were evaluated [28–30,33,37,40,41,46,49,53–55,57,58,67,71,74], and Pau et al., [40] also studied the gait

symmetry. Thirty-five papers evaluated kinematic parameters such as the hip, knee, and ankle joint angles, trunk and pelvic segments, and spinal range of motion [7,20,21,31,34,35,37,38,40,42–46,48,49,54,55,57,58,61,62,64,65,67–74,77,78]. Finally, 29 papers evaluated kinetic parameters [28,30,31,34,35,37,38,40–44,46,47,53,54,59,61,62,64,65,68–70,72–74,77,78,80].

Concerning sEMG data, the root means the square of muscle activation signal during the gait cycle was evaluated in [41], whereas the peak of compression tibiofemoral forces and rate of tibiofemoral loading in [68], and the individual muscle forces in [44,69].

3.4 DISCUSSION

In this systematic review, we identified and summarized the evidence provided by 43 original studies regarding the different technological and methodological strategies used to assess the human movement in obese subjects. To our knowledge, no systematic reviews on this topic were published so far.

Upon analyzing the literature and examining available technologies for human movement analysis, it appears evident that the majority of the adopted solutions are marker-based optoelectronic stereophotogrammetric systems. However, it is worth noting that most of the studies that use motion capture systems for gait analysis—even those directly assessing the impact of obesity—use standard kinematic marker sets or methodologies developed for non-obese individuals, thus not accounting for adiposity; these approaches were, namely, "Plug-in Gait", "Davis", and versions of the "Helen Hayes" marker set [32,36]. Although the literature confirms that it is extremely difficult to identify anatomical landmarks in obese individuals by using a palpatory approach [81], markers are usually placed on the skin trying to guess the placement in correspondence with the underlying anatomical references of interest [82], but without quantifying the error or estimating the possible impact on the final outcomes. In fact, the kinematic data derived from a (skin) marker-based motion capture system are extremely vulnerable to soft tissue artefacts (STAs) [19], which are caused by the relative movement of the tissues over the underlying bone reference [21]. It is evident that obese subjects are more sensitive to STAs, due to the presence of adipose tissue, which can thence increase the error in

estimating the overall kinematics. In order to mitigate this issue, several researchers used clusters of markers fixed to rigid plates, aiming at reducing the effect of skin movement by limiting relative marker motion [21,28,29,34,35,37,42,44,47,48,64]. Furthermore, a study presented an obesity-specific motion capture methodology that used a spring-loaded digitizing pointer to manually mark the ASIS landmarks and an additional marker on the iliac crest, which are used to define the pelvis segment [44]. However, the massive amount of STAs characterizing obese populations warrants further investigation of the overall accuracy of marker-based approaches, depending on the specific tasks and setup. To further counteract this problem, several studies proposed medical imaging approaches oriented to quantifying STAs and their effects and impacts on the kinematics of obese individuals. Among these studies, one was specifically focused on the use of MRI for studying STAs at the pelvis [21], which indeed represents the most critical segment due to the presence of the waist adipose tissue; however, the analysis was conducted on a small cohort of subjects who were classified as obese. Another research specifically analyzed knee kinematics during squatting while the subjects wore an exoskeleton, and STAs were estimated via biplane radiography [20]. Analyzing these papers, we can affirm that medical imaging approaches indeed returned the most reliable information directly focused on bone motions; for this reason, they can be considered as the basis to validate other methodologies. On the other hand, they are in fact invasive (e.g., ionizing radiation), difficult to use due to their inherent complexities, expansive, and bulky to be used in daily inpatient/outpatient setups or during daily clinical practice. Furthermore, to provide reliable information, these approaches require biomechanical subject-specific models, which require additional resources to be defined and reliably implemented. Moreover, it is important to highlight that, at present, the studies that used medical imaging techniques for assessing obese individuals were primarily focused on the pelvis and the knee joint; therefore, it is not possible to simply generalize the approach to other body joints or conditions.

Wearable sensors represent a viable solution to perform movement analysis since they are less expensive and more versatile, with respect to the marker-based optoelectronic stereophotogrammetric systems. Furthermore, they can be applied outside the

laboratory in free-living conditions, and can be used in an unrestricted area even for a long acquisition time [15–17]. Among wearable sensors, magneto-inertial measurement units (MIMUs) are the most promising ones [83,84]. However, from this systematic review, only five papers employed MIMUs in their study protocol so far. Gait was evaluated using either a single-sensor approach, that was previously validated in healthy and pathological individuals [33,45], or by deploying a 7-sensor setup, specifically addressing lower limbs [49,55,58]. Further, Pamukoff et al. [62] adopted electromagnetic wearable sensors to compare gait biomechanics between normal-weight and obese young adults. In addition to STAs, one of the main sources of uncertainties related to the use of wearable sensors is the presence of kinematics "crosstalk". This phenomenon can also affect marker-based systems and is linked to the error that can be made in the definition of the rotation axes around which the kinematics are decomposed (e.g., for the knee, the axes of flexion/extension, adduction/abduction, internal/external rotation) [85]; therefore, all the joint angles estimated out-of-sagittal-plane should be carefully interpreted. Moreover, wearable devices are also sensitive to STAs, which were specifically addressed by fixing the sensors over bones instead of muscles and using elastic bands and medical tape [49]. Most of the selected papers investigate the effect of obesity on biomechanics outcomes compared to a control group; unfortunately, only a few studies proposed a coherent approach for the evaluation of motion in obese people including a proper validation. Specifically, on this very topic, Lerner et al. [44] proposed an obese-specific marker set and compared the output with that obtained from a standard marker set designed for a normal-weight population. Staying on this subject, Horsak et al. [48] investigated whether test-retest reliability for three-dimensional gait kinematics in a young obese population is affected by the identification of the hip joint center; in particular, the authors assessed either a predictive or a functional hip joint center localization approach. Finally, Agostini et al. [55] validated a gait analysis system based on magneto-inertial sensors, both in normal-weight and overweight/obese subjects; the validation was performed with respect to a reference multichannel recording system providing direct measurements of joint angles in the sagittal plane through electrogoniometers, which indeed present inherent limitations.

From a deeper analysis of the included paper, we identified two main categories of limitations; the former is related to the population specifically involved in the studies, whereas the latter concerns the use of suitable technological solutions.

Concerning the first limitation, most of the evaluated studies involved in fact both males and females introducing a source of potential variability. In fact, obesity modifies the body geometry by adding mass to different regions and dissimilar fat distribution in males and females, and this could produce gender-related effects [33]. Moreover, the current literature did not consider that different body shapes (e.g., apple-shaped vs. pear-shaped) may change the biomechanics output [86]. Another limitation highlighted in the included papers is the absence of a stratification of the participants in terms of the severity of obesity. The lack of homogeneous groups reduced the generalizability of the results, making difficult the comparison among groups since it is not possible to reliably identify which one of these confounding factors directly influenced the measured parameters.

Second, in most of the analyzed articles, the authors focused on the analysis of different biomechanical properties characterizing the obese population, but they did not address the reliability of the technology specifically used to obtain those parameters/metrics. In fact, over 13 years of analyzed literature, only three papers proposed solutions for studying the movement of obese individuals and a proper validation of them; the majority of included papers only narratively referred to some specific limitations that have been noticed during the experimental procedures, but did not report quantitative information and/or possible strategies to mitigate them.

However, we are aware that these limitations could be ascribed to the lack of a non-invasive reliable method for the measurement of the movement specifically designed for obese individuals. Indeed, future studies should consider the use of optimization methods for reducing the influence of STAs, as well as suitable procedures for biomechanical modelling to properly mitigate the errors possibly associated with sensors/markers placement.

3.5 CONCLUSIONS

Obesity inherently requires the need to quantify the functional limitations due to the critical physical conditions. Indeed, the movement analysis through marker-based optoelectronic stereophotogrammetric systems is the most widespread approach in specialized laboratories; however, although it is considered reliable, this solution is particularly affected by soft-tissue artefacts. In recent years, wearable systems have been representing a viable solution to monitor the movement of obese subjects even at home during their daily activities, but the kinematics in the frontal and transversal plane should be carefully interpreted due to the presence of crosstalk. Soft tissue artefacts and kinematic crosstalk are still debated topics in human motion analysis literature, especially for obese subjects. The general problem related to the STAs issue could be addressed by employing medical imaging techniques, which can represent the basis for the validation of more agile solutions. In fact, the proposed medical imaging approaches are expensive, difficult to use due to their inherent complexities, bulky, and resource-consuming.

From this systematic review emerges the urgency for further research to account for the effects of subcutaneous adiposity on kinematic data collection and analysis, and the need for dedicated, feasible, and reliable solutions that may improve the accuracy of the measurements in the obese population.

4. MATERIALS AND METHODS

The aim of this research was to validate inertial measurement units, which are ubiquitous, non-invasive and versatile, with respect to a marker-based system that is accurate, but can be employed only in a specialized laboratory. This chapter illustrates the different methodological steps used in this validation and the technologies exploited.

In this frame, a preliminary series of tasks was defined, including: stabilometry, gait analysis, trunk movements, sit to stand, lifting of loads, step and reaching. Furthermore, a marker set protocol was identified so as to locate the anatomic points where markers and sensors should have positioned for complete and accurate assessment of the movements.

In order to verify the agreement among the technologies, the procedure was preliminary tested at the Politecnico di Milano on a control group of normal-weight subjects (15 women and 14 men, average age 23 years, BMI is 22.2 kg/m^2). The acquisition was simultaneously performed by using an IMU-bases system (Awinda, Xsens, Netherlands) and an optoelectronic system (Smart DX400, BTSBioengineering, Italy).

Eventually, the same procedure was carried out on a group of obese patients (17 women and 6 men, average age 46 years, BMI is 41.6 kg/m2) in Istituto Auxologico Italiano, Ospedale San Giuseppe, Oggebbio (VB). The adopted technologies were IMUs by Xsens and the optoelectronic system by Vicon. All the subjects gave their informed consent and the study was approved by the local IRB.

Then the outputs of the optoelectronic systems, the spatial coordinates of the markers recognized by the infrared cameras, were labelled. The quaternions associated to the body segments were extrapolated through the IMU system.

After postprocessing, it was decided to analyze the commonest movements focusing only on the upper limbs, which indeed represent one of the main novelty of the project:

- *Frontal lift of the right and left arm:* the subject is asked to look ahead. According to the protocol, he performs the movement while sitting. The stool is positioned in such a way that the angle between tibia and femur measures 90°. Before starting, the arms are stretched along the trunk. At the signal, the subject flexes

and extends the limb under consideration as much as he can. The gesture is executed at natural velocity six times with each arm. The whole task is repeated twice for each arm.

- *Lateral lift of the right and left arm:* the subject is asked to look ahead. According to the protocol, he performs the movement while sitting. The stool is positioned in such a way that the angle between tibia and femur measures 90°. Before starting, the arms are stretched along the trunk. At the signal, the subject abducts and adducts the limb under consideration as much as he can. The gesture is executed at natural velocity six times with each arm. The whole task is repeated twice for each arm.
- *Reaching of a target:* the subject is asked to look ahead. According to the protocol, he performs the movement while sitting. The stool is positioned in such a way that the angle between tibia and femur measures 90°. Before starting, the arms are stretched along the trunk. At the signal, the subject extends the dominant arm and touches a target placed on a pole with the point of his fingers. The height of the target and its distance from the trunk are derived from the anthropometric measurements. They are equal respectively to the maximum height that the subject can reach and to the 80% of the length of his arm. This particular distance is chosen in order not to add any other component to the movement. Indeed, on average, a person can cover it with a complete extension of the arm and forearm, without bending the trunk. The gesture is executed at natural velocity six times with each arm. The whole task is repeated twice for each arm.

This choice was due to the fact that in the literature there are several studies concerning the analysis of the movements involving the lower locomotion system, but few on the upper system.

MVN and modified plug-in-gait protocol were exploited to obtain motion information.

Acquired data were specifically analyzed by using dedicated processing and analysis workflow (Matlab, The Mathworks, US). As far as the optoelectronic systems were concerned, the positions of the markers were acquired, then a specific filtering and

interpolating procedure on the coordinates was applied in order to increase SNR and reduce occlusions impact.

In the static acquisition, a reference system centered in the joint was created for each body segment. Thereafter, these systems were projected in the dynamic acquisitions matching marker-marker via singular value decomposition.

As far as the IMU-based system was concerned, the reference systems were derived from quaternions directly provided by the acquisition SW, thus by exploiting the embedded calibration procedure. The products of the roto-translation matrixes associated to the adjacent segments describe the movement of the articulations. The 3-D joint angles were obtained through the Euler decomposition.

A statistical study involving these kinematic data was addressed. Similarity metrices were adopted, such as linear fit, coefficients of multiple correlation (CMC), RMSD and Mean Absolute Variability (MAV); variations were assessed also point by point with Statistical Parametric Mapping (SPM) and the range of motions were compared with Bland – Altman analysis.

4.1 ACQUISITIONS

4.1.1 LABORATORIES

The assessment of the control group took place in the "Luigi Divieti" Motion Analysis Laboratory of the "Politecnico di Milano" (Milano, Italy), which is located in the Department of Electronics, Information and Bioengineering.

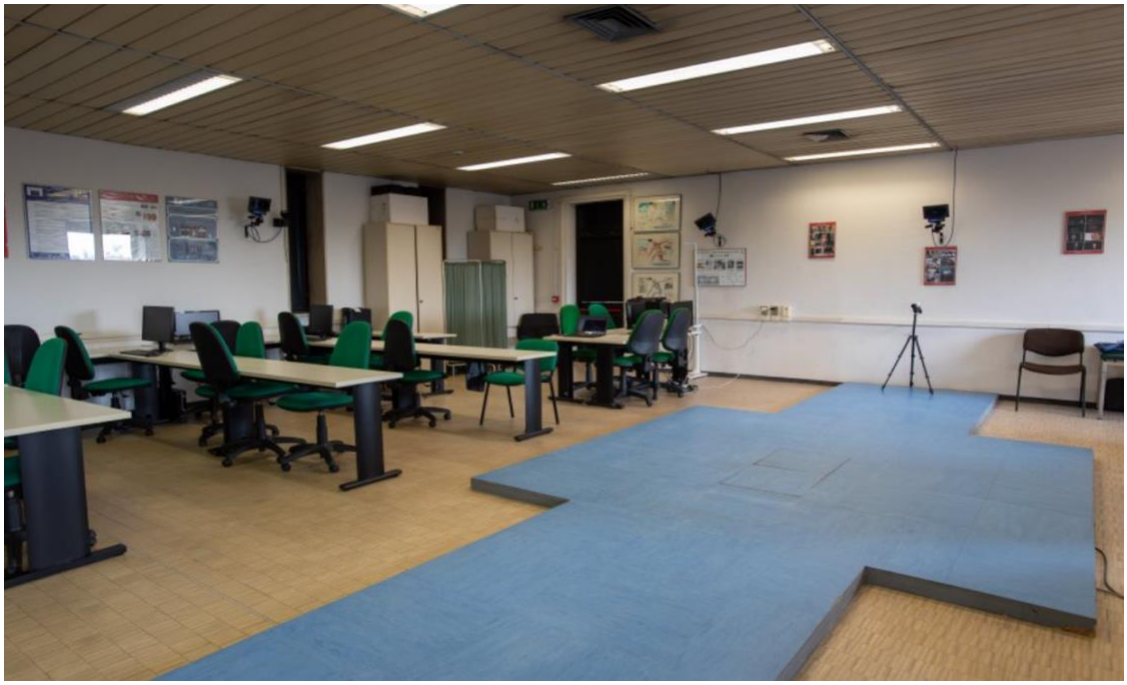

Figure 10: Luigi Divieti motion lab

This laboratory (Figure 11) is equipped with an optoelectronic system of motion analysis, which has 8 infrared cameras (SMART DX400, BTSBioengineering, working at 100Hz), two force platforms used to measure the ground reaction forces, an electromyograph and a videorecording system.

The cameras designed for the SMART system present several advantages: accuracy, flexibility and non-invasiveness. SMART provides advanced motion capture technology to universities and research centers, as well as to companies, thanks both to its quality in three-dimensional reconstruction algorithms and calibration, and to its original architecture. SMART (Figure 12) is a powerful, modular and easy-to-use motion capture system.

SMART, with all its various applications, has been the tool that has been used throughout the period of development of the thesis, to optimize and implement the protocols for motion analysis examined.

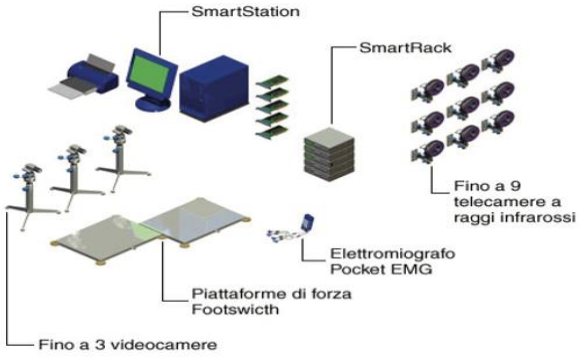

Figure 11: SMART components

Cameras of the SMART DX400 has a sensor resolution of 1 Mpixel. The maximum sampling rate is 300 Hz, but the highest resolution is reached at 100 Hz. It has an accuracy of 0,3 mm in a 4x3x3m volume. The system provides the three-dimensional coordinates of the retroreflective markers which were placed on the subjects' body according to the protocol. The markers are hit by infrared rays every 0,01 s. Each reflected ray is recorded by the camera which is coaxial to the source. Human movement can be reconstructed once the 3-D coordinates of the interesting points are known. The passive markers are spheres with a radius of 7 mm which reflect infrared light. They are attached to the subject, and they track landmarks of the human body. Motion capture systems employing them, like Smart DX400, are easy to handle and do not require any cables. The temporary hiding of some markers during the recordings causes problems in movement reconstruction. They are typically hidden by clothes or by body parts. This problem is partially reduced with the adoption of multiple cameras. Another solution is the use of clusters of markers mounted in such a way that at least three of them are visible. In return, the analysis algorithm becomes more complex.

SMART Capture is a specific software provided with the SMART DX400, which is used to analyze the static or dynamic acquisitions. As starting the program, the system is checked to ensure that the infrared cameras are connected to the computer and set up correctly.

The first step is the calibration of the system. It begins with the definition of the volume, the physical space in which the movements to be evaluated are performed. To make the SMART system stable and ready for image acquisition, the directions of the three main axes (X, Y and Z), which are the bases of the 3D system, are defined by means of a right-handed triad. The entire volume is manipulated in the three directions with the rod of one of the three axes, which is removable from the triad, in order to provide the cameras with an infrared indication of the margins of the space to be captured. The positions of the markers and their movements are what is recorded by the cameras. Only points that represent the reflecting spheres should appear on the screen.

SMART Tracker is a dedicated SW able to reconstruct the three-dimensional position of each marker from the images of each camera, acquired by SMART Capture. The first step is to create a model, a stick figure functional to the movement analysis. It is possible to apply a model that assigns a name to each marker (which can directly indicate an anatomical landmark or a point necessary to indirectly determine the landmark by means of a specific calculation protocol). After the creation of the model, the single points of this scheme must be associated to the markers represented in the acquisition file (labelling). It is also possible to graphically visualize the force platforms and the resulting force vectors.

In the second phase, the obese participants were evaluated at the Movement Analysis Lab of Ospedale San Giuseppe, Istituto Auxologico Italiano, Piancavallo (VB), Italy, using an optoelectronic system with six cameras (460 VICON; Oxford Metrics Ltd, Oxford, UK) with a sampling rate of 100 Hz and two force platforms (Kistler, CH; length 600mm; width 400 mm) with a sampling rate of 500 Hz. The reflective markers were spherical with a diameter of 14 mm.

All the functionalities described above, operated by the SMART software needed to manage the acquisitions with the optoelectronic system by BTSBioengineering, are performed through the Nexus software as far as the VICON system is concerned. Data are organized in a hierarchical structure, with information stored in relevant nodes.

For the analysis, the portable system provided by Xsens was integrated to these systems, which includes the IMU sensors, the respective battery chargers, a trigger (Awinda Station) and the USB flash drive containing the acquisition and analysis programs. In the previous chapter several details of the systems have been provided, and hereinafter further information about its use are given.

4.1.2 PARTICIPANTS

Only adult subjects were involved, both female and male. We excluded people affected with conditions that could have influenced their motion pattern, such as musculoskeletal disorders, neurological disorders, genetic pathologies like down or Prader-Willi syndrome and pregnancy.

Thirty normal-weight people, 15 men and 15 women aged between 20 and 30 years were assessed as control group; their average BMI was 22,2 kg/m^2. As case group, in Istituto Auxologico San Giuseppe, 23 obese patients (BMI > 30 kg/m^2), 17 women and 6 men aged between 18 and 75 years were assessed; their average BMI was 41,6 kg/m2.

4.1.3 SUBJECT MEASUREMENTS

The following steps were always repeated in the same order to ensure that the acquisitions were carried out in a critical and repeatable manner:

- Markers and sensors were placed on the body segments according to a modified plug-in gait protocol. The normal-weight participants wore sportswear to reduce the shift of clothes and the connected errors. Few obese subjects accepted the sportswear, rather they chose adherent clothes.
- Anthropometric measurements were taken. They were used to create proportioned models and to derive the joint angles.
- Calibration of both systems. For the XSens system, there was an actual calibration procedure. For the optoelectronic system, a video lasting a few seconds with the subject in T-pose was registered, which was the basis for the analysis of the dynamic acquisitions.
- Execution of the required tasks at normal speed.

- At the end of the acquisitions, the markers and sensors were removed. Then, the setup was sterilized and rearranged for the next test.

When the consent was signed, the volunteer was measured with a soft tape (Figure 13) and weighed by means of the force platform. These measurements are necessary to calibrate the wearable system and to obtain the joint angles as output of the optoelectronic system.

The measurements considered for the optoelectronic system are:

- Mass [Kg];
- Height [m]: the height of the subject from the floor to the top of the head with the subject standing flat on both feet (1);
- Inter ASIS distance [m]: the distance between the iliac crests. This measure is necessary when markers cannot be placed directly on the ASIS (2);
- Leg length [m]: measured between the ASIS and the medial malleolus (3);
- Knee width[m]: distance between the lateral and medial femoral epicondyles (4);
- Ankle width [m]: distance across the malleoli;
- ASIS-Trochanter-Distance [m]: between the ASIS and greater trochanter (5);
- Shoulder offset [m]: offset from the base of the acromion marker to shoulder joint center (6);
- Elbow width [m]: width of elbow along flexion axis (7);
- Wrist width [m]: width of wrist along flexion axis (8).

From these measures the positions of the joint centers were obtained through the specific "plug-in gait" procedure, implemented in Matlab.

The measurements considered for the wearable system instead are:

- Height [m] (1);
- Foot length [m] (9);
- Shoulder height [m]: from the ground to C7 (10);
- Shoulder width [m]: distance between distal tips of the acromion in T-pose (11);
- Elbow span [m]: distance between elbows in T-pose (12);
- Wrist span [m]: distance between wrists in T-pose (13);

- Arm span [m]: distance between the right fingers and the left fingers in T-pose (14);
- Hip height [m]: from the ground to the greater trochanter (3);
- Inter ASIS distance [m] (2);
- Knee height [m]: from the ground to the lateral epicondyle (16);
- Ankle height [m]: from the ground to distal tip of lateral malleolus (15).

In contrast to the previous ones, these are inputs to MVN Analyze before the IMU calibration.

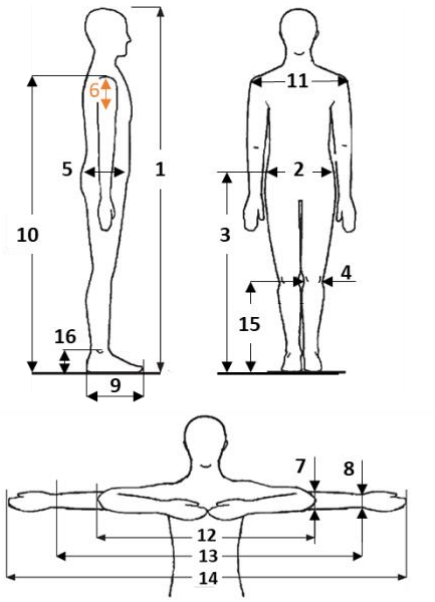

Figure 13: Anthropometric measurements

An example of the collected measurements can be seen in the Table 2.

Sesso	M	F	M	M	M	F	F	M	M	M
	MA01	FA02	SL03	ML04	PE05	FF06	CS07	FF08	SS09	PM10
mass (Kg)	67	64	74	68,5	98,8	66	64	68	59	72,5
height (m)	1,75	1,68	1,80	1,82	1,90	1,585	1,63	1,87	1,65	1,63
inter-ASIS distance (m)	0,24	0,25	0,265	0,21	0,225	0,225	0,27	0,27	0,22	0,29
leg length (m)	0,91	0,84	0,93	1,00	1,02	0,895	0,955	1,015	0,87	0,85
knee width (m)	0,12	0,12	0,105	0,09	0,11	0,085	0,10	0,11	0,10	0,125
ankle width (m)	0,07	0,07	0,07	0,07	0,075	0,065	0,065	0,075	0,07	0,07
ASIS-troc distance (m)	0,13	0,15	0,09	0,06	0,125	0,105	0,16	0,09	0,06	0,08
shoulder offset (m)	0,07	0,055	0,07	0,06	0,065	0,045	0,095	0,10	0,08	0,08
elbow width (m)	0,075	0,07	0,07	0,07	0,09	0,065	0,08	0,08	0,07	0,08
wrist width (m)	0,06	0,055	0,065	0,06	0,07	0,05	0,05	0,06	0,06	0,065
foot length (m)	0,27	0,25	0,28	0,27	0,29	0,24	0,23	0,29	0,25	0,255
shoulder heigth (m)	1,38	1,36	1,47	1,52	1,57	1,30	1,34	1,55	1,36	1,33
shoulder width (m)	0,33	0,31	0,42	0,385	0,455	0,375	0,40	0,39	0,395	0,415
elbow span (m)	0,88	0,86	0,85	0,9	0,94	0,775	0,83	0,898	0,825	0,79
wrist span (m)	1,37	1,35	1,43	1,48	1,47	1,26	1,29	1,45	1,31	1,29
arm span (m)	1,80	1,72	1,80	1,90	1,87	1,62	1,58	1,87	1,62	1,66
hip height (m)	0,91	0,84	0,93	1,00	1,02	0,895	0,935	1,015	0,87	0,85
inter-ASIS distance (m)	0,24	0,25	0,265	0,21	0,225	0,225	0,27	0,27	0,22	0,29
knee height (m)	0,55	0,49	0,49	0,55	0,54	0,47	0,46	0,515	0,48	0,44
ankle height (m)	0,08	0,08	0,11	0,1	0,105	0,09	0,07	0,105	0,10	0,10

Table 3: Example of subject measurements

4.1.4 EXPERIMENTAL SETUP

The initial idea was to adopt the plug-in gait[10] protocol consisting of:

- Regarding the upper body (Figure 14):
    - 4 markers on the head: two forward, over the temple (RFHD: right front head, LFHD: left front head), two back in a horizontal plane of the front head markers (RBHD: right back of head, LBHD: left back of head).
    - A marker near the seventh cervical vertebra C 7. This is the most prominent spinal process on the back of the neck.
    - A marker near the 10th thoracic vertebra T 10.
    - Two markers on the anterior part of the thorax CLAV and STER, respectively on the junction of the clavicles (where clavicles meet the sternum) and on the sternum (above the xiphoid process).
    - A marker on the right scapula (RBAK) acts as an anti-symmetry marker strictly for auto-label purposes.
    - 1 marker on each shoulder, placed on the acromio-clavicular joint (RSHO, LSHO: right/left shoulder).
    - A marker on the central part of each humerus (RUPA, LUPA: Right/Left upper arm).
    - A marker on the outside of the right elbow, placed on lateral epicondyle approximating elbow joint axis, and similarly on the left (REL, LEL: right/left elbow).
    - 2 markers on each wrist (RWRB, LWRB internally, RWRA, LWRA externally).
    - One marker, placed on the dorsum of the hand, on the extremity of the second metacarpal for both the right and left hand LFIN, RFIN.

[10] "Plug-in gait reference guide", Vicon Motion System, 2018

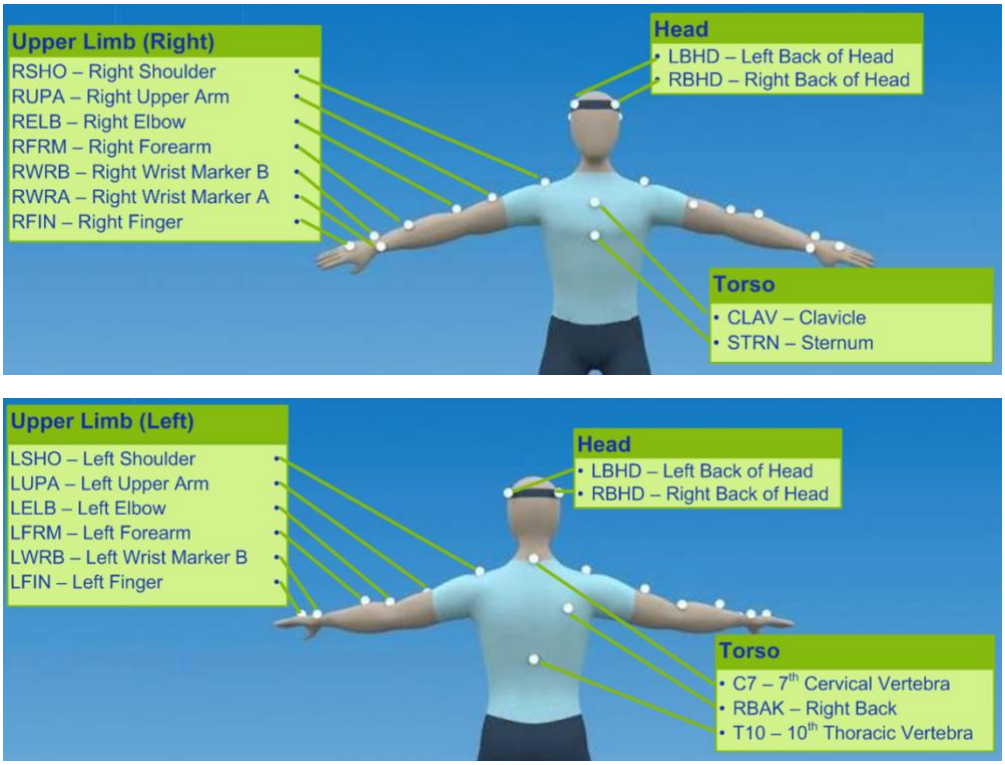

Figure 14: Plug-in gait upperbody, front view and back view

- Regarding the lower body (Figure 15):
    - RASI, LASI on both right and left anterior superior iliac spine.
    - Two markers are also placed symmetrically on the superior iliac spine posteriorly RPSI, LPSI. Alternatively, a single sacral marker SACR is used, placed on the sacral vertebra.
    - A marker for each femur at middle height: LTHI, RTHI (left/right thighbone).
    - One marker on each knee, positioned externally (RKNE, LKNE).
    - One marker for each tibia, positioned internally (RTIB, LTIB).
    - One marker on each malleolus, positioned externally (RANK, LANK).
    - One marker on the right and one on the left calcaneus (RHEE, LHEE).
    - A marker on the end of the second metatarsal, on the dorsal surface of the foot RTOE, LTOE.

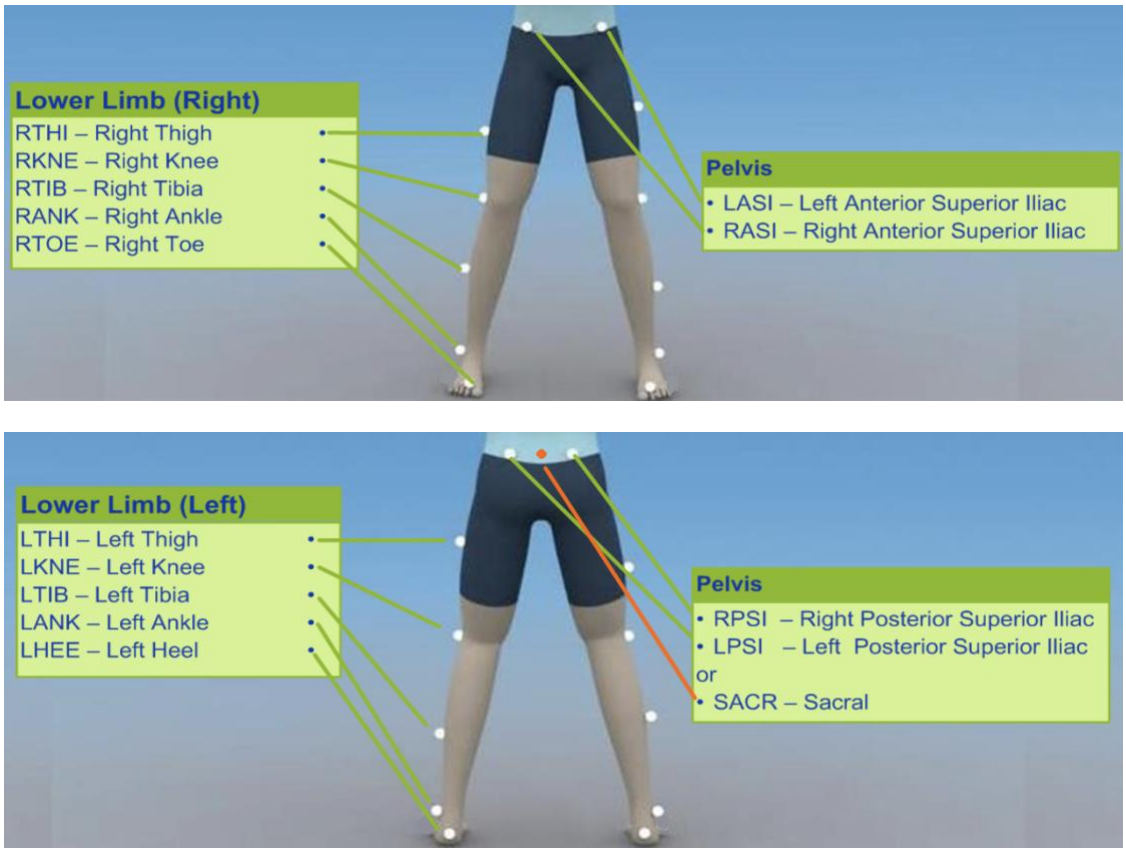

Figure 15: Plug-in gait lowerbody, front view and back view

This marker set, however, was slightly modified in order to obtain more reliable information during the execution of the motion, even when considering obese subjects. The markers on the head were eliminated, since it was preferred to focus on the limb movements. Also the marker on the scapula, which was judged to be of minimal interest, was eliminated.

Subsequently, some adjustments were performed with the aim of reducing the artefacts that typically affect the measurements of obese people's movement. In fact, the markers on the iliac crests were removed, because their shifts from the ideal position would have been too significant.

In their place, these landmarks were individuated by palpation and pointed out in additional static acquisitions by means of a structure called probe (Figure 15 on the right) moulded with a 3D printer. On its end three markers were present. During

postprocessing, the positions of the ASISs were derived by means of a specific Matlab function, even if these are not visible in overweight subjects.

Instead of the posterior iliac markers a rigid structure was applied next to the sacral vertebrae. Initially it consisted of 4 markers, but it was replaced with a cluster of 3 markers, more in accordance with the body structure.

Also considering the entity of obese subjects' soft tissue, in each segment of the limbs a cluster was introduced. The structures (Figure 16 on the left) were produced with a 3D printer, supported 4 markers and one inertial sensor. In this way, in each segment there was no longer only one marker, but 4 rigidly bound together, which provided redundant information and promoted a reduction of soft tissue artefacts.

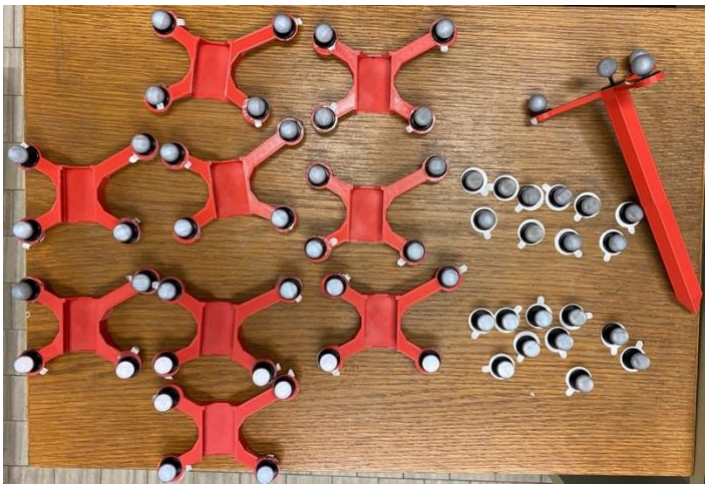

Figure 16: Plastic clusters, single passive markers with adhesive and a probe for the anterior iliac crests

Finally, on the joints where only one marker was present, such as elbow, knee and ankle, a second marker was added on the opposite side, which facilitated the search of the corresponding joint center.

As for the hands, the marker on the second metacarpus was moved to the third metacarpal; lastly, as for the feet, the marker on the second metatarsus was replaced by two markers on the first and on the fifth metatarsus respectively.

In Figure 17 the adopted protocol is reported.

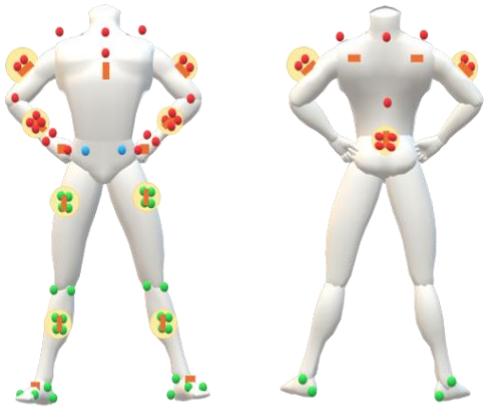

Figure 17: Modified Plug-in gait model. Red spots represent markers on the upper body, green spots represent markers on the lower body, blue spots represent the points indicated with the probe, orange rectangles represent the IMUs, yellow circles represent clusters of markers and IMU.

To further enhance the reduction of soft-tissue artefacts, elastic bands, part of the Xsens suit, were employed. They anchored the clusters along the limbs and made the setup adhere to the body. The single markers were attached to anatomical landmarks with double-sided adhesive.

Concerning the Xsens system, sensors were placed within the clusters on arms, forearms, femurs, tibias, and sacral vertebrae. Others were sticked with double-sided tape to the hands, scapulae and sternum; besides, IMUs were located on the feet inside the patients' socks and on the forehead with a band. The final configuration can be seen in the following image (Figure 18).

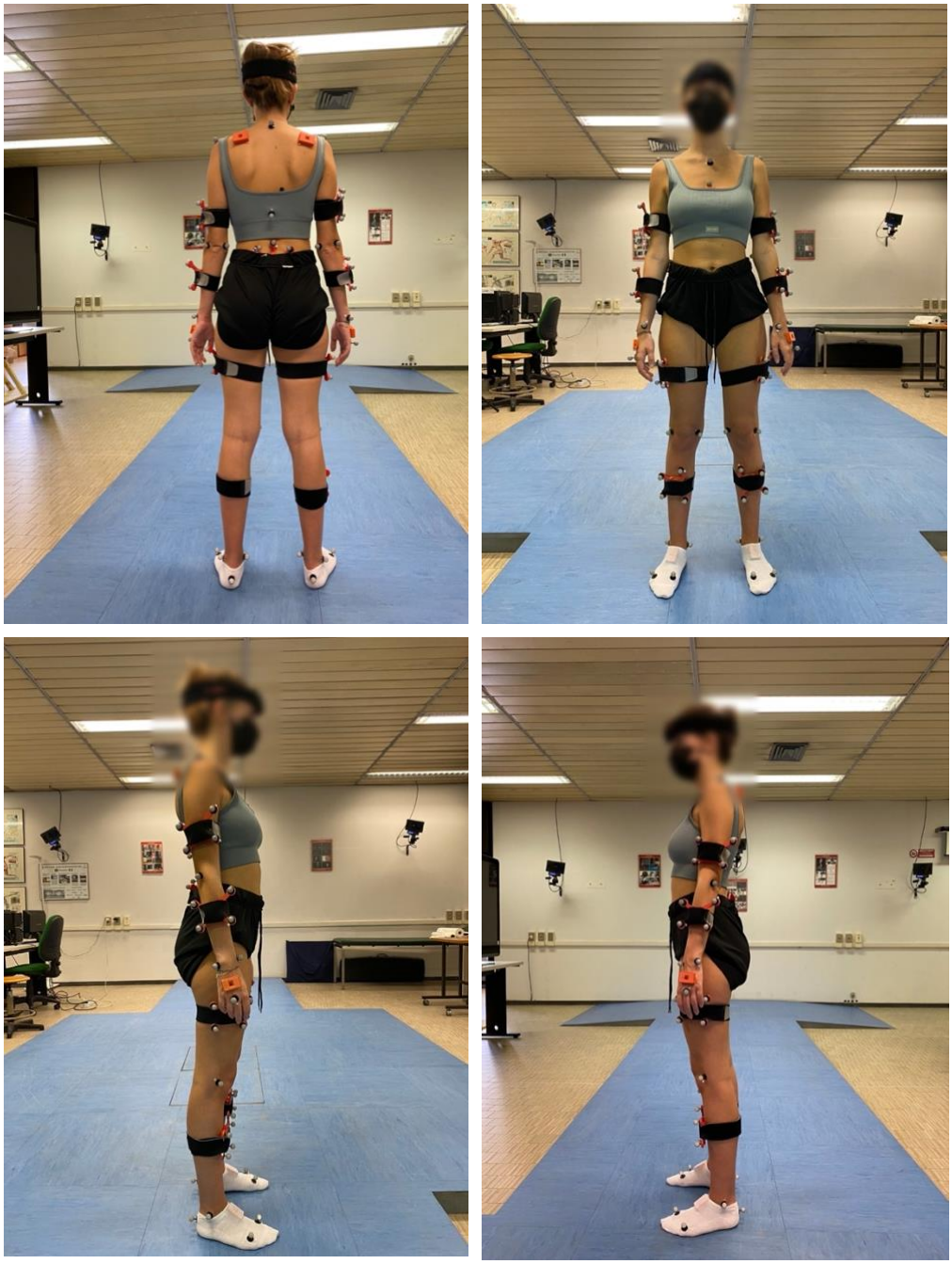

Figure 12: Final configuration of reflecting markers and IMUs

In order to obtain repeatable acquisitions, the sensors were placed in a specific orientation: inside the clusters and the headband with the micro-USB port facing upwards, in other cases facing leftwards.

An ID code is associated to the devices, in fact on each one an indication explains where it must be positioned (Figure 19).

Figure 13: ID Xsens sensor

4.1.5 SYSTEM CALIBRATION

Once the equipment is set, both the systems must be calibrated.

4.1.5.1 IMU CALIBRATION

It is crucial to perform segment calibration, in order to align motion detectors with body segments. One must have as good a calibration as possible to ensure very accurate results and excellent performance. It should be kept in mind that system calibration is not mandatory, but is always recommended.

To carry out this step, it is important, first of all, to verify that all sensors are recognized by the MVN Analyze software, second, to have a space where subjects can walk back and

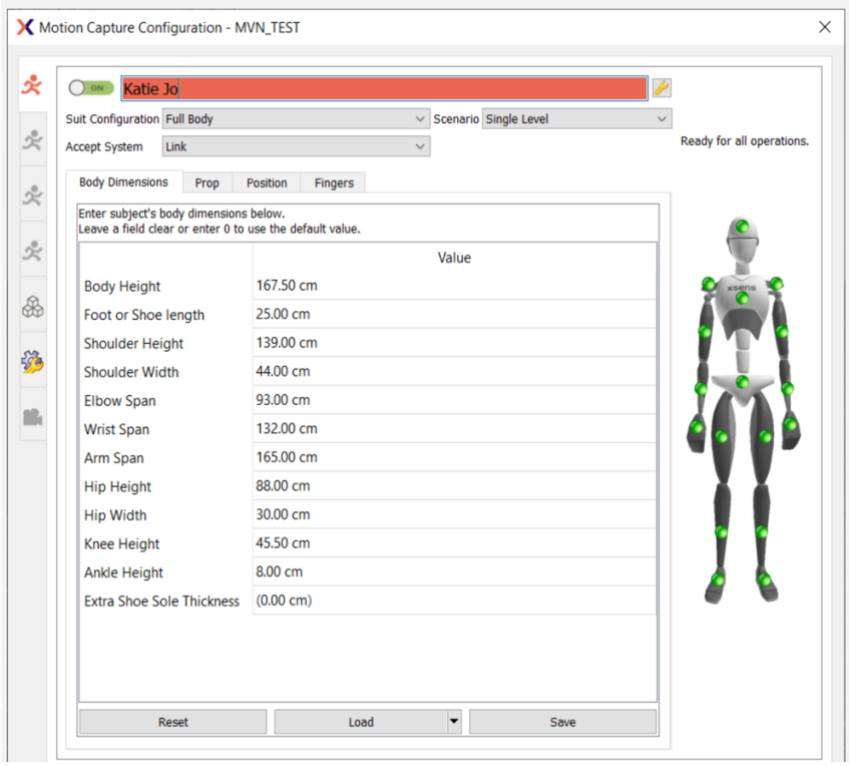

Figure 14: MVN motion capture configuration

forth for 5-10 meters and third, it is necessary to insert anthropometric measurements (Figure 20).

For this project the chosen calibration procedure included the N-pose (static neutral position) and walking. It was also possible to select the T-pose. Once this choice had

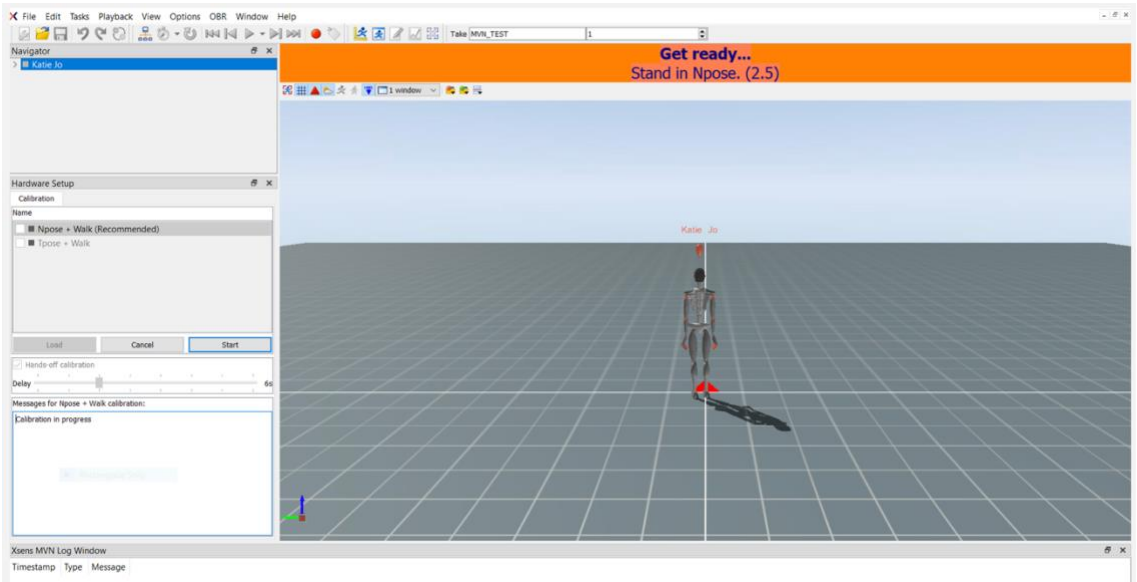

Figure 21: MVN avatar during calibration

been made, a 3D virtual space was created, where an avatar moved and reproduced the gestures during the exercises. (Figure 21).

Each person was asked to stand in a neutral position looking ahead. Once the calibration started, following the avatar, the individual was asked to remain in a static pose for a few seconds, then to walk forward and to return to the initial position with the chest always in the frontal plane of the measurement environment.

The system was able to comment on the quality of the previously estimated calibration parameters and to display warnings if problems had been detected.

There are four levels of calibration quality: good, acceptable, poor and fail. In this study, the quality of the control group calibration was good in such a manner that the results were as accurate as possible. As for obese patients, who could not stand repeated trials, sometimes the calibrations were only acceptable.

4.1.5.2 T-POSE CALIBRATION

Once the infrared cameras had been calibrated and the acquisition volume had been defined, for each subject another type of calibration was carried out for the optoelectronic system. That was necessary for the definition of the local reference systems of the body segments in dynamic acquisitions, in order to derive the joint angles and the various kinematic parameters of interest in the three main planes (sagittal, transverse and frontal).

Figure 22: T-pose for the calibration of the optoelectronic system

In this case, the T-pose (Figure 22) was selected. It was maintained by the subject for a few seconds, so that all the markers on the body were registered.

The subject was asked to step onto a force platform and assume the T-pose. At that point, the static acquisition was initiated.

Two other acquisitions were required for the evaluation of the position of the right and left iliac crest. As previously explained, single markers were not suitable to locate their exact coordinates. Thus, a probe was employed, which is a pointed structure that touches the iliac crest and has 4 markers on the other side, one is central and 3 surround it.

The calibration of the probe itself consisted of the recording of 10 rotations of the structure with its tip leaned on a base. Thanks to these recordings, it was possible to reconstruct the coordinates of the iliac crests in the dynamic acquisitions in postprocessing by means of a specific Matlab routine. This information was the starting point to find the joint centers of the lower limbs.

4.1.6 MOVEMENT DESCRIPTION

At this point, the actual trial began. The acquisition of the exercises was done simultaneously with both the optoelectronic and the inertial system. When we worked with SmartDx400, it was possible to exploit the trigger provided by the Xsens connected to both systems, on the other hand with 460VICON the synchronization happened in postprocessing.

The start and stop of the recording were controlled by MVN Analyzer via the "start recording" and "stop recording" button, these signals were then sent to the trigger (Awinda Station) which launched SMART Tracker.

A difference to consider for the successive steps was that the wearable system records at a sampling rate of 60 Hz, whereas the optoelectronic system at 100 Hz. This means that 60 and 100 frames are recorded for each second, respectively.

When both systems were activated, they acquired the same movement: BTS received information regarding the global coordinates of each marker displayed by the cameras, while the IMU sensors gathered information regarding displacement, speed and acceleration.

Before proceeding with the next movement, it was necessary to save the trials in both softwares: to facilitate the search it was chosen "InitialSurname_InitialName_#trial_Exercise_#repetition" (ex:PE05_LatDx01) with the extension ".tdf" for BTS system, ".c3d" for Vicon and ".mvn" for Xsens.

The exercises required by this clinical trial were multifaceted and involved movements of all the parts of the body, so that the accuracy of these sensors could be assessed in a general way, involving lower limbs, upper limbs and trunk. The only element left out was the head.

Below the exercises are reported in the exact order in which they were repeated each time. The tests were carried out facing the plane observed by more infrared cameras in order to have the best possible recording. Gestures were performed at a self-established speed, so that they resulted as natural as possible.

- *Stabilometry*: the patient was asked to maintain a neutral static condition, characterized by an upright position with the arms along the trunk for 60 seconds on a force platform. This examination evaluates and quantifies a person's balance by analyzing the adaptive mechanisms of the central nervous system involved in the control of the posture.
- *Walk*: two trials were performed in which the subject walked along the walkway at self-determined speed, stepping on the force platforms. The analysis systems recorded only the central part of the exercise, since in the extreme areas an optoelectronic system cannot detect all the markers.
- *Gait termination*: it is similar to the just described exercise, but the subjects did not walk the entire walkway. They stopped once they reached the force platforms. There were 4 trials of this task: in two of them the patient stopped on the second force platform, in the others he stopped with one foot in front of the other while maintaining balance, so that one foot was on one platform and one foot on the other.
- *Torsion*: the test was carried out on a dynamic platform and was repeated twice; the subjects started in N-pose and rotated the trunk around the vertical axis, first

to the right, then to the left. Six repetitions were required, with a short pause between them.

- *Forward flexion of the trunk*: the test was carried out on a dynamic platform and was repeated twice; the subject started from N-pose and bent the trunk forward. Six repetitions were required, with a short pause between them.
- *Bending*: the test was carried out on a dynamic platform and was repeated twice; the subject started in N-pose and bent laterally the trunk, first to the right, then to the left. Six repetitions were required, with a short pause between them.
- *Frontal lift of the upper limb*: the test was carried out on a dynamic platform and was repeated 4 times, twice with the right arm and twice with the left arm. The subject was sitting on a stool with the arms along the sides. The movement consisted in raising the arm ahead, as high as possible. Six repetitions were required, with a short pause between them.
- *Lateral raising of the upper limb*: the test was carried out on a dynamic platform and was repeated four times, twice moving the right arm and twice the left arm. The subject was sitting on a stool, with the arms along the sides. The movement consisted in raising the arm laterally, as high as possible. Six repetitions were required, with a short pause between them.
- *Sit to stand*: the test was performed on a dynamic platform and was repeated twice. The subject was sitting on a stool, with the arms along the sides. The movement consisted in standing up from the chair and then sitting down again. Three repetitions were required, with a short pause between them.
- *Lifting objects*: the test was carried out on a force platform and was repeated twice, starting from N-pose. The movement consisted in lowering, raising after having grabbed a medium size load and leaning it back onto the ground. The weight was a plastic box containing 2 kg. Three repetitions were required, with a short break between them.
- *Ascent and descent from a step*: the test was carried out on a dynamic platform and was repeated twice, starting from N-pose. The movement consisted of

stepping on and off a step. Three repetitions were required, with a short pause between them.

- *Reaching a target*: the test was carried out on a force platform and repeated twice, starting from N-pose. The gesture consisted in moving the dominant arm towards the target, a passive marker positioned on a tripod. It was placed at a distance from the trunk equal to 80% of the arm length. Six repetitions were required, with a short break between them.

When the acquisitions were finished, the patient was undressed of all markers, sensors, clusters and bands which were then disinfected with alcohol. The IMUs were put in charge in the appropriate compartments and new adhesive tape was sticked on the base of the markers. At this point the next acquisition could begin.

Afterwards, only the movements involving the upper limbs, which are generally less considered in the literature, were examined during the statistical analysis.

4.2 DATA ELABORATION

4.2.1 LABELLING OF THE OUTPUT OF THE OPTOELECTRONIC SYSTEM

The acquisitions obtained through the optoelectronic systems were examined. As already mentioned, the models assigned a label to each marker of interest with the name of the corresponding landmark and connected them in order to draw the stick figure. This made it easier to observe the human silhouette and its movements. In fact, the abovementioned models were applied to both static and dynamic acquisitions.

Seven different models were created for this project:

- Model 1 (Figure 23): coherent with the first kind of cluster on the sacrum, applicable to the acquisitions of the normal-weight subjects from 1 to 13;

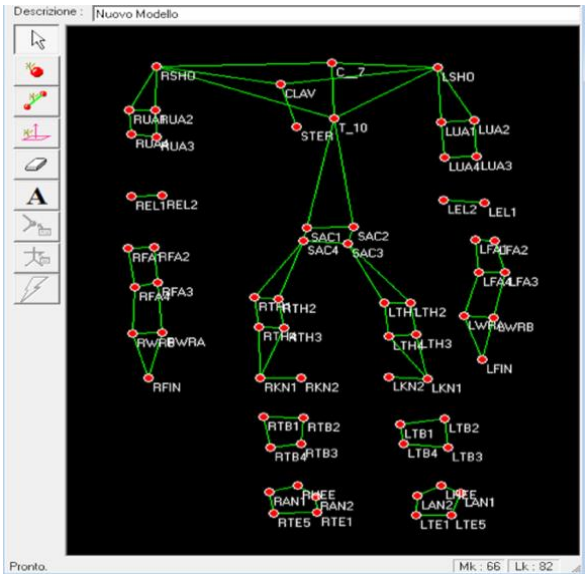

Figure 23: Model 1

- Model 2 (Figure 24): applicable to the remaining subjects' acquisitions.

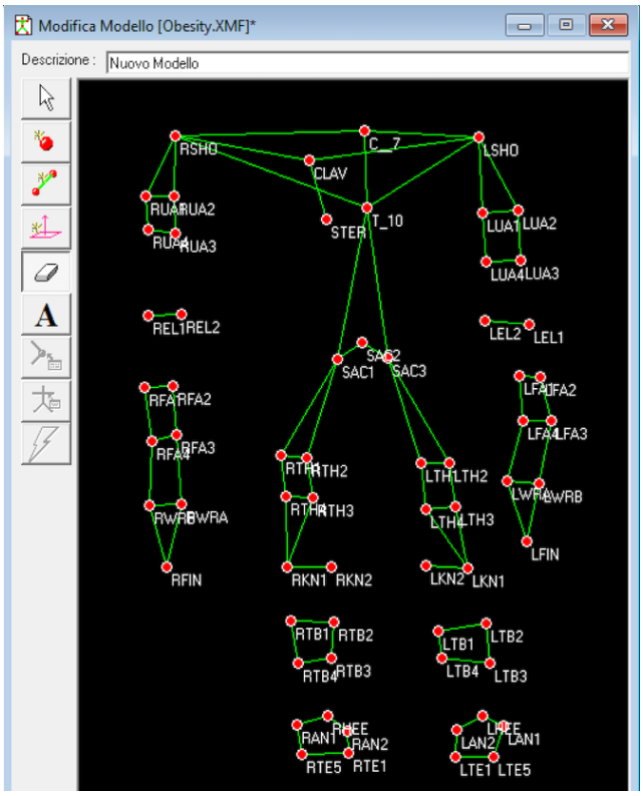

Figure 24: Model 2

The difference between these two models lies in the cluster used on the sacral vertebrae; in fact, in the former a 4-marker cluster was used, in the latter a 3-marker cluster. It was realized that the first type did not fit well to the human structure and often detached.
So, a more comfortable different shape was adopted, which allowed the subject to perform the exercises in optimal conditions.

- ASIS-right (Figure 25, two models, one for each type of sacral cluster): model that includes all markers from the previous models. Four markers representing the probe located on the right ASIS were added. Thus, it is exploited for the acquisition of the right iliac crest.

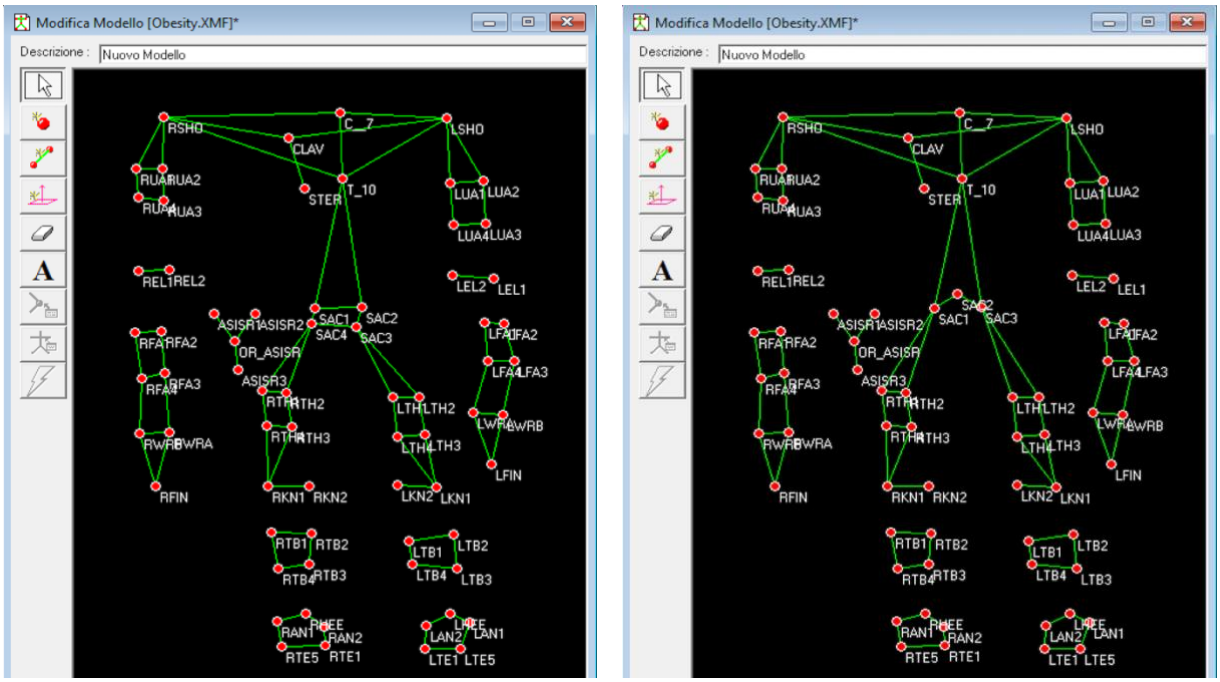

Figure 25: ASIS_right model

- ASIS-left (Figure 26, two models, one for each type of sacral cluster): model that includes all markers from the previous models to which four markers representing the probe located on the left ASIS were added. Thus, it is exploited for the acquisition of the left iliac crest.

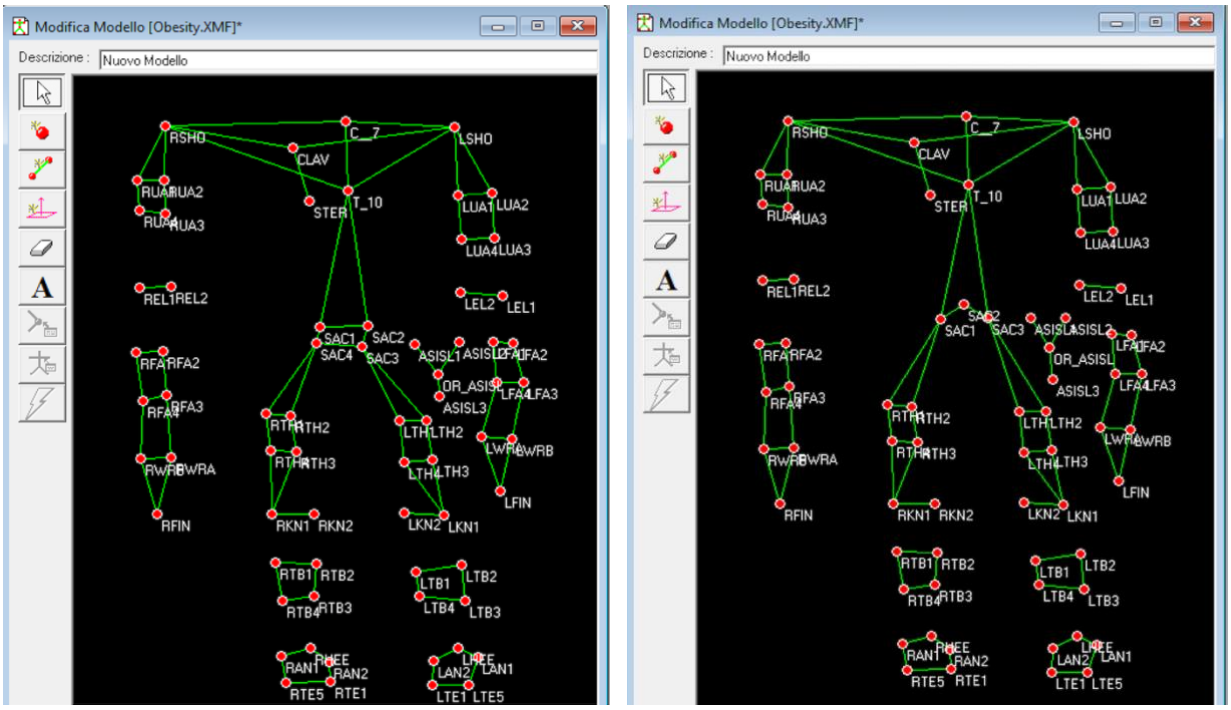

Figure 15: ASIS_left model

- Probe (Figure 27): four marker model, which allows to associate a name to each marker in the recording of the probe alone. This trial in combination with the other static acquisitions, as already mentioned, allowed to obtain the coordinates of the iliac crests through a series of mathematical steps.

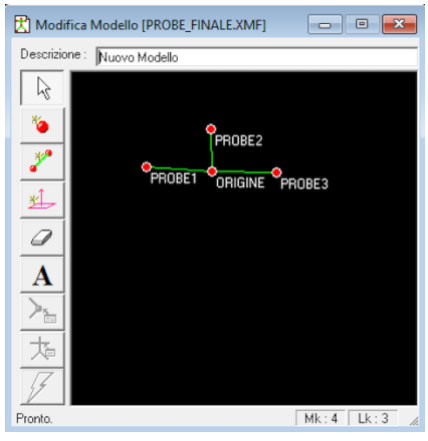

Figure 16: Probe model

4.2.2 IMU VIDEO ANALYSIS

The acquisitions were elaborated in such a way to get the "*.mvnx*" extension. MVNX is a human readable, XML format which can be imported to many other software programs, including Matlab® and Excel. This format contains the most information, including the sensor data, segment kinematics and joint angles, as well as the subject information needed to recreate a 3D visualization of a character. The pieces of information are:

- quaternions, linear and angular acceleration and velocity of the 23 segments;
- 3D joint angles of 22 joints. The Euler angles are calculated by applying the Z-X-Y and X-Z-Y order decompositions;
- Center of mass position of the body.
- Contact data indicating which contact point was detected as ground contact;
- 3D Orientation, acceleration and magnetic field data of the 17 measurement units.

The MVN Fusion Engine calculates the position, orientation and other kinematic data of each body segment with respect to an earth-fixed reference system. The axes are defined as:

- X pointing to the local magnetic north;
- Y pointing west according to right-hand rule;
- Z pointing up following the direction of the acceleration gravity vector.

The axes of each segment local reference system are aligned with this global reference when the subject is standing in the T-pose.

The MVNX file starts with the XML version, then the root element "*mvnx*" with a reference to the XSD (XML Schema Definition) and the MVNX version. This is followed by a field "mvn", containing the MVN Analyze/Animate version and build details with which this MVNX file was produced, followed by the comments. The file continues with session information, including the suit label, the sample frequency, the number of segments calculated, the date when the recording took place and the filename of the original recording on which the MVNX file is based. The next section contains mesh scale and labeling information for the segments. The mesh scale is used for scaling of the visualization of the character in MVN Analyze/Animate.

The section "*segment*" defines the positions of connecting joints and anatomical landmarks with respect to the origin of that segment. The sensor data is a list of the names of segments measured with the measurement units. The "*joints*" section is a list of the names of joints with the corresponding segments and connections. The "*ergonomic joint angles*" section is a list of the joint angles used in ergonomic analysis, of the segments and connections for each joint. The "*foot contact definition*" section is the list of the foot contact points and their index in the foot contact array for every frame. If the point is in contact with the ground, the value is 1, whilst if it is not in contact, the value is 0.

The "*frames*" section is opened with the segment, sensor and joint count. The data of all parameters are contained within this section, including the calibration pose data. The frame type "*tpose*" describes the positions and orientations of all segments in the T-pose. The MVN anatomical frame is used to calculate the joint angles.

4.3 PROCESSING OF THE OUTPUT OF THE OPTOELECTRONIC SYSTEM

After labelling the acquisitions, a Matlab code was developed for the analysis of the spatial coordinates obtained by means of the optoelectronic systems in order to derive the kinematic data.

4.3.1 INTERPOLATION AND FILTERING

The code is divided into two parts, a first part in which the static file of each subject is retrieved and a second part in which the dynamic file is analyzed.

In both cases the acquisitions were read in order to extract the data regarding the frequency, the labels and the track matrix, which contains the coordinates of all the markers corresponding to the labels. For each marker three columns represent the global x, y and z coordinates respectively, the rows correspond to the time frames. This was made possible thanks to the Matlab function "*tdfReadData3D*".

It was possible to calculate the sampling period as the reciprocal of the sampling frequency, useful information to draw graphs or to derive kinematic data as a function of time.

It should also be taken into account that some videos were cut at the beginning or at the end, so that only the most important frames were saved. However, once these files were imported into Matlab, the cut frames were not completely absent but were described as NaN (meaning Not a Number) matrixes having as rows the number of cut frames. To ensure that only the actual frames were processed, a function was written to eliminate the excess rows. This function "*toglіereNAN*" is visible in the appendix. It returns as output the matrix of traces without the rows of NaNs and the new number of frames.

At this point it was possible to associate the coordinates of the markers to the corresponding labels. 65 matrixes, one for each marker, were derived with the function "*name_position*". They had 3 columns, one for each dimension of the space, and the number of rows was equal to the number of frames.

These signals were filtered and interpolated in order to increase SNR and reduce occlusion impact. This step was performed by means of three functions: "*interpolazione*", "*butterworth*", "*predictMissingMarker*".

Throught "*interpolazione*" the NaN rows were replaced with new values obtained thanks to the Matlab function "interp1". The NaN lines represented the frames in which a marker had not been visible to the cameras. It must be kept in mind that this procedure was possible only in the case in which the marker had been sensed for most of the time. Instead, when the absence was relevant, the interpolation did not work properly.

"interp1" performed linear interpolation and returned values at specific points of a function. The NaN lines were removed by means of the Matlab function "*rmmissing*". The inputs were the marker coordinates obtained from "*name_position*" and the interval of interpolation, that was, in this case, from the first to the last frame.

"*predictMissingMarker*" searched the NaNs and filled these gaps by exploiting the correlation structure in the marker coordinates. In input a matrix containing the coordinates of all the markers was passed, the output was the same matrix with the NaNs replaced by interpolated values.

After having interpolated the coordinates of all the markers, a Butterworth low-pass filter was adopted. "*butterworth*" consists of these functions:

- *"butter*" and *"filter"*: are both Matlab functions: the first returns the coefficients of the Butterworth digital low-pass filter, receiving as input the order and the normalized cutoff frequency. From the literature it is clear that the degree of filtering varies between 2 and 4 and the cutoff frequency between 5 and 12Hz. "*filter*" is applied, which receives as input the previous coefficients and the matrix on which the filtering itself must be applied (marker coordinates), which uses the rational transfer function. All the information regarding the various inputs and outputs of the Matlab functions are easily available on the application itself with the command "help".

Having obtained all filtered signals, the static and dynamic study differs.

4.3.2 STATIC ACQUISITION: REFERENCE SYSTEMS AND JOINT CENTERS

As already mentioned, the acquisition of the static pose is used to define local reference systems for each body segment and the respective roto-translation matrices, which are composed of four columns representing the 3 cartesian verses and the origin of the system itself.

First of all, the average values of the marker coordinates, already interpolated and filtered, were defined through the function "*mean*".

In order to verify that all the steps were correctly carried out, the human shape was recreated by plotting the points representing the markers in a 3D graph.

The manuals of XSens and of the plug-in gait protocol were followed for the creation of the reference systems, in such a way to obtain joint angles referred to the same axes from both the analysis systems. More precisely, the construction of the axes was done by following the instructions of the plug-in gait protocol, but the verses were consistent with the MVN model.

Focusing on the upper body, one started by defining a reference system in the chest, and then proceeded coherently to the shoulders, elbows and wrists.

Regarding the chest reference system, a Z axis was initially defined, then a pre-axis X and a Z axis that was perpendicular to the previous ones and finally the X axis that was perpendicular to Y and Z.

The Z axis was constructed to point upward and was obtained from the difference between two midpoints: the former between the clavicle and the seventh cervical vertebra landmarks; the latter between the sternum and the tenth thoracic vertebra landmarks. The pre-axis X was derived in the same way but involving the midpoint between sternum and clavicle and the midpoint between T_10 and C_7. In this way, the direction of the axis is forward. The Y-axis pointed to the left. To ensure its perpendicularity to the previous axes, the "*cross*" function was used. This function defines the orientation of the axis, depending on the order of the input axes. Following the right-hand rule, one is able to find the exact order to be entered in the function.

To ensure that the X axis is also perpendicular, the pre-axis X was replaced by a new axis, also obtained with the *"cross"* function, between the Y axis and the Z axis.

The versor of each axis was then computed, throught the "*unit*" function and the origin of the axes was then defined. In this case, the origin of the axes coincided with the clavicle marker from which the size of the marker sphere was subtracted so that the origin was really on the body and not on the marker.

As already anticipated, the 4x4 roto-translation matrix was written having as columns respectively the global coordinates of the versors X, Y, Z and the origin. The last row contained the array [0,0,0,1].

These roto-translation matrices were used to find the local coordinates of markers, and joint centers in the static acquisition, which were exploited to obtain the coordinates of the joint centers and the roto-translation matrices in dynamic acquisitions through singular value decomposition and to extrapolate the joint angles.

From the reference system of the thorax, it was possible to calculate the coordinates of the articular centers at static level. To do this the chord theorem was exploited and a function was implemented based on this principle.

Three points were determined, in order to define a plane: a previously calculated articular center, a real marker placed on the joint to be studied, of which the offset had been previously measured and a marker interposed between the two involved articular centers. The name of the theorem is "chord" precisely because the two joint centers and the plane-definition marker lie on a circumference.

For the upper part of the body, two versions of "*chord function*" were implemented: in the second one the marker interposed between the two joints was replaced by an axis, which could anyway identify the plane.

The function defined 4 versors:

- V_x: versor obtained from an axis generated by the difference between the marker on the joint of interest and the previous joint center.
- V_t: in the first case obtained from the difference between the marker interposed between the two joints and the previous joint center, in the second case the versor of the plane-definition axis. It is a preparatory axis.
- V_z: versor that was found by finding an axis perpendicular to V_t and V_x with the "*cross*" function.
- V_y: versor obtained by finding an axis perpendicular to V_z and V_x with the "*cross*" function.

At this point a reference system was created whose origin was the midpoint between the previous joint center and the marker on the joint.

As already seen above, the roto-translation matrix was extrapolated consisting of 4 columns, each having the global values of the coordinates of the unit vectors and the origin. This matrix is used to calculate the local coordinates of the known center and of the marker on the articulation, by multiplying the global coordinates by the inverse of the roto-translation matrix.

Knowing the local coordinates, it was possible to exploit the function "*circcirc*" implemented by Matlab that allowed to obtain as outputs the coordinates of the intersections between two circumferences.

In this case the circumferences were:

- Circumference with center in (0,0) in local coordinates, meaning centered in the origin of the axes just described, with radius equal to half the distance between the marker on the joint to be studied and the known joint center.
- Circumference centered in the marker on the joint to be studied and in the plane defined by the 3 points. The radius in this case instead was given by the offset of

the involved joint, the distance between the marker on the joint and the joint center.

In this way two intersection points were obtained as outputs and the appropriate one, representing the coordinates of the joint center, had to be chosen.

In the first version of the "*chord function*", the local coordinates of the plane-definition marker were calculated. If the Y-coordinate of this point was positive then the intersection with negative ordinate was chosen, or vice versa. This is because, as shown in Figure 28, the joint center and the plane-definition marker were on opposite sides of the diameter, which implied having in local coordinates discordant values in ordinate.

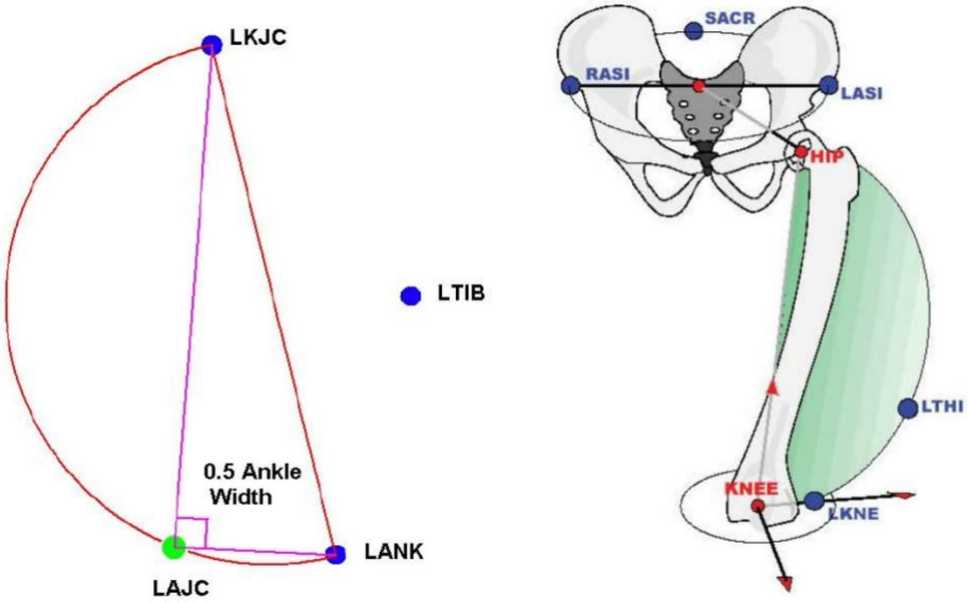

Figure 17: Schematic representation of the "chord function" applied to joints of the human body

At this point, by multiplying these local coordinates by the abovementioned roto-translation matrix, the 3D global coordinates of the joint center were obtained.

As for the second case, the point with negative ordinate was chosen (by construction) and converted into global coordinates as explained.

As far as the shoulders were concerned, the method used for both right and left was the same. The second version of the function was used, so in input instead of the plane-definition marker interposed between two joints a longitudinal axis was used, obtained

as an axis perpendicular to the X axis of the chest, directed outward, and the axis obtained as the difference between the marker of the shoulder, respectively right and left, and the origin of the chest, directed transversely. The previously calculated thoracic origin located below the clavicle marker was used as the known joint center in both cases. The markers placed on the joint of interest were RSHO and LSHO, respectively, and finally the offset of interest given as input was the anthropometric measure "shoulder_offet".

With regard to the right and left elbow, the articulation of the shoulder of the considered limb was used as known joint; the external markers of the elbows REL1 and LEL1 were the markers on the joint; the average positions of the clusters on the arms were the plane-definition markers, and the halved value of the parameter "elbow_width" was the offset.

However, the "*chord function*" was not employed to find the coordinates of the wrist joint centers. On the other hand, the midpoint between the two wrist markers, RWRA and RWRB (for the left LWRA and LWRB) was adopted. It was necessary to subtract the value of the wrist thickness in the direction of the abdo/adduction axis, obtained as an axis perpendicular to the flexion-extension axis (difference between the wrist markers) and the intra-extra rotation axis (difference between elbow joint and midpoint of the wrist markers).

Finally, an articular center for the hand was found through the "*chord function*". It received as input the already known joint center of the wrist; RFIN or LFIN were the markers on the joint; the average position of the markers on the wrists was chosen as marker interposed between the two joint centers and the halved value of the thickness of the hand was the offset.

Once all the interesting joint centers were found, they were exploited as reference system origins in the corresponding segments in order to successively calculate the joint angles between adjacent segments in dynamic acquisitions.

The technique for creating reference systems for the arm, forearm and wrist was always the same, therefore, it was decided to write a function that summarized the steps for each segment.

The function "*reference_system*" received as an input the origin of the system, a preliminary Z-axis and two markers. The Y-axis was obtained from the difference between these two markers (real or virtual), the X-axis from the cross product between the Y-axis and the Z pre-axis. The final Z-axis was computed with the cross product between the X-axis and the Y-axis. At the end, all the vectors were normalized.

The order of the markers and the order of the inputs of the cross function were essential because it allowed to obtain reference systems consistent the ones described in the MVN manual. In output the function "*reference_system*" returned the corresponding roto-translation matrixes.

"*reference_system*" function was exploited for the construction of both right and left arm, forearm, and wrist reference systems.

- Two roto-translation matrices were defined for the upper arm: rot_RUA and rot_LUA, referring to the right and left arm, respectively. They were obtained from the "*reference_system*" function that received as input the joint center of the shoulder of the studied limb, as pre_axis Z, the Z axis of the thorax, directed transversely. The choice of markers and their position was slightly different from one arm to another, in fact, the right arm received as marker 1 the joint center of the shoulder and as marker 2 the joint center of the elbow, marker 1 and 2 were inverted for the left arm.
- For the forearm rot_RFA and rot_LFA were calculated. The inputs to "*reference_system*" were as origin the respective joint centers of the elbow, as pre_axis Z, the same used for the upper arm. For the right limb as marker 1 the joint center of the elbow was assigned and as marker 2 the one of the wrist, for the left arm the two markers were reversed.
- Finally for the hand rot_RFIN and rot_LFIN were obtained by giving as input the articular centers of the wrist as origin, the usual Z-axis, and, as markers for the right limb, the former was the wrist center, the latter was the one of the hand. They were inverted for the left limb.

The reference systems were centered in the joint centers with the verses visible in the image below (Figure 29). The red arrows indicate the X-axis, the green ones the Y-axis, and the blue ones the Z-axis.

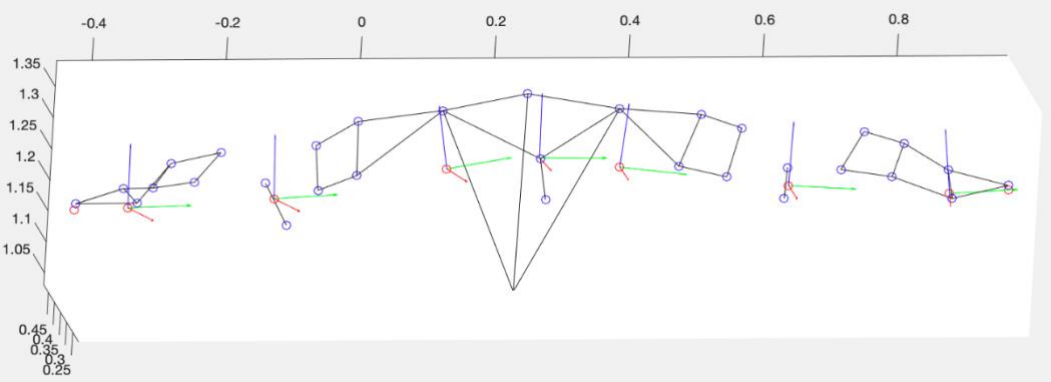

Figure 18: Frontal-top view of the upper body in T-pose with joint centers and reference systems

The constructions followed the kinematic model implemented in MVN system in the XSens manual (Figure 30), in order to grant consistency in the two analysis systems.

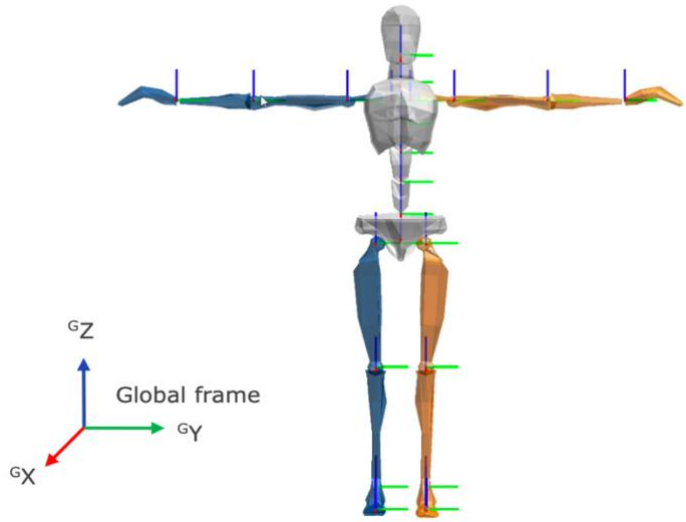

Figure 30: XSens reference systems in T-pose

As the second-to-last step in the static acquisition analysis, the local coordinates of the markers and joint centers were evaluated by multiplying the inverse of the roto-translation matrices by the global coordinates of the data of interest. Example: to obtain the local coordinates of the markers in the cluster on the upper arm (RUA1, RUA2, RUA3,

RUA4), their global coordinates were multiplied by the inverse of the rot_RUA roto-translation matrix.

On the other hand, two types of local coordinates were derived for joint centers or markers on the extremities of the body segments, in fact both roto-translation matrices of the adjacent segments were exploited.

Example: to obtain the local coordinates of the markers on the shoulder (RSHO or LSHO), their global coordinates were multiplied by the inverse of the roto-translation matrix, in one case considering rot_TORACE and in the other rot_RUA (or rot_LUA).

These coordinates were used in the analysis of dynamic acquisitions to obtain, by means of a series of mathematical steps, the joint angles.

As the last step of the static analysis, the plots of the reference systems with their respective origins projected on the human body were obtained, in order to get a graphical feedback of the obtained results.

4.3.3 DYNAMIC ACQUISITION: JOINT ANGLES

Once the static analysis was over, the joint angles of the dynamic movements were derived. First of all, the coordinates of the markers had been interpolated and filtered.

In order to extrapolate these angles, two functions were used: "*svdRegistration*" and "*joint_rotation*". The former allowed to obtain in output the global coordinates of the joint centers during the acquired movements and the rotation matrixes positioned in the joint centers.

The latter allowed to derive the joint angles describing the reciprocal motions of two body segments from their roto-translation matrices.

Analyzing more in detail these functions, "*svdRegistration*" consisted of a "for" loop with a number of cycles equal to the number of frames of the dynamic acquisitions and received in input four elements:

- A matrix including the global coordinates of the markers close to the joint to be studied in the dynamic acquisition;
- A matrix consisting of the local coordinates of the static acquisition of the same markers, placed in the same order as the previous matrix;

- The weights to be attributed to each marker of the matrix: for the analysis of the acquisitions of the control group, each weight was equal to 1 because there were no areas in which soft tissue artefacts were more relevant than others. In the future, for acquisitions of obese subjects, the weights of the coordiunates of the markers more prone to these artefacts will be reduced;
- A matrix containing one or more articular centers of the static acquisition in local coordinates, of which the global coordinates in the dynamic acquisitions were needed; usually the positions of the proximal and distal articular centers of the examined segment were recalled.

Receiving these data as inputs, a roto-translation matrix and the joint center of interest were obteined.

For the thorax, the global and local matrices included the marker coordinates of clavicle, sternum, C_7, T_10, right and left shoulder. While the matrix of joint centers in local static coordinates included the joint centers of thorax, right and left shoulder.

Regarding the shoulders, the matrices include the global and local coordinates of the shoulder marker, of the four markers on the upper arm and of the two markers on the elbow. Regarding the right shoulder, all the mentioned markers belonged to the right limb and the same was for the left limb. The matrix of joint centers in static local coordinates included the shoulder and elbow joint centers of the studied limb.

For the elbow, the markers and joint centers of the involved limb were used. The matrices included the four forearm markers, the two elbow markers, and the two wrist markers; the joint centers recalled instead are those of the elbow and wrist.

For the right and left wrist, the matrices included the hand marker and the two wrist markers while in the joint center matrix, there was only the wrist joint center.

Once the "*svdRegistration*" function had been used to obtain the roto-translation matrices of each body segment, the "*joint_rotation*" function was applied which received as inputs roto-translation matrices of two adjacent segments (the distal and the proximal one) and compiuted the corresponding Euler angles describing the movement of the articulation.

In this way six Nx3 matrices were obtained, one for each joint (right and left shoulder, elbow and wrist). The rows corresponded to the frames and the columns to the 3 dimensions of the space.

The "*joint_rotation*" function, which derived the joint angles from two roto-translation matrices, was based on five basic functions:

- *tform2quat*: Matlab function that compiuts quaternions from roto-translation matrixes. Quaternions are complex numbers describing a vector field and can be exploited to describe the rotations of a system joined to a rigid body with respect to a fixed system. They thus have the same function as roto-translation matrices, but provide information only about rotations and not translations;
- *quatconj*: Matlab function exploited to calculate the conjugate of the proximal quaternion;
- *quaternion*: Matlab function to obtain an array of quaternions. It was used to be sure that Matlab would actually read the array obtained from tform2quat as a quaternion;
- *eulerd*: receiving as input a quaternion (product of the previous quaternions) and the rotation sequence, it is able to return the rotation angles in degrees, in the order of the input sequence. Euler angles describe in another way the rotation of a reference system with respect to another one, thus making it possible, in this setting, to obtain the magnitude of the joint angles in the three main directions by evaluating the reciprocal position of two adjacent segments.

  For each joint, it was subsequently mandatory to rearrange the output so that the joint angle matrix had as columns, the rotation angles around X, Y, and Z of one system relative to the other one. Regarding the lateral lift movement, as described in the manual, the order of decomposition for wrists and elbows was ZXY, whereas for the shoulder was XZY.

  As for the frontal lift of upper arm (flexion-extension movement), the manual was not followed because the output curves were consistent between one system and another, but not consistent with the performed movement; in fact, the outputs were an excessively wide abduction/adduction curve and a flexion/extension

curve with sign variations within the same movement. The obtained results improved by modifying the rotation sequence from XZY to YXY and satisfied the expectations.

To facilitate the comparison between the output data from the optoelectronic system and the output data from the IMU-based system, it was necessary to modify the angles by translating them by 90° or changing their sign.

To confirm that the output data were meaningful and there was consistency between the two systems, at least qualitatively, it was decided to plot the curves of the angles in the three dimensions of each joint with respect to the acquisition time.

An example is shown in the image below (Figure 31) where it is possible to observe the movement of the shoulder during a lateral arm raise. The red curve represents the angle with respect to the X-axis, which characterizes the adduction/abduction movement, the green curve represents the angle with respect to the Y-axis, which characterizes the intra/extra rotation movement, and the blue curve represents the angle with respect to the Z-axis, which characterizes the flexion/extension movement.

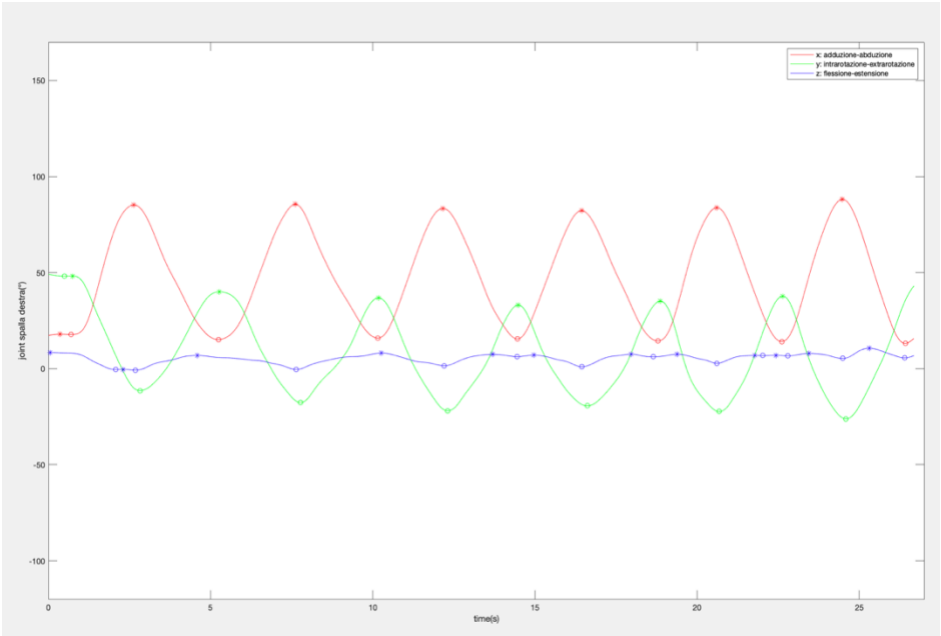

Figure 31: shoulder joint angles during lateral lift movement

After evaluating the conformity of the curves, the values of interest for a statistically significant comparison between the two analysis systems were extrapolated. These

values were the maxima, minima of the curves, and the ranges of motion for each repetition within the exercise.

For each movement, the most involved joint and the main axis of rotation were considered. For example, for the lateral arm raise, the abdo/adduction axis of the shoulder was chosen. From this curve, the six intervals representing the six repetitions of the gesture were then individuated. The other angles were divided into the same interval and within each one of them the maximum, minimum and range of motion of the curve, the difference between the maximum and minimum, were found.

This process was accomplished through the use of three functions:

- *"MIN_SPALLA"*: allowed to find the coordinates of the local minima of the joint angle of abdo/adduction of the shoulder, with regard to the lateral lift, and of the flexion/extension angle of the same joint, with regard to the frontal lift and reaching movements, and finally to plot the curve of the Euler angle evidencing the minima. The reason is that the focus was more on the upper limb analysis. If the shoulder is not the most involved joint in the analyzed movement, it is sufficient to modify the Euler matrix in input, by inserting the one of interest.
- *"Intervalli"*: function that divided the Euler angles of each joint into six intervals individuated by the coordinates of the minima of the shoulder, more precisely by the frame corresponding to each minimum. Before applying this function, it was visually checked that the minima chosen to divide the intervals were correct; since the curves were not perfect sinusoids, there might have been local minima not representing the end of an interval.
- *"MAX_MIN"*: allowed to find the minimum and maximum of the Euler angles in the three dimensions for each interval. As outputs, the values of the maximum, of the minimum and also the frames in which they were located were obtained for completeness of information.

Finally, through the function "*graficoMaxMin*" the curves of the joint angles with their respective maxima and minima were plotted.

In order to facilitate the statistical analysis, each maximum and minimum, in the three directions of each joint, and the ranges of motions were saved as a Matlab file.

Considering a single acquisition, 6 maxima, 6 minima and 6 ranges of motion were obtained for each direction, for each joint involved in the movement (elbow, wrist and shoulder). An example of the classification of these values is shown in the Table 4.

PE05	LATDX01	
SPDX		
	MAX X	ROM X
264	85.2314689	67.9059296
762	85.5702982	70.4379328
779	83.7820248	67.8810319
1233	82.2882625	66.840382
2062	83.8445793	69.4415229
2449	88.118941	74.9656209
		media max
	MIN X	84.8059291
1	17.3255393	media min
525	15.1323654	15.2271924
1016	15.9009929	media rom
1447	15.4478805	69.5787367
1880	14.4030564	
2643	13.1533201	

Table 4: Max, min and ROM classification

The averages of these values were then calculated for the repetitions of the same exercise in the three dimensions of the space. An example is shown in Table 5 below.

SPDX		X	
	MAX	MIN	ROM
PE05-LATDX01	84.80593	15.22719	69.57874
PE05-LATDX02	109.9292	12.08476	97.84448
SS09-LATDX01	142.9595	14.73968	128.2198
SS09-LATDX02	141.9257	14.06948	127.8562
GGal16-LATDX01	148.0009	19.25443	128.7465
GGal16-LATDX02	137.7069	21.80669	115.9002
RA20-LATDX01	153.3398	9.89505	143.4448
RA20-LATDX02	151.8201	10.08529	141.7348
MMan21-LATDX01	119.2382	22.96786	96.27031
MMan21-LATDX02	120.3024	23.06394	97.23843
MontA22-LATDX01	143.7647	27.28851	116.4761
MontA22-LATDX02	147.6803	27.49736	120.1829
GD23-LATDX01	132.6213	17.90274	114.7185
GD23-LATDX02	147.9202	16.65454	131.2657
TT25-LATDX01	152.5983	22.40371	130.1946
TT25-LATDX02	150.8278	23.6487	127.1791
CutS26-LATDX01	160.8225	5.963161	95.8299
CutS26-LATDX02	166.7521	7.883272	158.8689
PG27-LATDX01	146.3853	18.48024	127.905
PG27-LATDX02	145.7649	19.35462	126.4103
NA29-LATDX01	135.0788	20.48436	114.5945
NA29-LATDX02	139.9651	21.5223	118.4428

Table 5: Average max, min and ROM of the same exercise

At this point, the optoelectronic system was ready for a statistical comparison with the IMU-based system.

4.4 PROCESSING OF THE OUTPUT OF THE IMU-BASED SYSTEM

The data acquired with the IMU-based system were analyzed with a specific Matlab routine. The "*load_mvnx*" function was employed to read information contained in MVNX files.

The "*joint_rotation*" function, described above, was used to perform the angle decomposition. All the joints of the anatomical model were considered except for the ones connected to T4, which were described through the protocol adopted with the optoelectronic system. According to the cinematic chain the abduction, flexion and rotation angles of the proximal segment were computed with respect to the distal segment. The conjugate quaternion of the proximal segment was multiplied by the one describing the distal segment. Then the Euler angles were calculated by means of the "*eulerd*" function with the "*frame*" option, described in the previous part, present in the *Robotic Systems* Toolbox. The decomposition order was Z-X-Y for most of the joints. As far as shoulder movements were concerned, X-Z-Y was chosen for abduction and Y-X-Y for flexion. The obtained outputs were compared with the ones directly computed by the Xsens system and contained in the MVNX file. Some corrections were introduced in order to compensate for the different orientations of the decomposition axes, which were selected in the Matlab function and in Xsens. The inverse sinusoidal functions sometimes produced discontinuities on the angles because they individuated the outputs in different periods. The "*checkContinuity*" function eliminated this error. Furthermore, the noise was reduced thanks to a third order Butterwoth filter with cut-off frequency equal to 1 Hz.

Once the interpolated and filtered outputs of the joint angles were obtained, the movements were analyzed. By knowing that the movement consisted of six repetitions, it was possible to divide the acquisition in the six intervals, exactly as it happened with the output of the optoelectronic system. By using the functions "*MIN_SPALLA*", "*graficoMaxMin*", "*intervalli*" and "*MAX_MIN*" it was possible to calculate the maximum, minimum and range of motion of each interval. Then, the averages of these parameters were calculated for each exercise in the transverse, sagittal and longitudinal direction.

At this point also the inertial system was ready for a statistical analysis, a validation with respect to the optoelectronic system.

4.5 STATISTICAL ANALYSIS

Statistical analysis was approached in the same manner for all the tasks, and it was decided to merge the results of the right arm raise with the ones of the left arm raise because there were no asymmetries in the acquired subjects.

The issue refers to the data comparison and the assessment of the deviation of the movement pattern under analysis from reference data through a few meaningful indices. The need to assess the similarity between curves is encountered both to compare the datasets obtained using the two different instrumentations and for comparing data related to the control group to the ones related to obese subjects.

In general, the comparison between pairs of kinematic curves is performed by computing the Pearson's correlation coefficient (R), which allows for quantifying the strength of a linear relationship between the two curves (i.e., their shape similarity, independently from their amplitude or their mean difference), the root mean square error (RMSE) which provides a positive global index, or the coefficient of multiple correlation (CMC) which is helpful when the reliability of a group of curves is under analysis.

Another approach consists in computing the difference between parameters assumed to be representative of the entire curve, such as the range of motion (ROM), or computing the mean difference between the mean values of the curve under analysis (Pa) in respect of the mean value of the reference curve (Pref). Some indices were proposed to compare the ROM of the two curves in order to quantify the differences in terms of pattern amplitude, such as the ratio index (RIROM = ROMPa/ROMPref) or the symmetry angle. Conversely, the mean difference (MD = $Pa - P$ref) is used to assess a vertical shift (offset) between the curve under analysis and the curve used as reference.

Another commonly adopted approach consists in calculating the differences between the curves in correspondence of specific events. However, for each curve several points can be extracted and their selection could be arbitrary, and it implies a loss of information about the entire pattern and hence it can be critical.

4.5.1 SHAPIRO-WILK TEST

The Shapiro-Wilk test was applied to each column of values through the Matlab function "*swtest*" which requires as input only the column vector itself. This function returns the parameter H equivalent to 0 or 1: 0 when the distribution of the values is normal, 1 when it is not. In the case in which the quantity of 0 is greater than that of 1, a parametric analysis is performed, otherwise a non-parametric one.

Having verified that the distribution of most of the samples was normal, the statistical parametric analysis was chosen. This test was performed to define the type of statistical inference approach (parametric/non parametric), to be used in the Statistical Parametric Mapping (SPM), which was implemented to assess the differences in the waveform corresponding to specific joint angles acquired by the IMU-based or marker-based systems.

4.5.2 T-TEST / WILCOXON RANK SUM TEST

This kind of parametric test was carried out thanks to the Matlab function "*ttest*". It requires in input the two column vectors representing the same values; the first vector contained the values extrapolated with the optoelectronic system, the latter contained the ones extrapolated with the inertial system. It verifies that the input data have a normal distribution with mean equal to zero. The alternative is the rejection of the null hypothesis at the 5% significance level. In output, in addition to this result, the p-value, a value between 0 and 1, is obtained. The lower it is, the more the result is statistically significant and therefore the validity of the null hypothesis is more questioned. The corresponding non-parametric test is the Wilcoxon rank sum test, which was implemented by using the function "*ranksum*" in Matlab. Both these tests were used, according to the normality of the data distribution, in SPM.

4.5.3 PEARSON CORRELATION COEFFICIENT

In addition to the t-test, a test assessing the correlation between the two analysis systems was also addressed.

In statistics, the Pearson correlation index (also called linear correlation coefficient or Pearson correlation coefficient or Bravais-Pearson correlation coefficient) between two variables, is an index that expresses any linear relationship between them.

The employed Matlab function was "*corrcoef*", which received as inputs the two corresponding columns and returned two values, ρ_{xy} and p-value. The former is an index that expresses a possible relationship of linearity between the two variables, the latter indicates that the correlation is strong if it is below the level of significance (default 0.05).

More precisely:

- If $\rho_{xy} > 0$: the variables X and Y are directly correlated, or positively correlated;
- If $\rho_{xy} = 0$: the variables X and Y are directly uncorrelated;
- If $\rho_{xy} < 0$: the variables X and Y are defined inversely correlated, or negatively correlated.
- If $|\rho_{xy}| < 0.3$: there is weak correlation;
- If $0.3 < |\rho_{xy}| < 0.7$: there is moderate correlation;
- If $|\rho_{xy}| > 0.7$: there is strong correlation.

4.5.4 BLAND-ALTMAN ANALYSIS

It is a graphical method which allows to visually evaluate the level of agreement between two variables. In Matlab the "*blandaltman*" function was used which received as inputs the two variables to be compared (derived from the two analysis systems) and drew a graph describing their agreement.

If the differences are randomly distributed around the zero value and none is excessively high, then the measurements are in agreement. The Bland-Altman plot shows, the value of the differences with respect to the average of the semi-sum of the two variables, $\frac{x+y}{2}$.

4.5.5 ROOT MEAN SQUARE DEVIATION AND MEAN ABSOLUTE VARIATION

RMSD represents the root square of the variance, evaluated sample by sample, between the curves and the averaged curve. Similarly, MAV measures the average of the difference between maximum and minimum values among the compared curves sample by sample.

4.5.6 COEFFICIENT OF MULTIPLE CORRELATION

The point is to determine the similarity of the different joint-angles expressed as a function of time during a movement-cycle.

The between-subject variability and the between-gait-cycle variability are the two main confounding factors to be ''excluded''. The study saw the protocols applied synchronously on each subject and differences between protocols were analyzed within each movement-cycle.

Kadaba et al. proposed the coefficient of multiple correlation (CMC) to measure the overall similarity of waveforms taking into account the concurrent effects of differences in offset, correlation, and gain.

For a subject and a joint-angle, the kinematics was measured synchronously through P protocols, on G motion-cycles and Fg was the number of frames measured for the g^{th} cycle. P waveforms were therefore available for each motion-cycle, one per protocol.

The aim was to measure the similarity among the P waveforms acquired by the P protocols within each cycle: (1) biological variability of the subjects' kinematics, (2) variability between normal-weight and obese subjects' kinematics, (3) variability in the propagation of the soft-tissue artefact. Altogether these three types of variability will be called herein ''between cycle variability''. The confounding factor to be excluded was therefore the cycle.

Since F changed from one cycle to the next, the normalization by the degrees-of-freedom was done within the summation over the cycles.

$$\mathrm{CMC} = \sqrt{1 - \frac{\sum_{g=1}^{G}\left[\sum_{p=1}^{P}\sum_{f=1}^{F}\left(Y_{gpf} - \bar{Y}_{gf}\right)^2 / GF_g(P-1)\right]}{\sum_{g=1}^{G}\left[\sum_{p=1}^{P}\sum_{f=1}^{F}\left(Y_{gpf} - \bar{Y}_{g}\right)^2 / G(PF_g - 1)\right]}}$$

where Y_{gpf}, ordinate at frame f of the waveform provided by protocol p at cycle g;

$$\bar{Y}_{gf} = \frac{1}{P}\sum_{p=1}^{P} Y_{gpf}$$

ordinate at frame f of the average waveform among the P waveforms for the cycle g;

$$\bar{Y}_g = \frac{1}{PF}\sum_{p=1}^{P}\sum_{f=1}^{F} Y_{g\,p\,f}$$

grand mean for the cycle g among its P waveforms. When, within each cycle, the variability of the P waveforms around their mean waveform is considerably smaller than the variance about their grand mean, CMC approaches 1. Otherwise, the CMC tends towards zero or even becomes a complex number. This is for example the case when the peak-to-peak amplitude of the P waveforms (ROM) is comparable with respect to the offset among them.

4.5.7 LINEAR FIT METHOD

A simple approach to perform a global comparison between curves through a few parameters with specific physiological meaning consists of linear fitting applied to two datasets plotted one versus the other (linear fit method, LFM).

Pa was the kinematic dataset under investigation to be compared with Pref, the reference dataset. They were time-normalized between two selected events. Since Pa and Pref were normalized in respect of the cycle, they resulted in two arrays of real numbers of the same length. It was hence possible to plot Pa against Pref, to define a set of points in a Cartesian coordinate system ((Xi; Yi) with i = 1 . . . N) where Pref values corresponded to x-values and Pa to y-values. The present method is based on applying a linear fit to the of points. This fitting minimized, in a least squares sense, the sum of the square vertical distances between the points and the fitting line (regression line):

$Ya = a1 \cdot P\text{ref} + a0$,

where Ya represents the linear function which approximated Pa values by means of a linear transformation of values of Pref; $a1$ is the angular coefficient; and $a0$ is the intercept of the fitting line. The goodness of the fit could be assessed by the coefficient of determination R^2 which coincides with, for the properties of linear fit, the square of the Pearson's correlation coefficient R.

The LFM relies on the interpretation of the values of R^2, $a0$, and $a1$ for assessing curve similarity between Pa and Pref.

The formulas for computing the above three parameters are

$$a_1 = \frac{\sum_{i=1}^{N} \left(P_{\text{ref}}(i) - \overline{P_{\text{ref}}}\right) \cdot \left(P_a(i) - \overline{P_a}\right)}{\sum_{i=1}^{N} \left(P_{\text{ref}}(i) - \overline{P_{\text{ref}}}\right)^2},$$

$$a_0 = \overline{P_a} - a_1 \cdot \overline{P_{\text{ref}}},$$

$$R^2 = \frac{\sum_{i=1}^{N} \left(a_0 + a_1 \cdot P_{\text{ref}}(i) - \overline{P_a}\right)}{\sum_{i=1}^{N} \left(P_a(i) - \overline{P_a}\right)^2},$$

with N the length of datasets (corresponding to the 100% of the cycle) and overline used for indicating the mean value of a dataset.

The meaning of LFM parameters is described below.

(i) $a1$ measures the mean variation of Pa for every one-unit change in Pref. It hence represents the amplitude scaling factor, that is, the factor for which Pref should be multiplied to match Ya except for a scalar addition.

(ii) $a0$ predicts this scalar addition (shift), that is, the value of Pa when Pref is equal to 0.

(iii) R^2 measures the strength of the linear relationship between Pa and Pref, that is, the percentage of variance in Pa that can be matched by the variance in Pref.

It should be noted that if Pa = Pref then the values of LFM parameters are $a1$ = 1, $a0$ = 0, R^2 = 1. Furthermore, the LFM has the advantage that, for its intrinsic linearity, the mean $a1$ and $a0$ values obtained from n comparisons of n different Pa - data sets with their mean pattern are equal to the ideal values: $a1$ = 1 and $a0$ = 0. This is the case when n curves of healthy subjects are compared with a reference pattern obtained as their mean. MD, which is generally adopted to assess the presence of a vertical shift, can be potentially affected by changes in amplitude. The problem of vertical shift is particularly important, for example, when tests are repeated and markers need to be replaced (potentially introducing an offset). On the other hand, the use of ROM (and hence RIROM and other related indices) can have some disadvantages: (1) it only compares the differences between the maximum and the minimum of the curves, independently from the data distribution; (2) the mean ROM of n curves can be very different from the ROM of the relevant mean curve, and it can affect the assessment of amplitude similarity. Differently from ROM, $a1$ takes into account the amplitude along the entire cycle. The RMSE has the problem that its values were similar over the different conditions and hence

its physiological meaning is difficult to be argued. More clear is the meaning of Pearson correlation coefficient R. However, the same information of R can be obtained in LFM through the R^2 value, which provides a measure of the shape similarity of two curves with a clear mathematical meaning (the percentage of variance of the dataset under analysis explained by a linear transformation of the reference one) and a clear physiological meaning (the pattern similarity despite possible amplitude differences or presence of a shift). R^2 resulted in an index for summarizing the waveform similarity.

LFM relies on the hypothesis that two motion patterns related to a specific joint are usually characterized by a similar waveform, given the intrinsic biomechanical constraints of the musculoskeletal system. In this respect, it is necessary to define when the hypothesis of linear relationship decays. Despite R^2 being high even for nonlinear transformations, it should be taken into account that for R^2 < 0.50 (i.e., less than 50% of Pa variance matched by Pref variance, corresponding to a R < 0.70) the relationship between Pa and Pref can be only partially described by means of a linear transformation and hence the values of $a1$ and $a0$ should be carefully handled. Second, the results of LFM depend on which dataset, between Pa and Pref, is chosen as reference. Finally, it should be highlighted that when a phase shift between Pa and Pref is present, this results in a reduction of shape similarity. Since curves were time normalized and expressed as a percent of the movement cycle this aspect was not critical.

5. RESULTS AND DISCUSSION

The curves representing the joint angles, which better characterize the analyzed upper limb movements, are here reported. For the frontal lift, the attention was focused on the flexion angle (Figure 32). The abduction angle was mainly considered in the assessment of the lateral lift movements (Figure 33). As far as the gesture of target reaching is concerned, the flexion angles of shoulder and elbow were examined in particular (Figure 34 and Figure 35). In the pictures the measures obtained with both the systems are plotted.

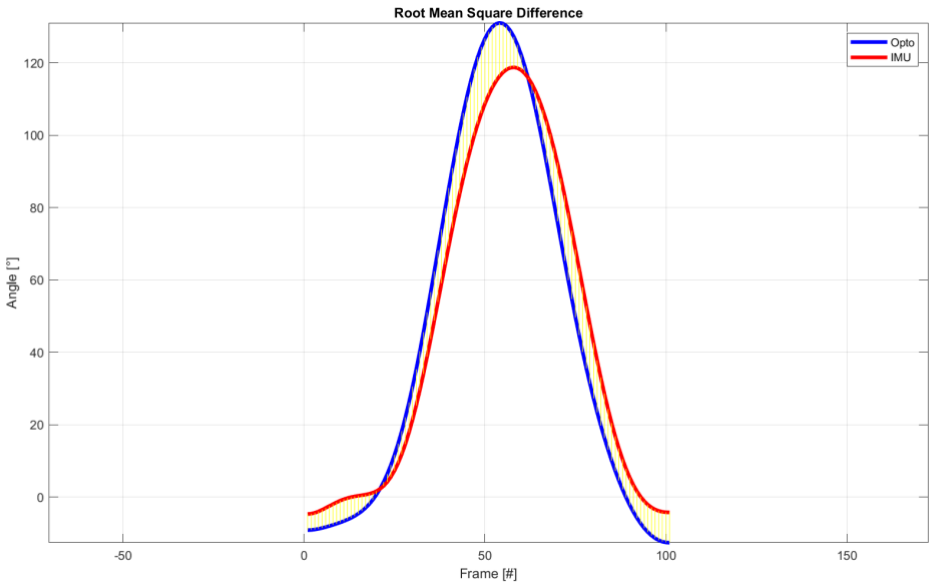

Figure 32: Normal-weight and obese subjects' flexion angles of the shoulder measured during frontal lift movement. The blue curve represents the values obtained with the optoelectronic system, the red curve represents the ones obtained with IMUs, yellow segments are their differences.

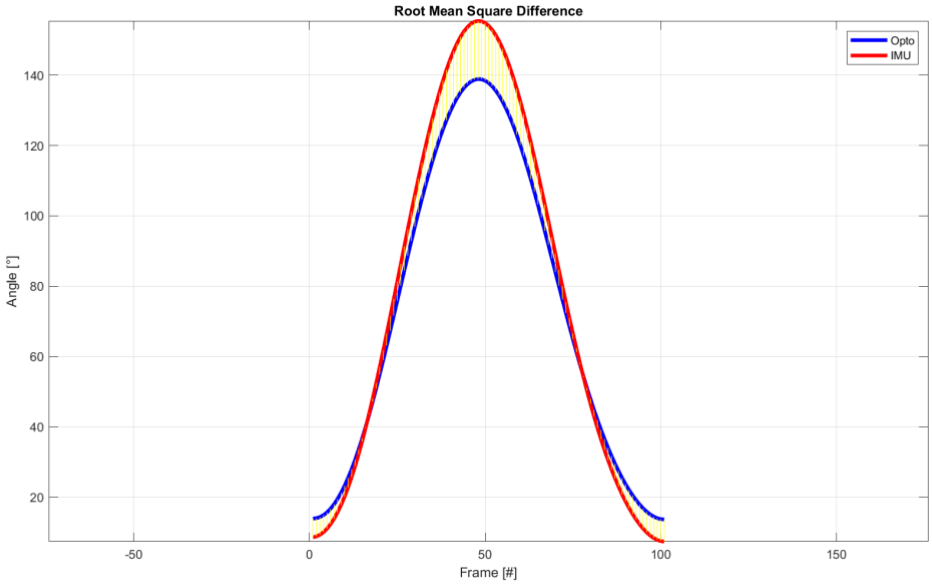

Figure 33: Normal-weight and obese subjects' abduction angles of the shoulder measured during lateral lift movement. The blue curve represents the values obtained with the optoelectronic system, the red curve represents the ones obtained with IMUs, yellow segments are their differences.

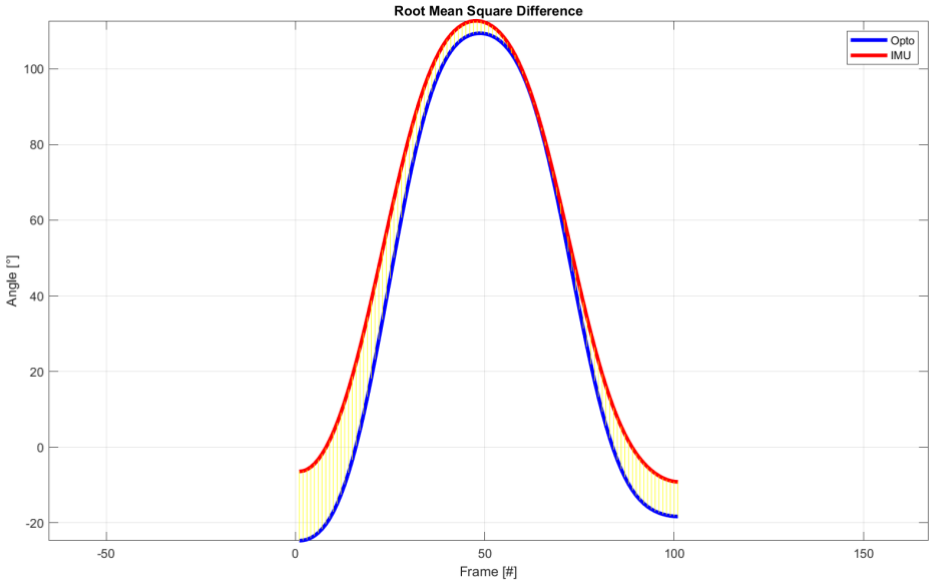

Figure 34: Normal-weight and obese subjects' flexion angles of the shoulder measured during reaching movement. The blue curve represents the values obtained with the optoelectronic system, the red curve represents the ones obtained with IMUs, yellow segments are their differences.

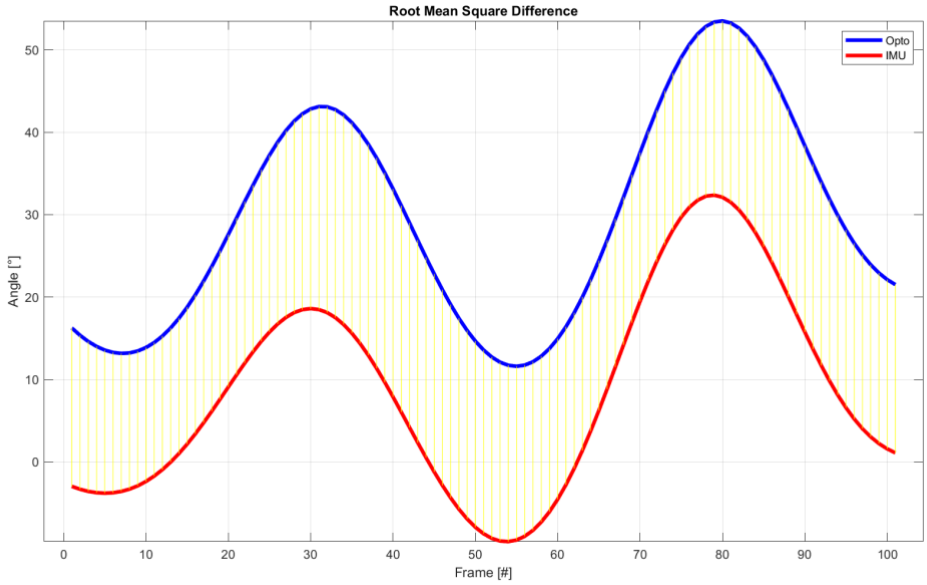

Figure 35: Normal-weight and obese subjects' flexion angles of the elbow measured during reaching movement. The blue curve represents the values obtained with the optoelectronic system, the red curve represents the ones obtained with IMUs, yellow segments are their differences.

At first, a statistical analysis was performed considering the most relevant points of the curves. Figures 36, 37 and 38 report the ROMs of the curves of the 3D joint angles acquired during normal-weight subjects' examinations.

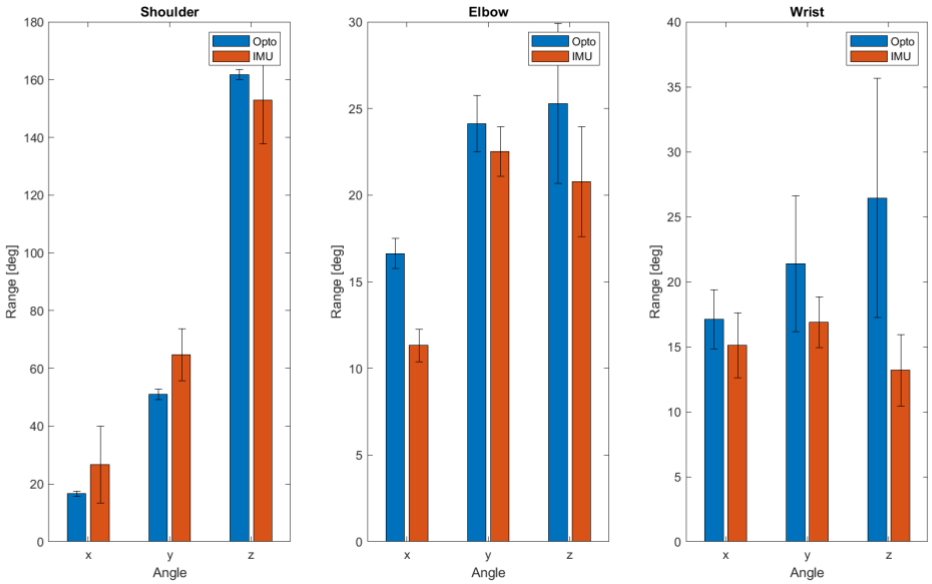

Figure 36: ROMs considering normal-weight subjects' 3D joint angles of shoulder, elbow and wrist measured during frontal lift movement. The blue columns represent the values obtained with the optoelectronic system, the red columns represent the ones obtained with IMUs.

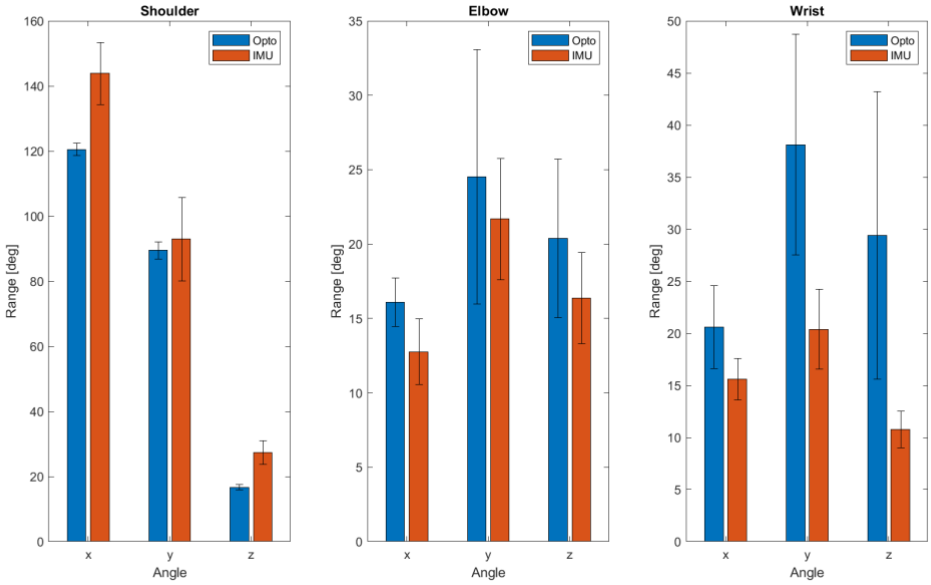

Figure 37: ROMs considering normal-weight subjects' 3D joint angles of shoulder, elbow and wrist measured during lateral lift movement. The blue columns represent the values obtained with the optoelectronic system, the red columns represent the ones obtained with IMUs.

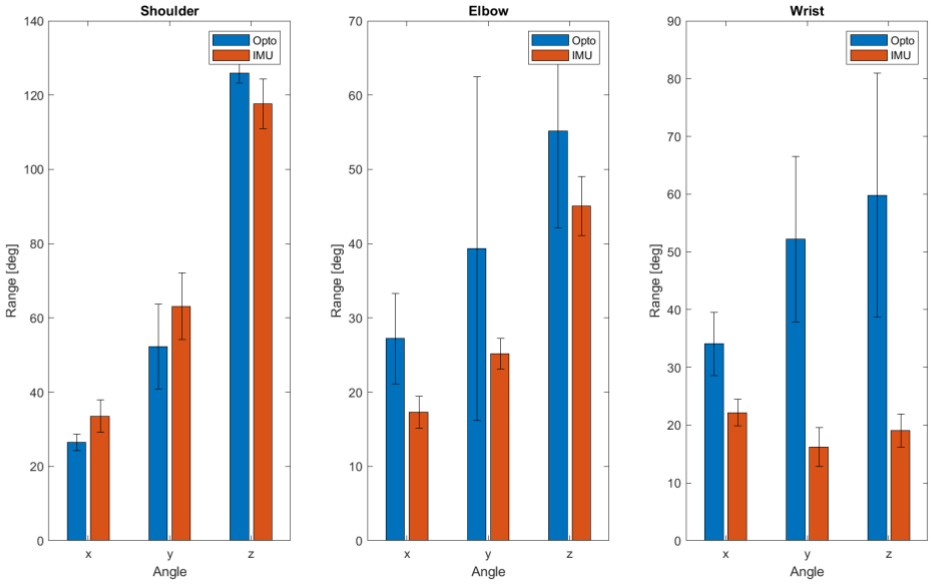

Figure 38: ROMs considering normal-weight subjects' 3D joint angles of shoulder, elbow and wrist measured during reaching movement. The blue columns represent the values obtained with the optoelectronic system, the red columns represent the ones obtained with IMUs.

The previous graphs represent the ROMs of normal-weight subjects' movements. Concerning the abduction angle of the shoulder, a remarkable difference around 20° between the ROMs was measured with the two systems during lateral lift movement. Also the ROMs of the wrist joint angles reached differences of 30°.

Their RMSE is of the order of units for the measures acquired through the optoelectronic system and of tens for the ones gathered with the IMU-based system. Conversely, regarding the other joints the RMSE is higher for the values acquired through the optoelectronic system.

Figures 39, 40 and 41 report the ROMs of the curves of the 3D joint angles acquired during obese subjects' examinations.

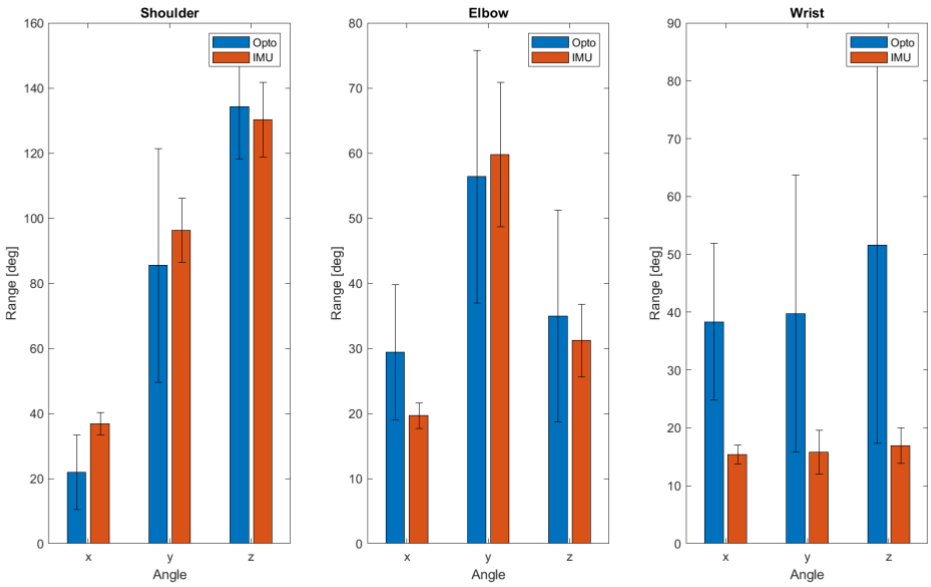

Figure 39: ROMs considering obese subjects' 3D joint angles of shoulder, elbow and wrist measured during frontal lift movement. The blue columns represent the values obtained with the optoelectronic system, the red columns represent the ones obtained with IMUs.

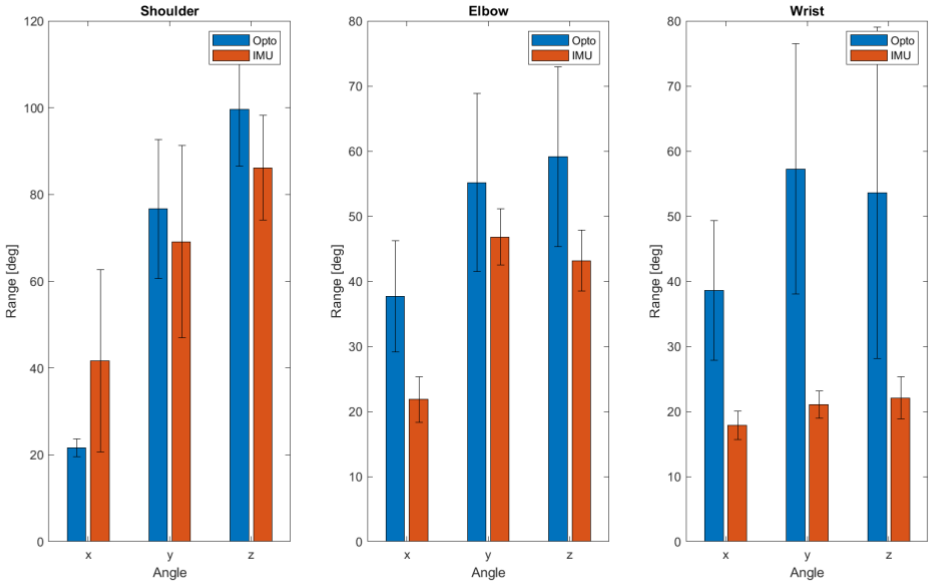

Figure 40: ROMs considering obese subjects' 3D joint angles of shoulder, elbow and wrist measured during lateral lift movement. The blue columns represent the values obtained with the optoelectronic system, the red columns represent the ones obtained with IMUs.

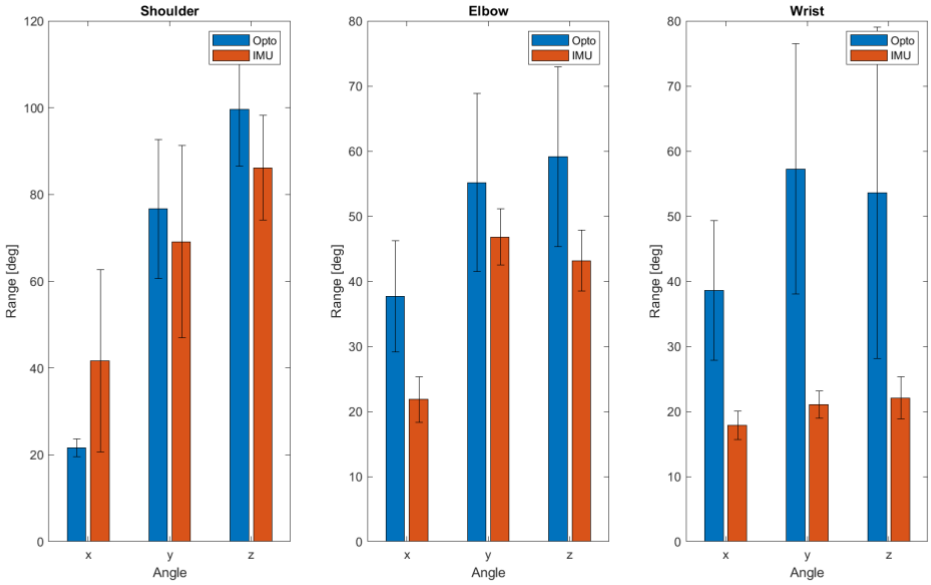

Figure 41: ROMs considering obese subjects' 3D joint angles of shoulder, elbow and wrist measured during reaching movement. The blue columns represent the values obtained with the optoelectronic system, the red columns represent the ones obtained with IMUs.

The previous graphs represent the ROMs of obese subjects' movements. The differences between the ROMs measured with the two systems are between 10° and 40°. The RMSE increases and reaches almost 20° with both the measurement systems, which could be due to soft tissue artefacts and to the two different protocols.

Bland-Altman plots were drawn taking into account the ROMs of the principal angles. The following images (Figure 42 – 45) represent the analysis concerning normal-weight subjects.

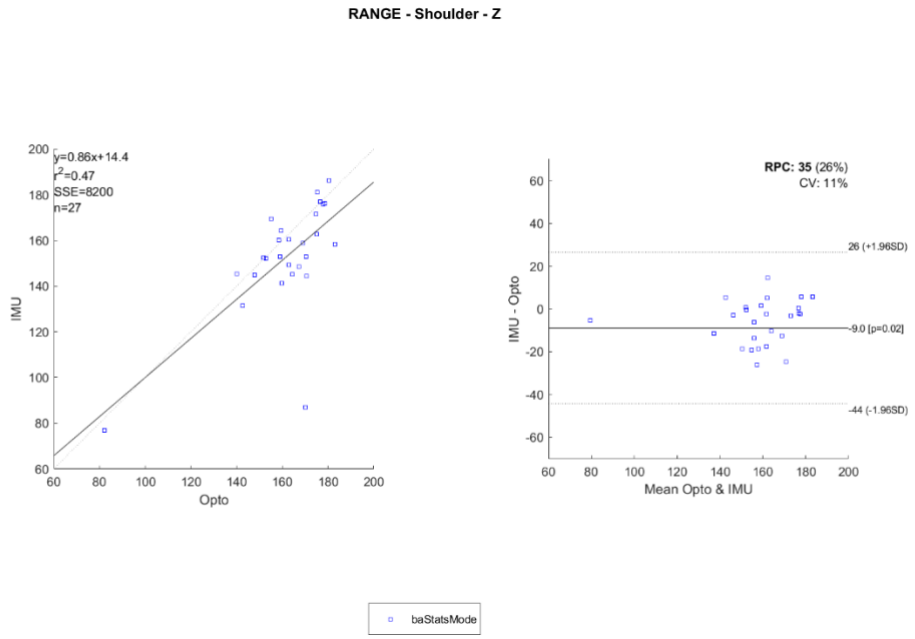

Figure 42: Bland-Altman plots of the ROMs considering normal-weight subjects' flexion angles of the shoulder during frontal lift movement.

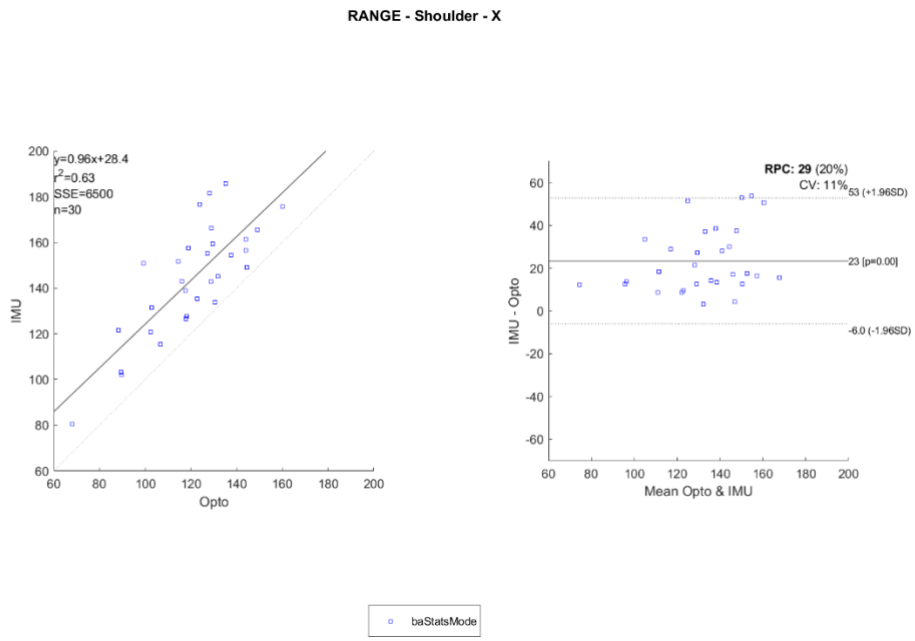

Figure 43: Bland-Altman plots of the ROMs considering normal-weight subjects' abduction angles of the shoulder during lateral lift movement.

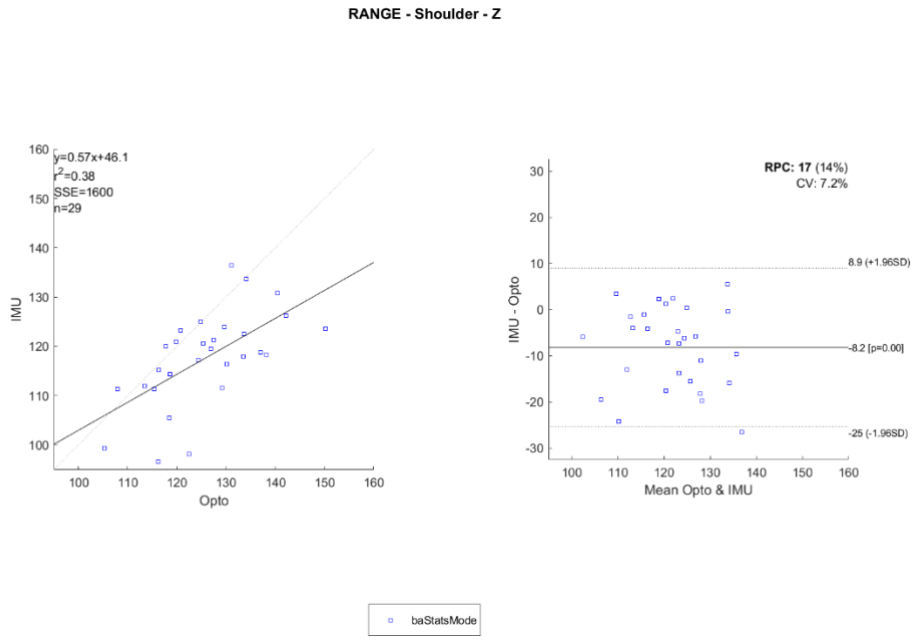

Figure 44: Bland-Altman plots of the ROMs considering normal-weight subjects' flexion angles of the shoulder during reaching movement.

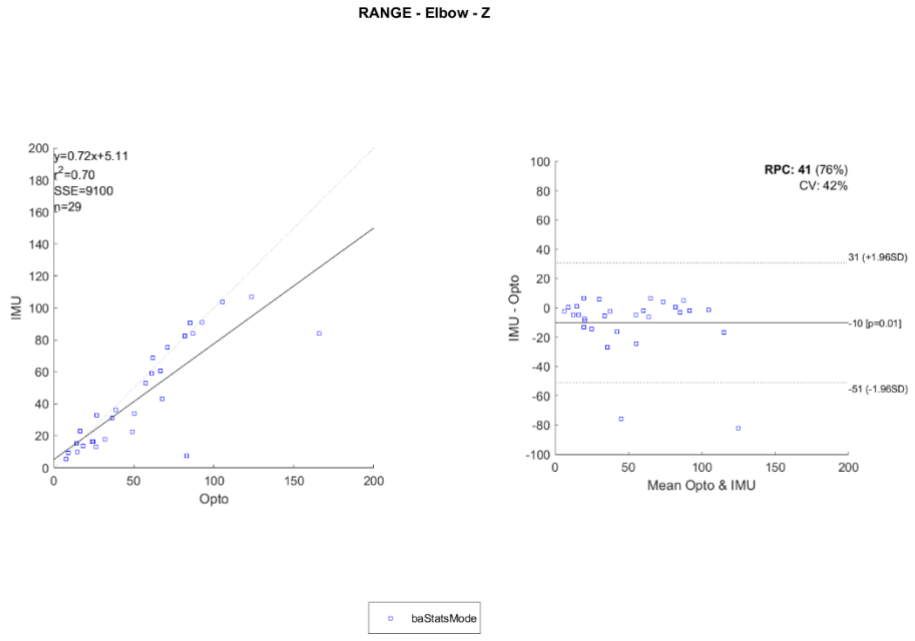

Figure 45: Bland-Altman plots of the ROMs considering normal-weight subjects' flexion angles of the elbow during reaching movement.

Bland-Altman plots of normal weight subjects' ROMs evidence that the obtained values generally fall within the acceptability range. The biases of the shoulder joint (almost 100°)

result relevant, the situation improves for the other joints. On the other hand, the relative standard deviations associated to the shoulder are good (around 10%), but the elbows present a worse situation (42%). Discrepancies connected to the adopted protocols or measurement errors have a greater impact on movements with a small amplitude. R^2 > 0,5, so the correlation turns out to be medium-high. The sums of squares errors (SSEs) are of the order of 10^4.

Figures 46 – 49 show the Bland-Altman plots drawn by taking into account the ROMs of obese subjects' movements.

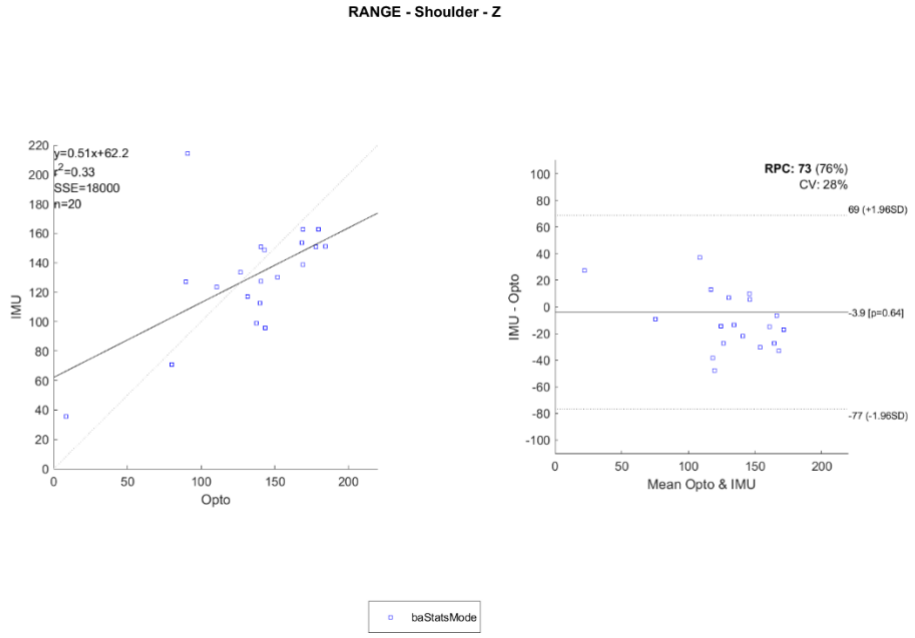

Figure 46: Bland-Altman plots of the ROMs considering obese subjects' flexion angles of the shoulder during frontal lift movement.

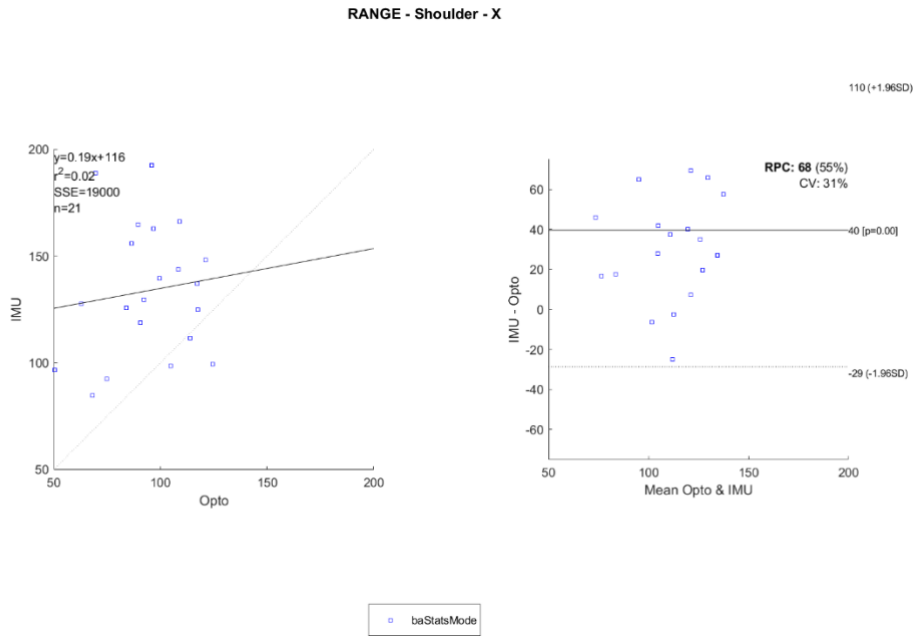

Figure 47: Bland-Altman plots of the ROMs considering obese subjects' abduction angles of the shoulder during lateral lift movement.

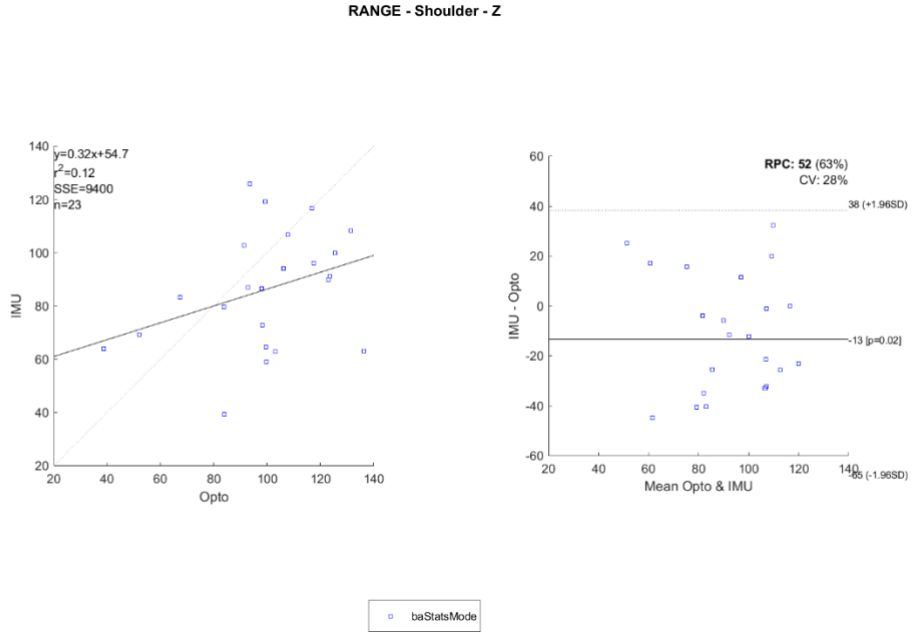

Figure 48: Bland-Altman plots of the ROMs considering obese subjects' flexion angles of the shoulder during reaching movement.

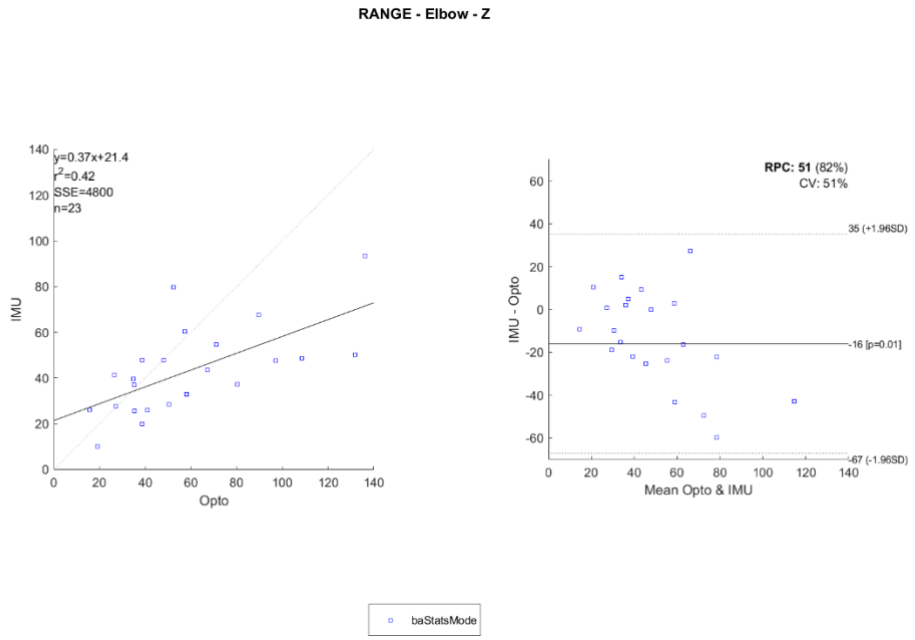

Figure 49: Bland-Altman plots of the ROMs considering obese subjects' flexion angles of the elbow during reaching movement.

Bland-Altman plots for obese subjects' ROMs evidence that obtained values generally fall within the acceptability range. Similarly to what happened with normal-weight subjects, the biases of the shoulder joint (almost 100°) result relevant, the situation improves for the other joints. The relative standard deviations (around 30%) are higher than the ones obtained with the normal-weight group. In this case $R^2 < 0,5$, so the correlation turns out to be poor. The SSEs are of the order of 10^5.

Repeatability indexes were calculated in order to provide a global view of the similarity of the curves representing the measures performed by means of the two systems. Figures 50, 51 and 52 represent the CMCs, RMSs and MAVs calculated in order to perform the validation in the normal-weight group.

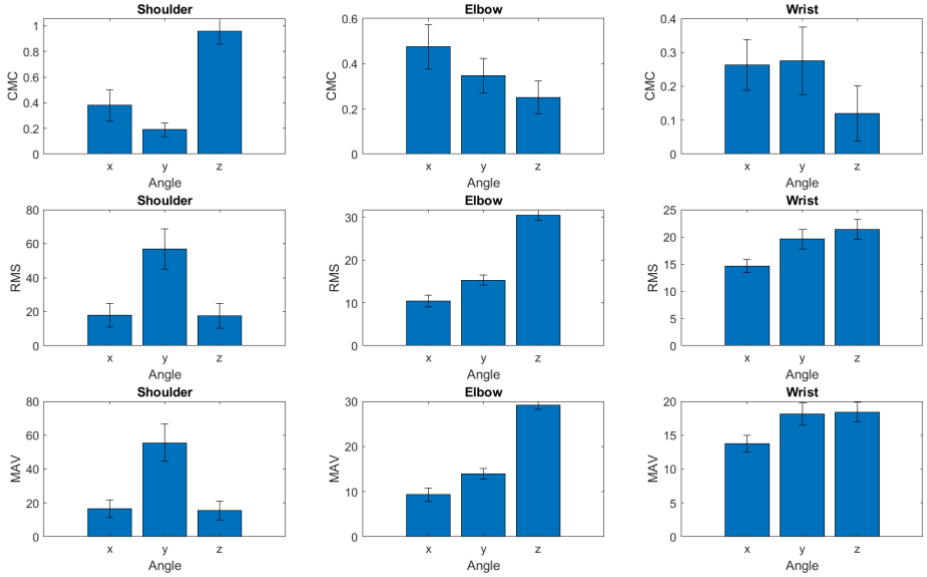

Figure 50: Repeatability indexes concerning the measurements obtained through the two systems of normal-weight subjects' 3D joint angles of shoulder, elbow and wrist measured during frontal lift movement.

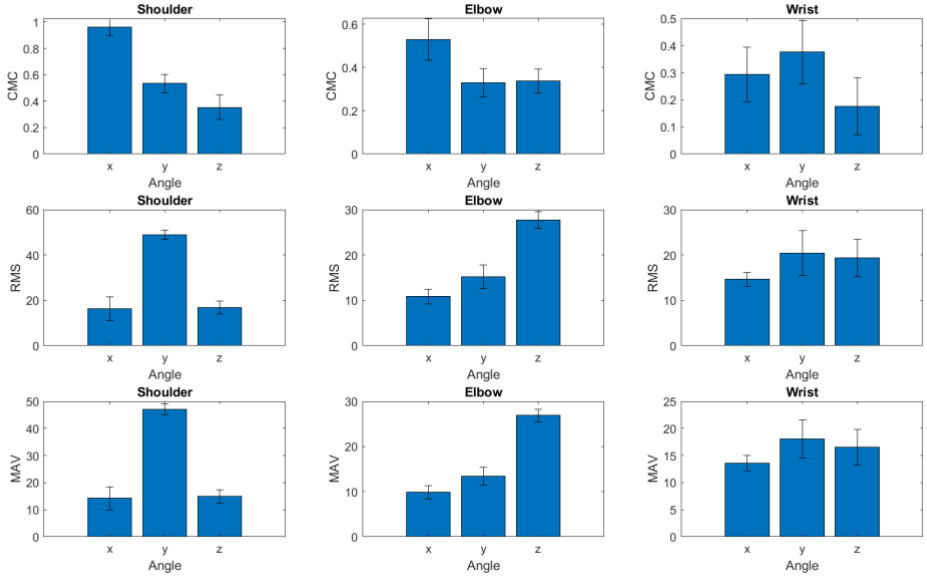

Figure 51: Repeatability indexes concerning the measurements obtained through the two systems of normal-weight subjects' 3D joint angles of shoulder, elbow and wrist measured during lateral lift movement.

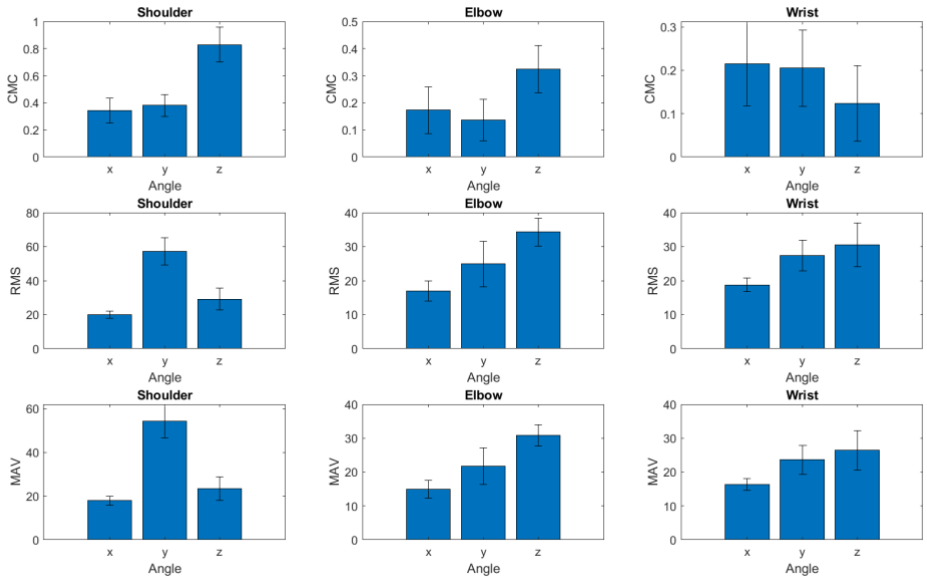

Figure 52: Repeatability indexes concerning the measurements obtained through the two systems of normal-weight subjects' 3D joint angles of shoulder, elbow and wrist measured during reaching movement.

CMC > 0,8 for the predominant angle of each movement as far as the shoulder joint is concerned. The correlation is good. The situation gets worse for the other angles. The RMS and MAV are between 20° and 60°.

Figures 53, 54 and 55 represent the repeatability indexes calculated in order to perform the validation in the obese group.

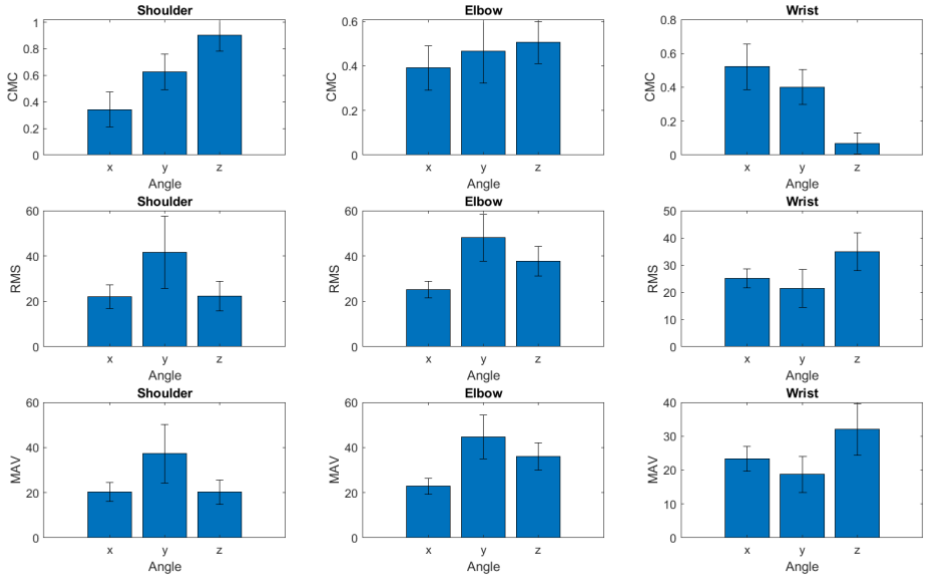

Figure 53: Repeatability indexes concerning the measurements obtained through the two systems of obese subjects' 3D joint angles of shoulder, elbow and wrist measured during frontal lift movement.

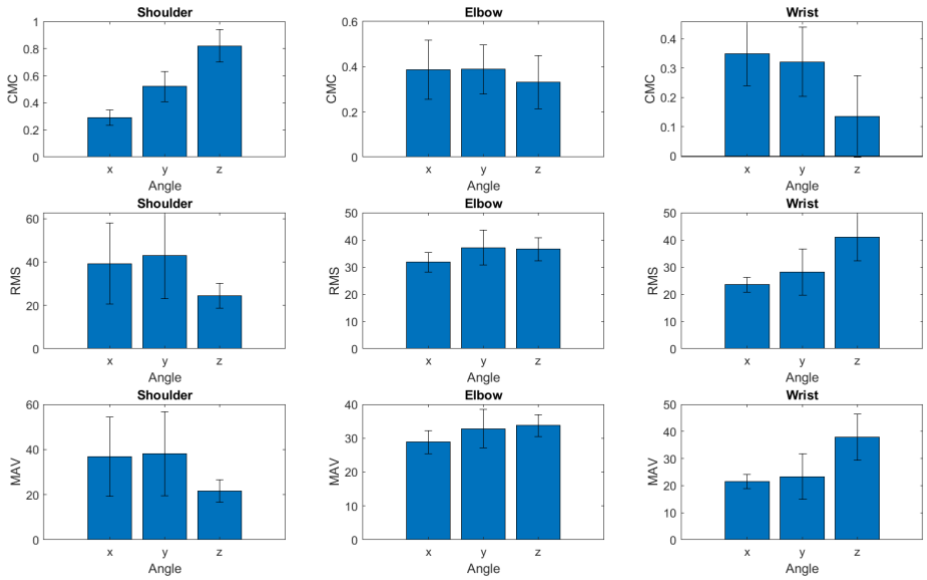

Figure 54: Repeatability indexes concerning the measurements obtained through the two systems of obese subjects' 3D joint angles of shoulder, elbow and wrist measured during lateral lift movement.

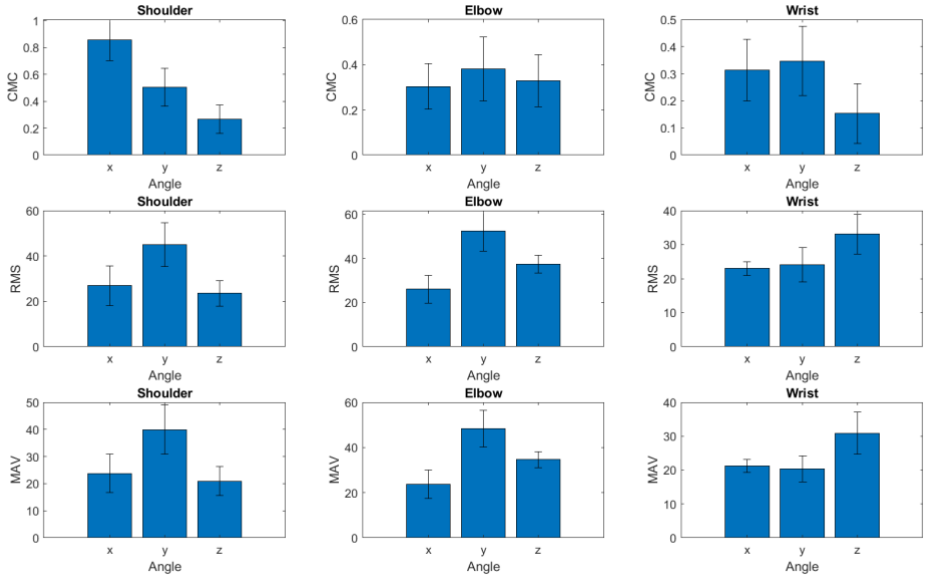

Figure 55: Repeatability indexes concerning the measurements obtained through the two systems of obese subjects' 3D joint angles of shoulder, elbow and wrist measured during reaching movement.

Similarly to what happened with normal-weight subjects, CMC > 0,8 for the predominant angle of each movement as far as the shoulder joint is concerned. The correlation is good. The situation gets worse for the other angles. The RMS and MAV are between 20° and 50°. The differences in RMS and MAV, which result slightly smaller for obese subjects, are probably due to different motion strategies.

The coefficients obtained through the linear regression method, when the tasks performed by normal-weight people were analyzed, are reported in Figures 56, 57, 58.

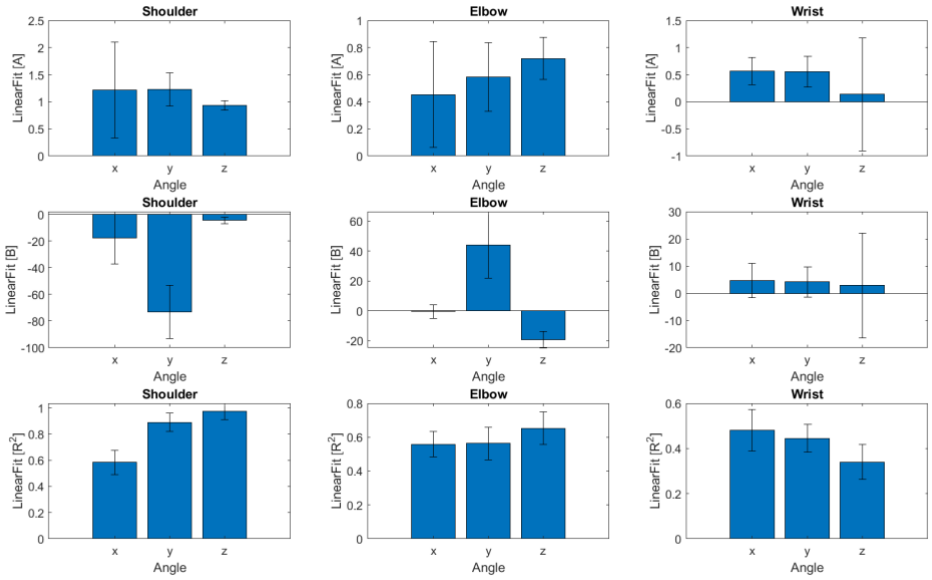

Figure 56: Linear fit parameters concerning the measurements obtained through the two systems of normal-weight subjects' 3D joint angles of shoulder, elbow and wrist measured during frontal lift movement.

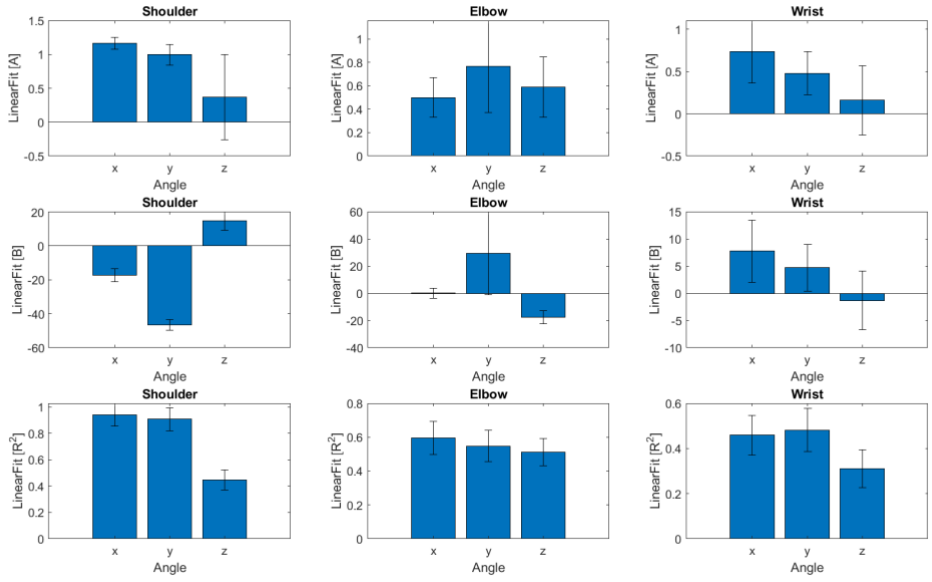

Figure 57: Linear fit parameters concerning the measurements obtained through the two systems of normal-weight subjects' 3D joint angles of shoulder, elbow and wrist measured during lateral lift movement.

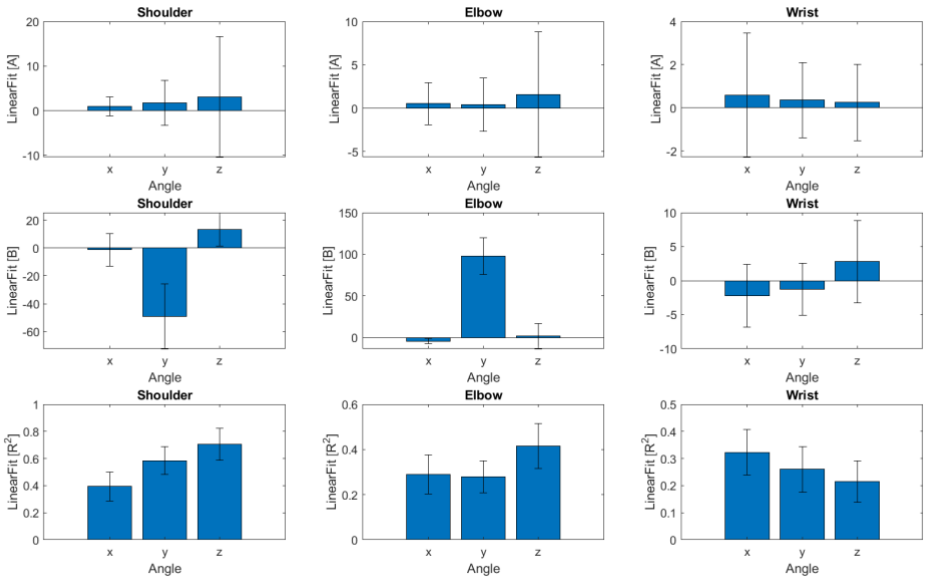

Figure 58: Linear fit parameters concerning the measurements obtained through the two systems of normal-weight subjects' 3D joint angles of shoulder, elbow and wrist measured during reaching movement.

The coefficients obtained through the linear regression method, when the tasks performed by obese people were analyzed, are reported in Figures 59, 60 and 61.

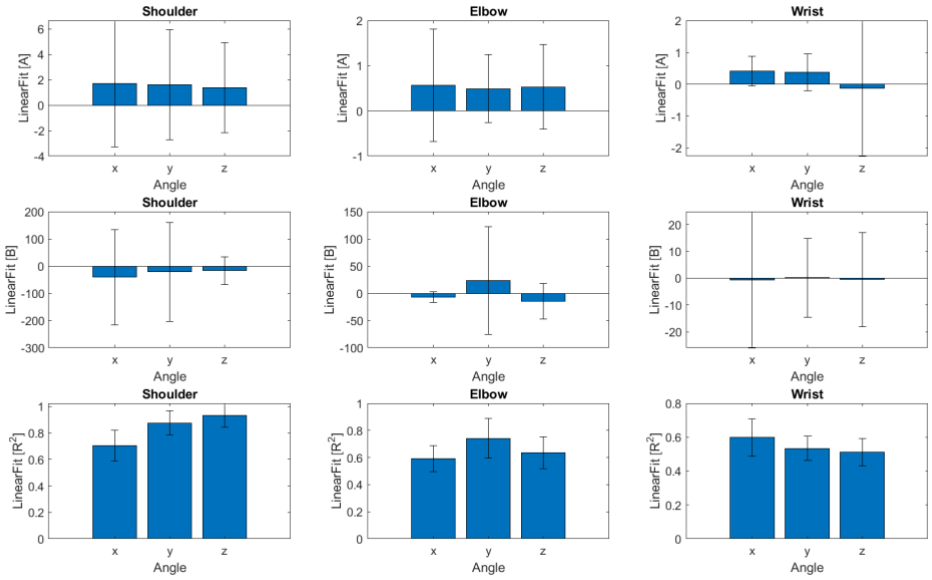

Figure 59: Linear fit parameters concerning the measurements obtained through the two systems of obese subjects' 3D joint angles of shoulder, elbow and wrist measured during frontal lift movement.

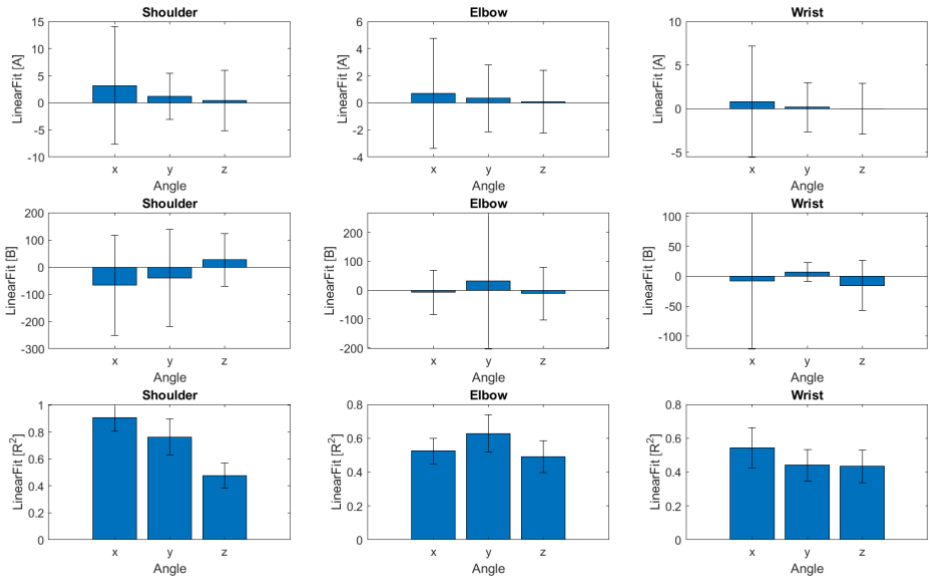

Figure 60: Linear fit parameters concerning the measurements obtained through the two systems of obese subjects' 3D joint angles of shoulder, elbow and wrist measured during lateral lift movement.

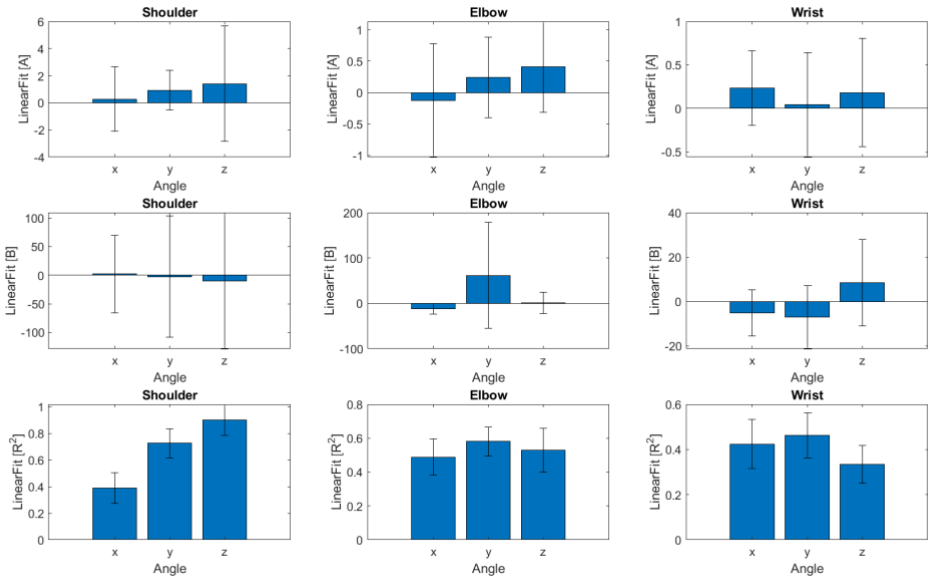

Figure 61: Linear fit parameters concerning the measurements obtained through the two systems of obese subjects' 3D joint angles of shoulder, elbow and wrist measured during reaching movement.

The angular coefficients found for normal-weight subjects are near 1, which indicates a good rate between the corresponding values obtained through the different measurement systems. These results are worse for obese subjects since they increased. In both groups the scalar addends are relevant, which means that the orientations between the reference systems constructed in the two models are not completely coherent. The R^2 values approach 1 for the most significant angles of each gesture, the Pearson coefficients indicate a strong correlation.

The mean and the standard deviation of the joint angle curves were computed point by point. On the left, the normality curves of the measures obtained by means of the two systems are drawn on the same graph. The plot reported on the right represents the correlation between these values. Figures 62 - 67 describe normal-weight subjects' movements.

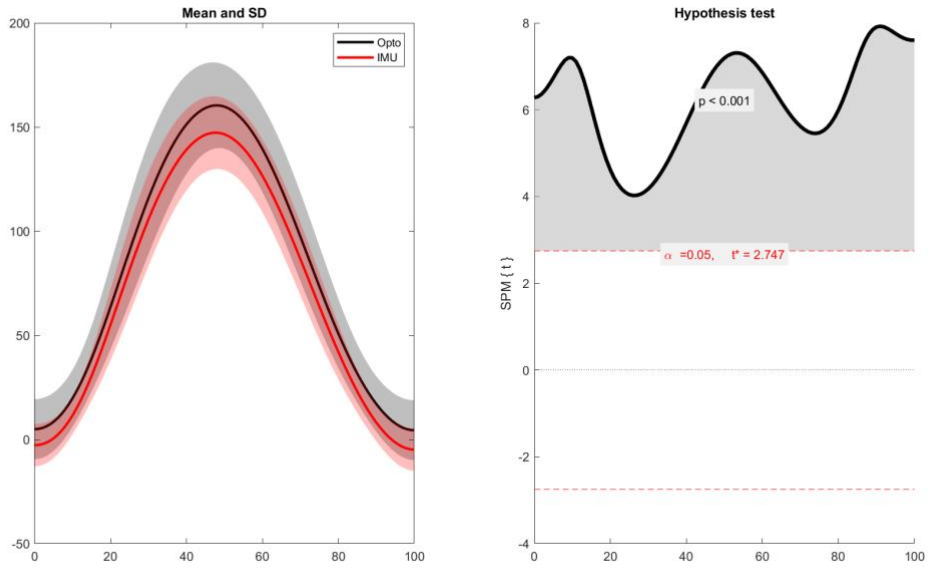

Figure 62: Normal-weight subjects' normality curves representing flexion angles of the shoulder measured during frontal lift of the right arm. The grey curve represents the values obtained with the optoelectronic system, the red curve represents the ones obtained with IMUs. On the right the correlation indexes.

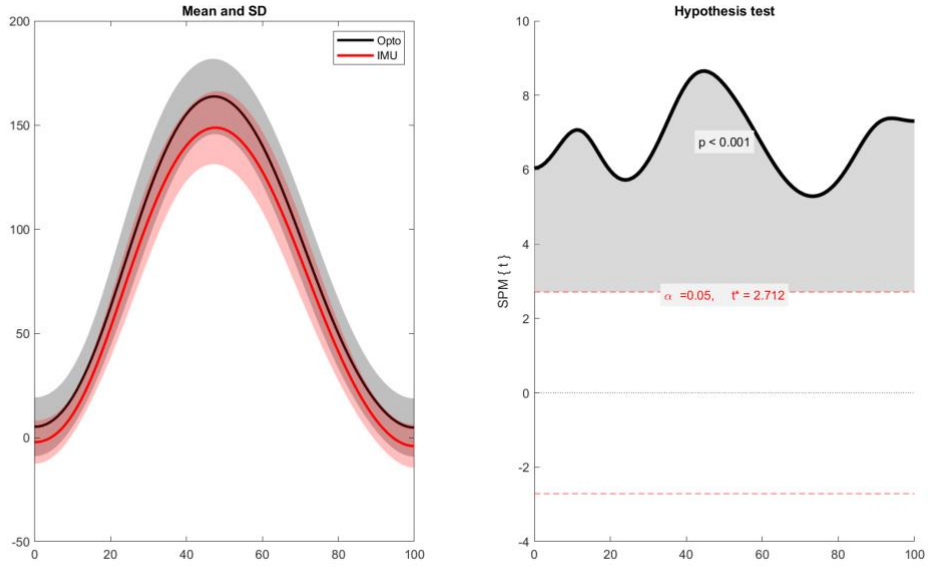

Figure 63: Normal-weight subjects' normality curves representing flexion angles of the shoulder measured during frontal lift of the left arm. The grey curve represents the values obtained with the optoelectronic system, the red curve represents the ones obtained with IMUs. On the right the correlation indexes.

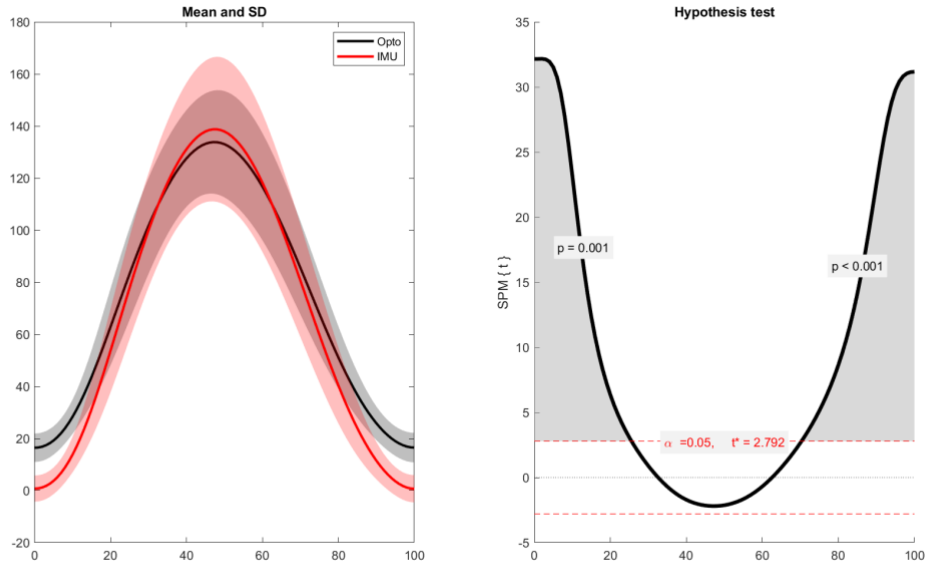

Figure 64: Normal-weight subjects' normality curves representing abduction angles of the shoulder measured during lateral lift of the right arm. The grey curve represents the values obtained with the optoelectronic system, the red curve represents the ones obtained with IMUs. On the right the correlation indexes.

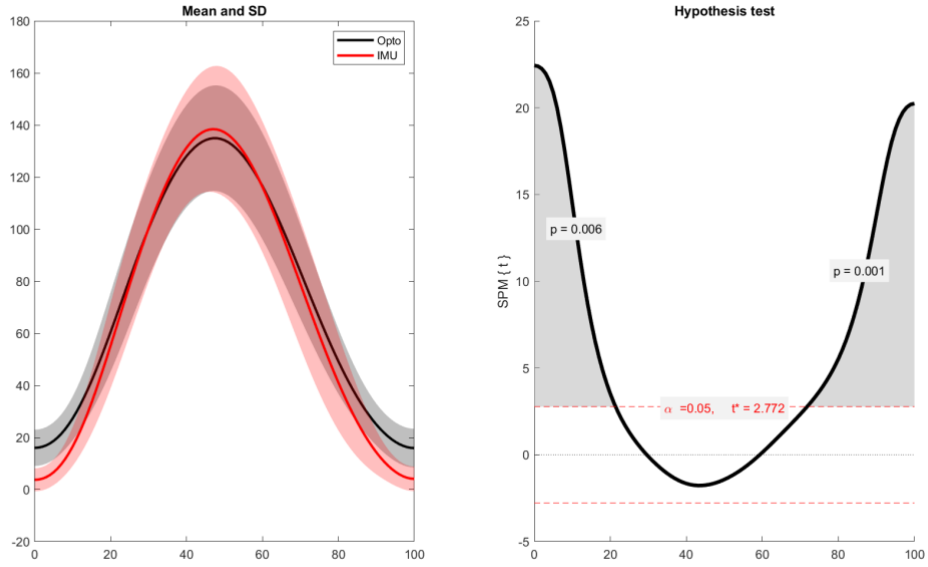

Figure 65: Normal-weight subjects' normality curves representing abduction angles of the shoulder measured during lateral lift of the left arm. The grey curve represents the values obtained with the optoelectronic system, the red curve represents the ones obtained with IMUs. On the right the correlation indexes.

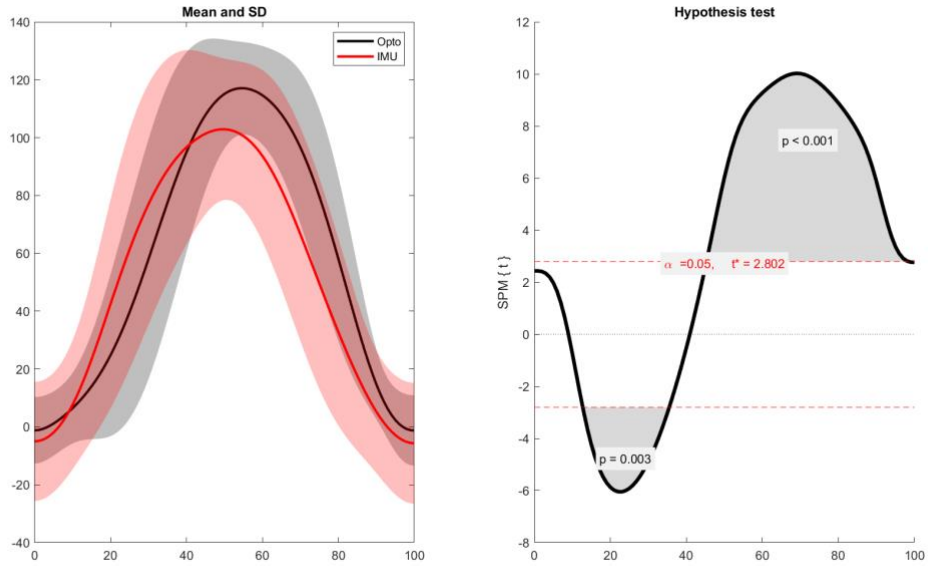

Figure 66: Normal-weight subjects' normality curves representing flexion angles of the shoulder measured during reaching movement. The grey curve represents the values obtained with the optoelectronic system, the red curve represents the ones obtained with IMUs. On the right the correlation indexes.

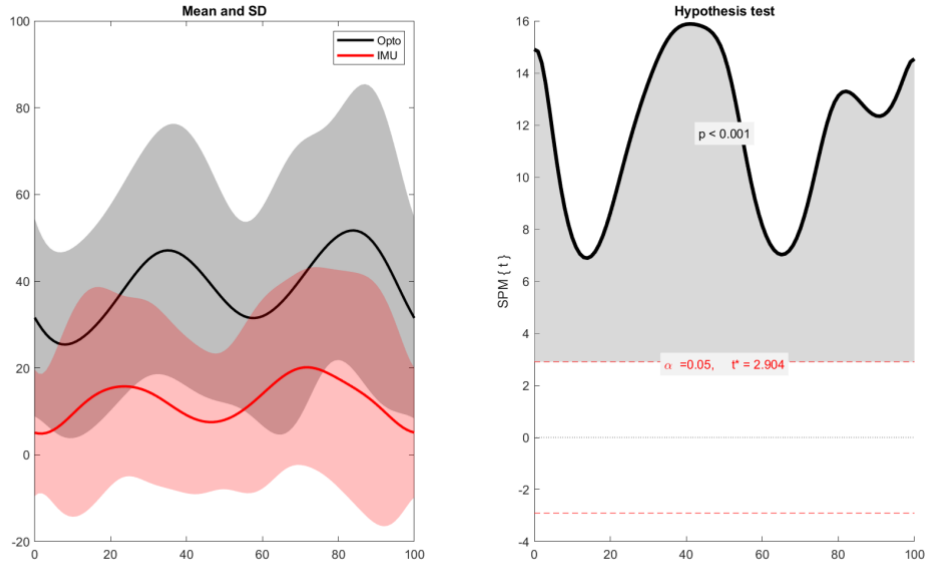

Figure 67: Normal-weight subjects' normality curves representing flexion angles of the elbow measured during reaching movement. The grey curve represents the values obtained with the optoelectronic system, the red curve represents the ones obtained with IMUs. On the right the correlation indexes.

In an analog way, Figures 68 - 73 describe obese subjects' movements.

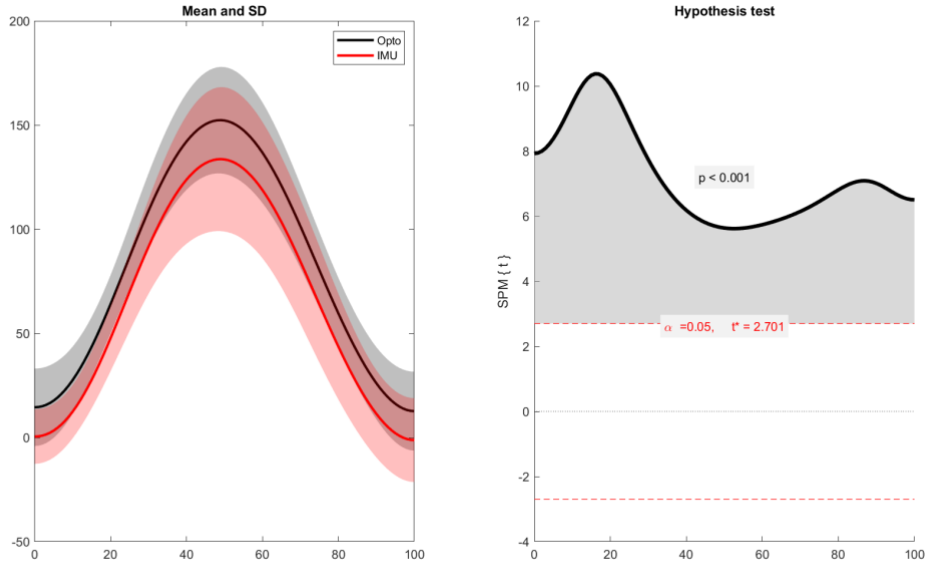

Figure 68: Obese subjects' normality curves representing flexion angles of the shoulder measured during frontal lift of the right arm. The grey curve represents the values obtained with the optoelectronic system, the red curve represents the ones obtained with IMUs. On the right the correlation indexes.

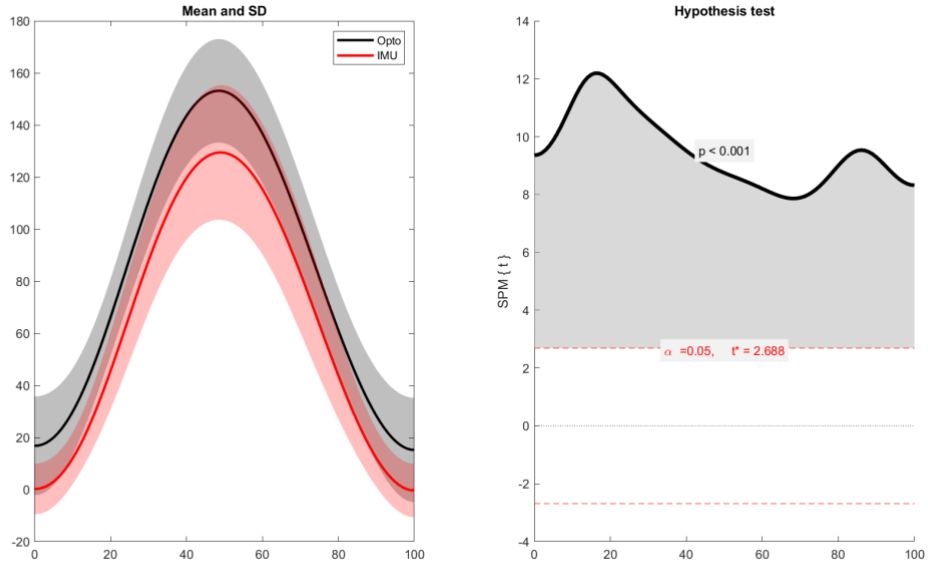

Figure 69: Obese subjects' normality curves representing flexion angles of the shoulder measured during frontal lift of the left arm. The grey curve represents the values obtained with the optoelectronic system, the red curve represents the ones obtained with IMUs. On the right the correlation indexes.

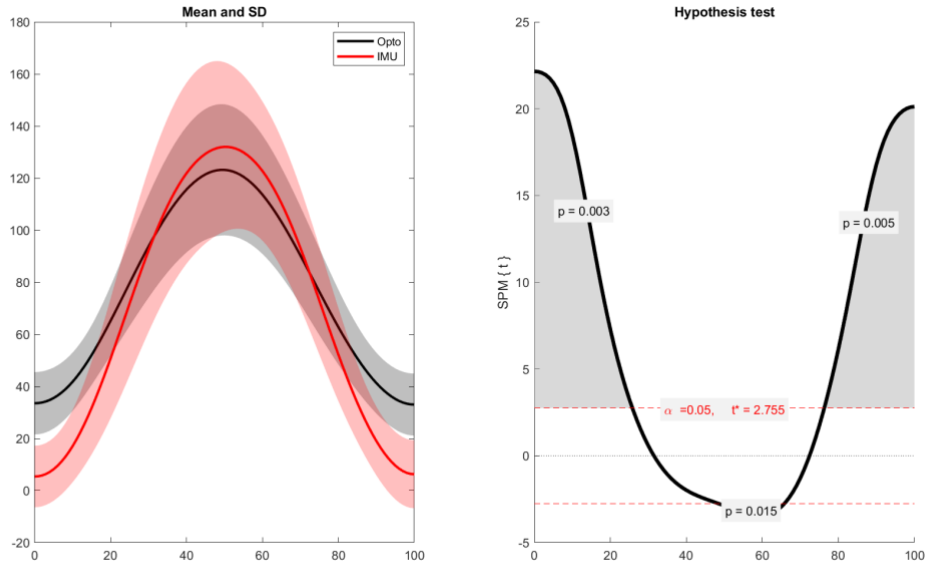

Figure 70: Obese subjects' normality curves representing abduction angles of the shoulder measured during lateral lift of the right arm. The grey curve represents the values obtained with the optoelectronic system, the red curve represents the ones obtained with IMUs. On the right the correlation indexes.

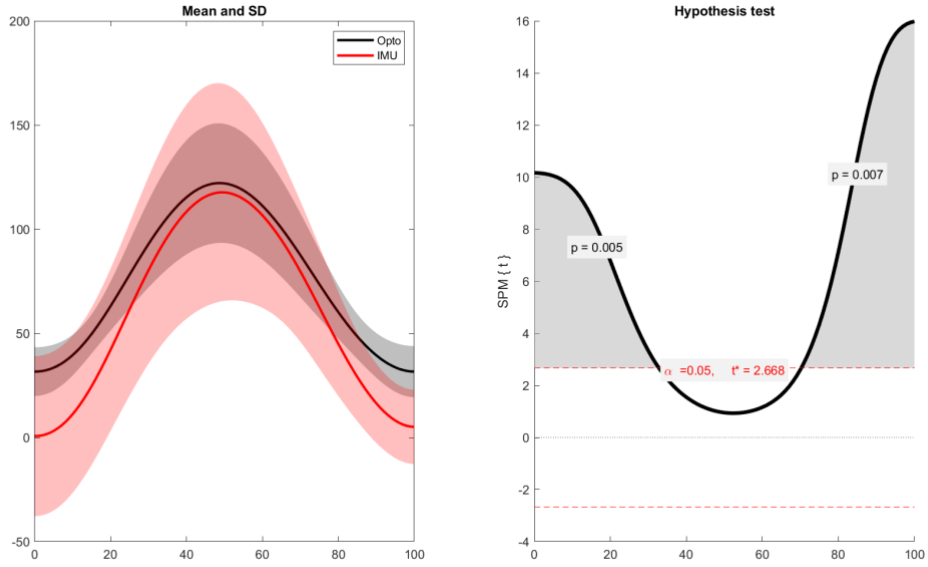

Figure 71: Obese subjects' normality curves representing abduction angles of the shoulder measured during lateral lift of the left arm. The grey curve represents the values obtained with the optoelectronic system, the red curve represents the ones obtained with IMUs. On the right the correlation indexes.

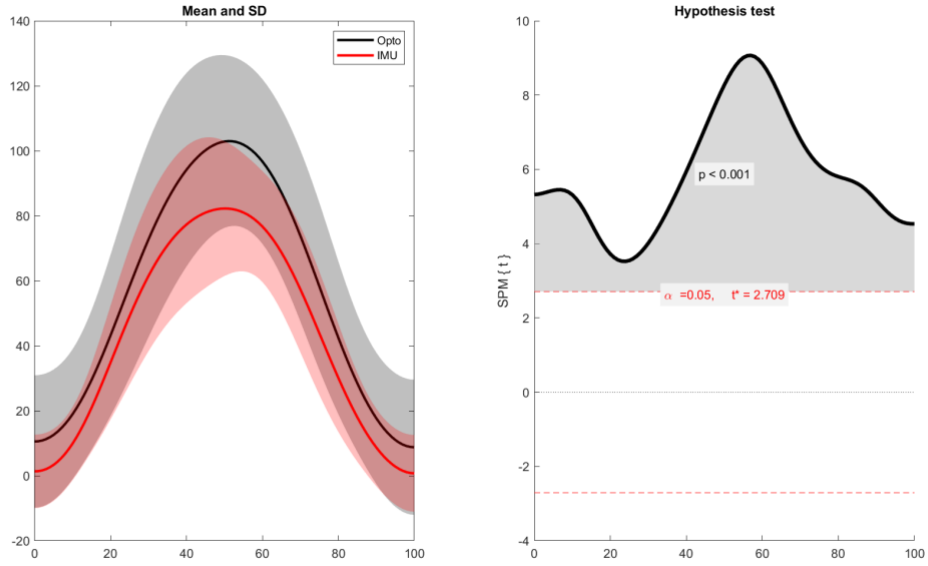

Figure 72: Obese subjects' normality curves representing flexion angles of the shoulder measured during reaching movement. The grey curve represents the values obtained with the optoelectronic system, the red curve represents the ones obtained with IMUs. On the right the correlation indexes.

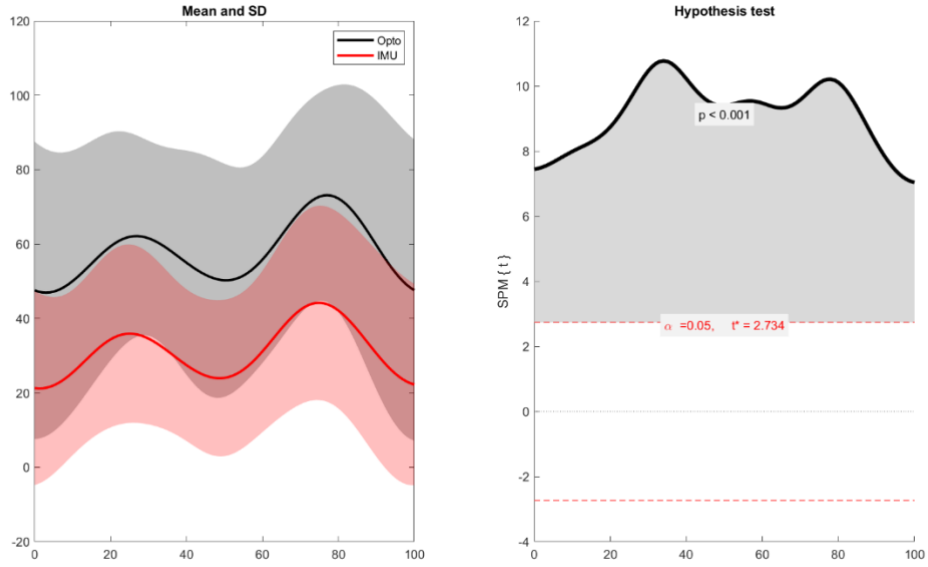

Figure 73: Obese subjects' normality curves representing flexion angles of the elbow measured during reaching movement. The grey curve represents the values obtained with the optoelectronic system, the red curve represents the ones obtained with IMUs. On the right the correlation indexes.

Both for normal weight and obese subjects, SPM vector field analyses generally found significance ($p < 0{,}001$). In both groups, the better results in terms of correlation were obtained in the plane in which the movement mainly took place. It was also noticed that the angles measured by means of the two technologies are closer to each other while lifting and lowering. At the beginning the biases are clearly visible. As shown above, wider ROMs were relieved through the optoelectronic systems around the z axis during the frontal lift and through the inertial system around the x axis during the lateral lift.

Figures 74 - 79 show the joint angle curves acquired by means of the IMU-based system. On the left, the normality curves of the measures obtained on normal-weight and obese subjects are drawn on the same graph. The plot reported on the right represents the correlation between these values.

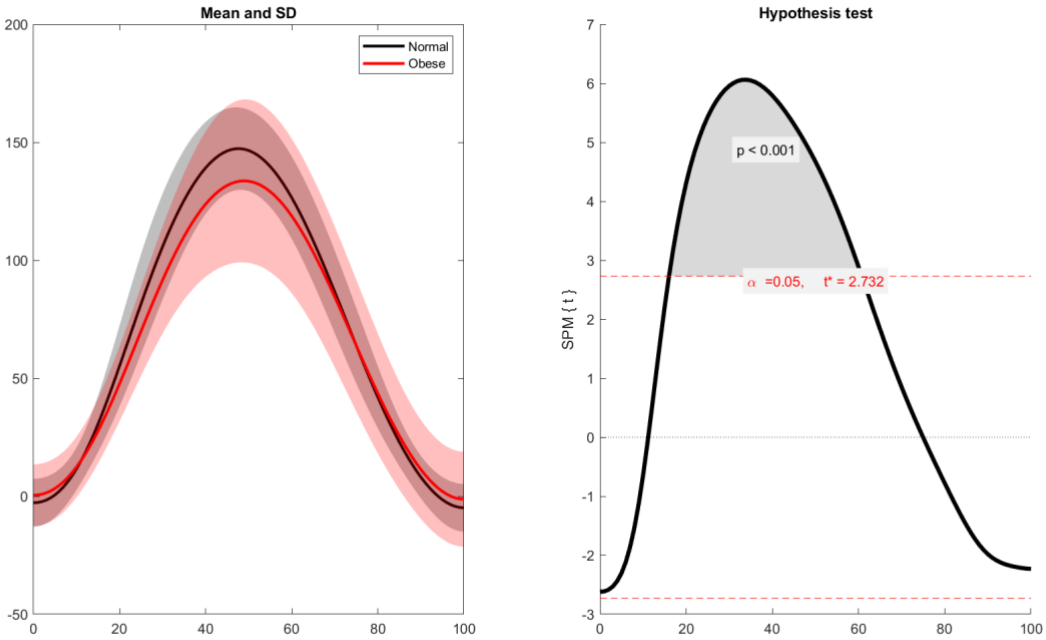

Figure 74: Normality curves representing flexion angles of the shoulder measured with IMUs during frontal lift of the right arm. The grey curve represents the measures of normal-weight subjects' gestures, the red curve represents the ones of obese subjects' gestures. On the right the correlation indexes.

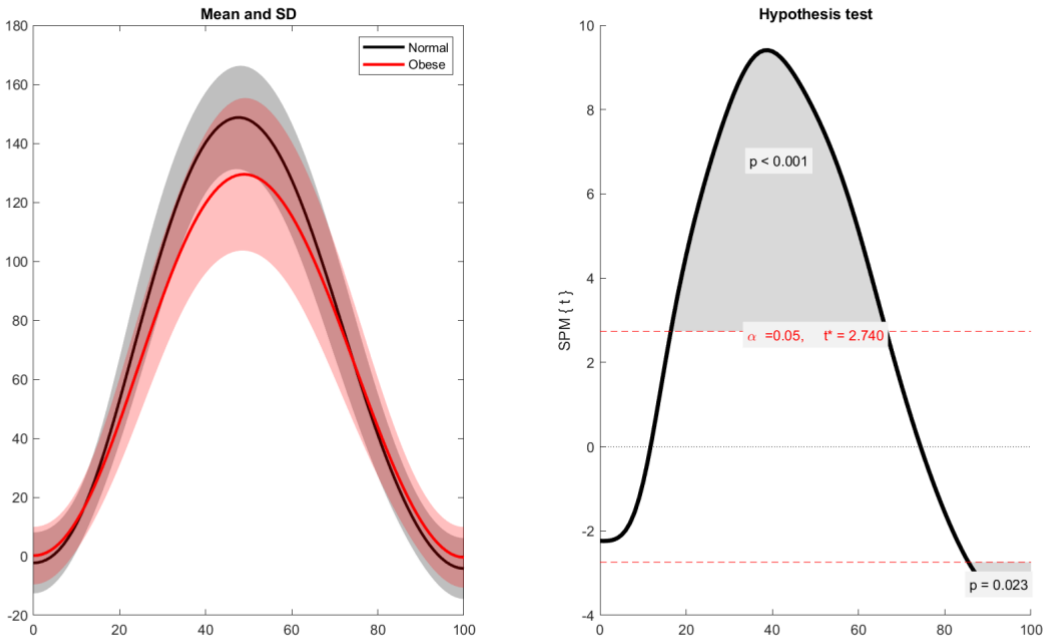

Figure 75: Normality curves representing flexion angles of the shoulder measured with IMUs during frontal lift of the left arm. The grey curve represents the measures of normal-weight subjects' gestures, the red curve represents the ones of obese subjects' gestures. On the right the correlation indexes.

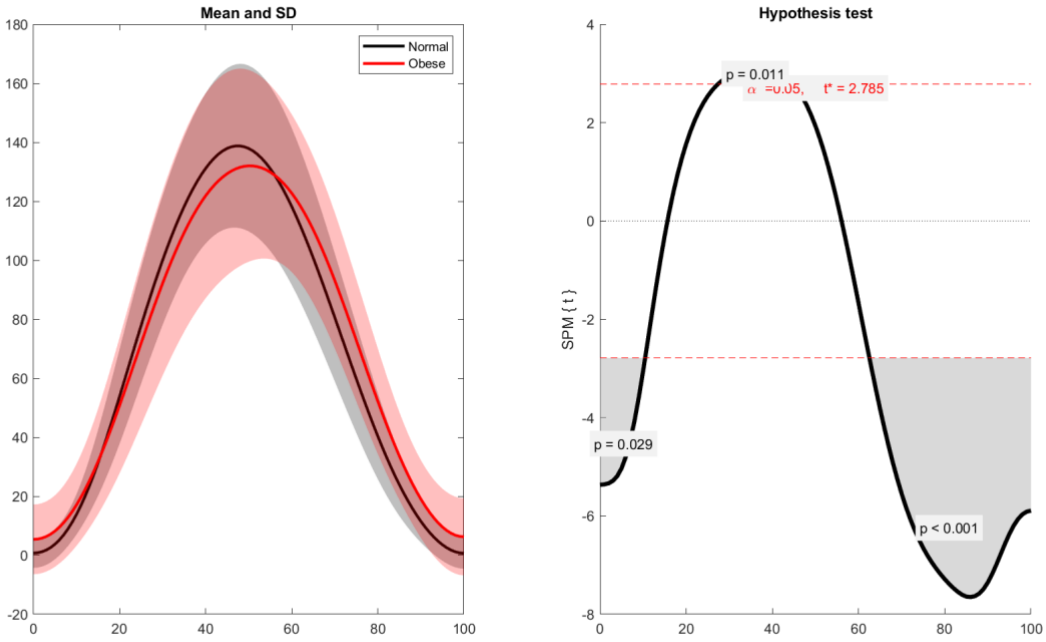

Figure 76: Normality curves representing abduction angles of the shoulder measured with IMUs during lateral lift of the right arm. The grey curve represents the measures of normal-weight subjects' gestures, the red curve represents the ones of obese subjects' gestures. On the right the correlation indexes.

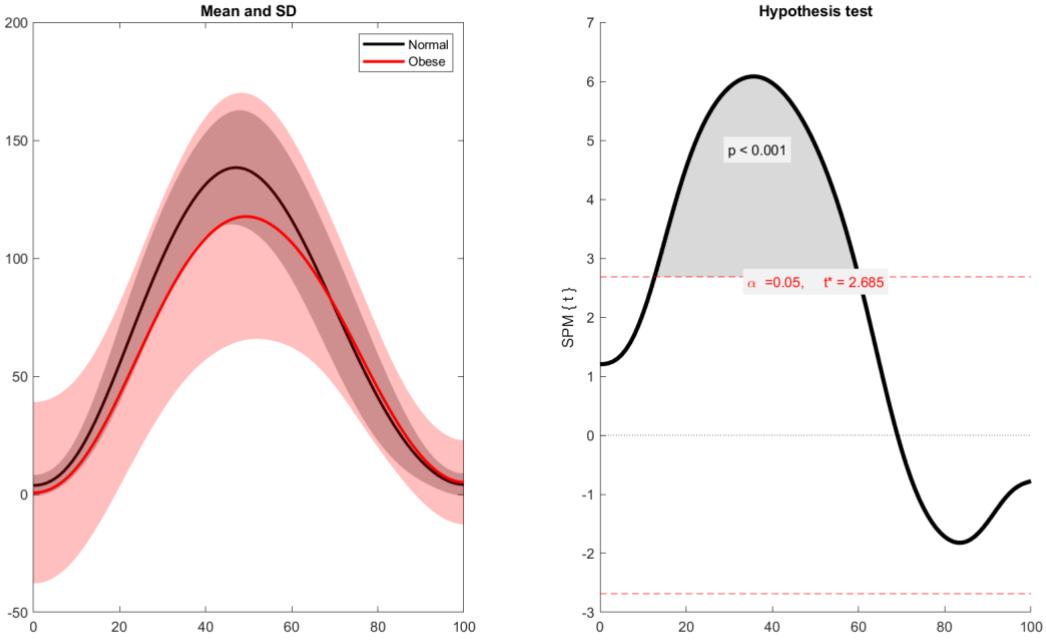

Figure 77: Normality curves representing abduction angles of the shoulder measured with IMUs during lateral lift of the left arm. The grey curve represents the measures of normal-weight subjects' gestures, the red curve represents the ones of obese subjects' gestures. On the right the correlation indexes.

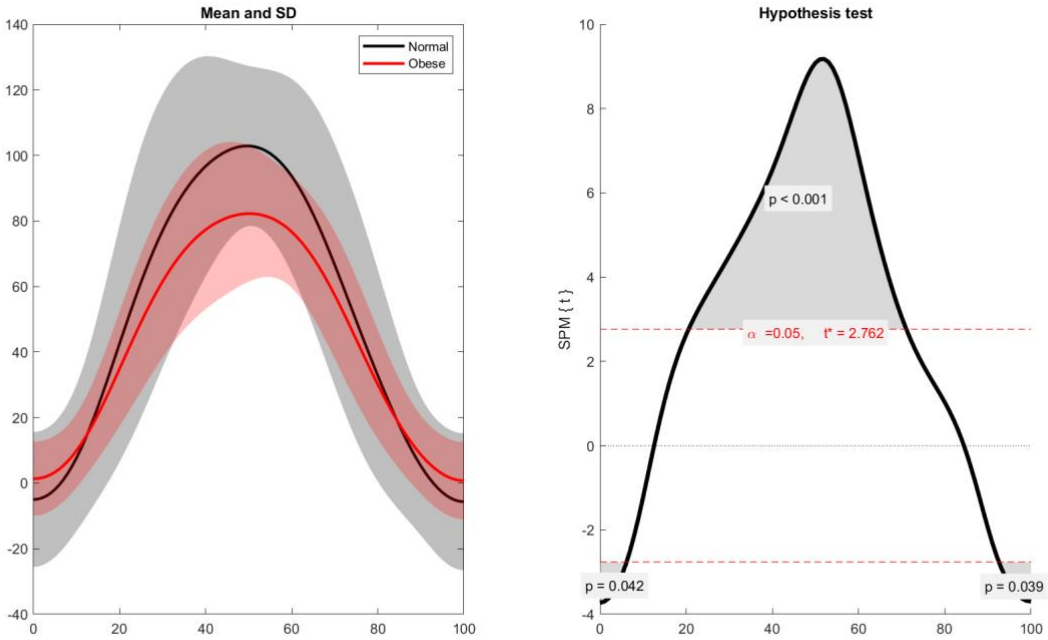

Figure 78: Normality curves representing flexion angles of the shoulder measured with IMUs during reaching movement. The grey curve represents the measures of normal-weight subjects' gestures, the red curve represents the ones of obese subjects' gestures. On the right the correlation indexes.

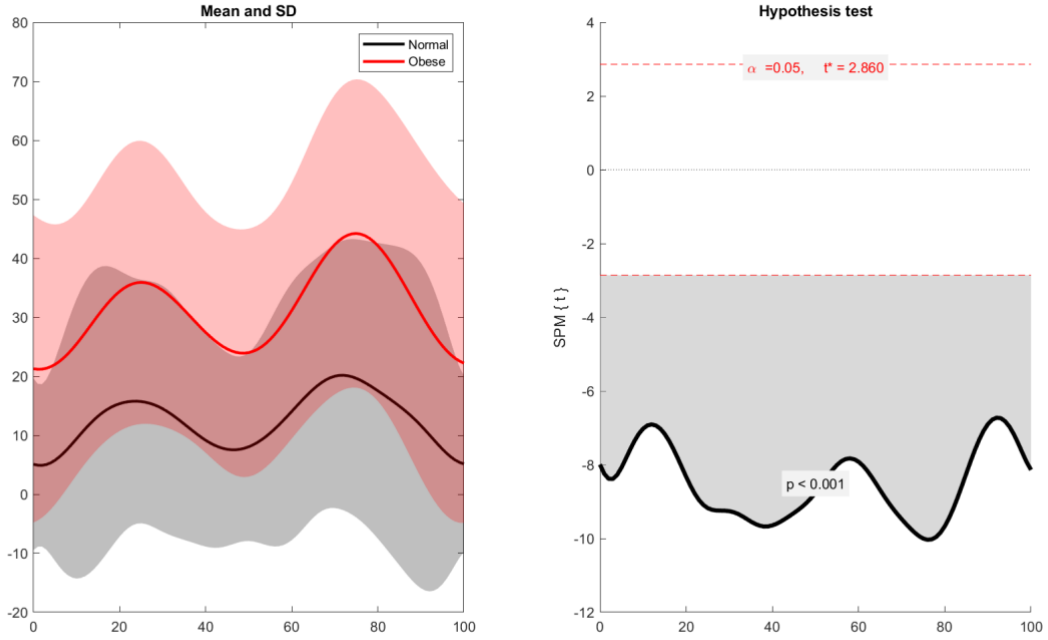

Figure 79: Normality curves representing flexion angles of the elbow measured with IMUs during reaching movement. The grey curve represents the measures of normal-weight subjects' gestures, the red curve represents the ones of obese subjects' gestures. On the right the correlation indexes.

In an analog way, Figures 80 - 85 show the joint angle curves acquired by means of the optoelectronic systems.

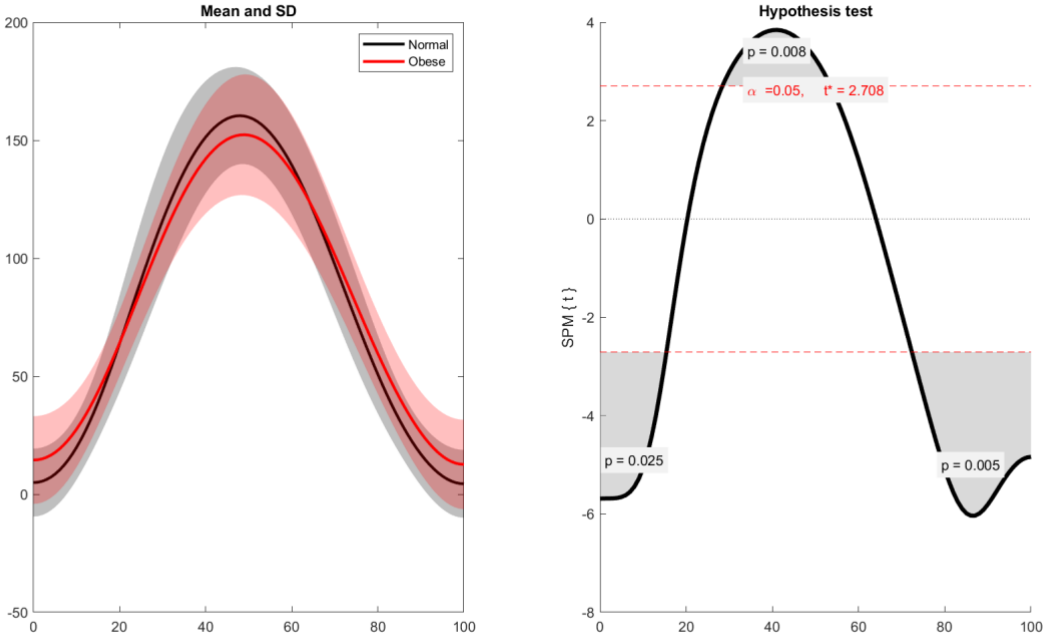

Figure 80: Normality curves representing flexion angles of the shoulder measured with an optoelectronic system during frontal lift of the right arm. The grey curve represents the measures of normal-weight subjects' gestures, the red curve represents the ones of obese subjects' gestures. On the right the correlation indexes.

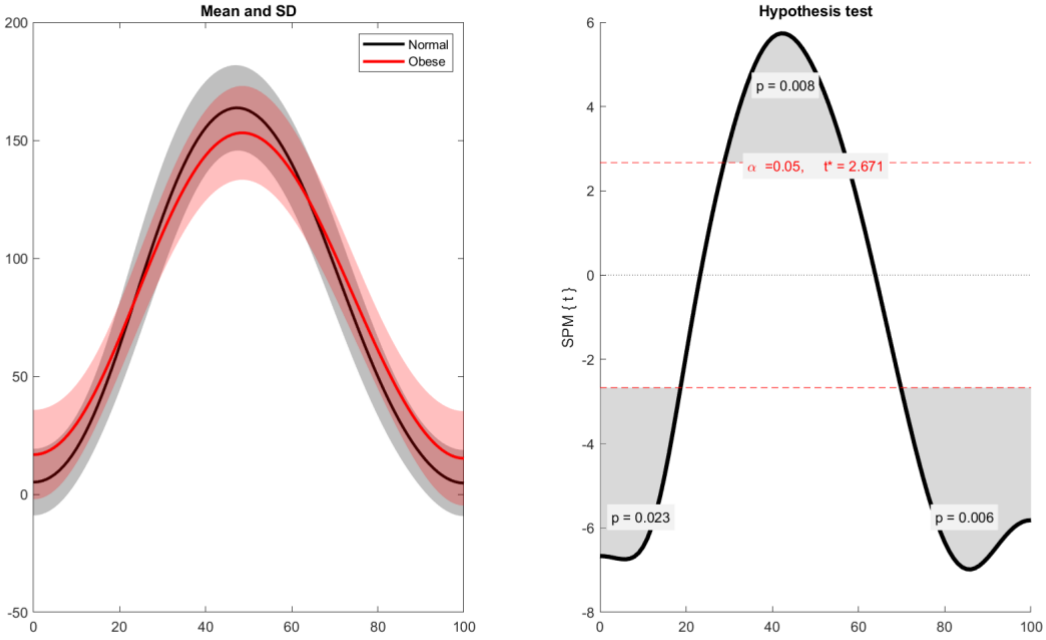

Figure 81: Normality curves representing flexion angles of the shoulder measured with an optoelectronic system during frontal lift of the left arm. The grey curve represents the measures of normal-weight subjects' gestures, the red curve represents the ones of obese subjects' gestures. On the right the correlation indexes.

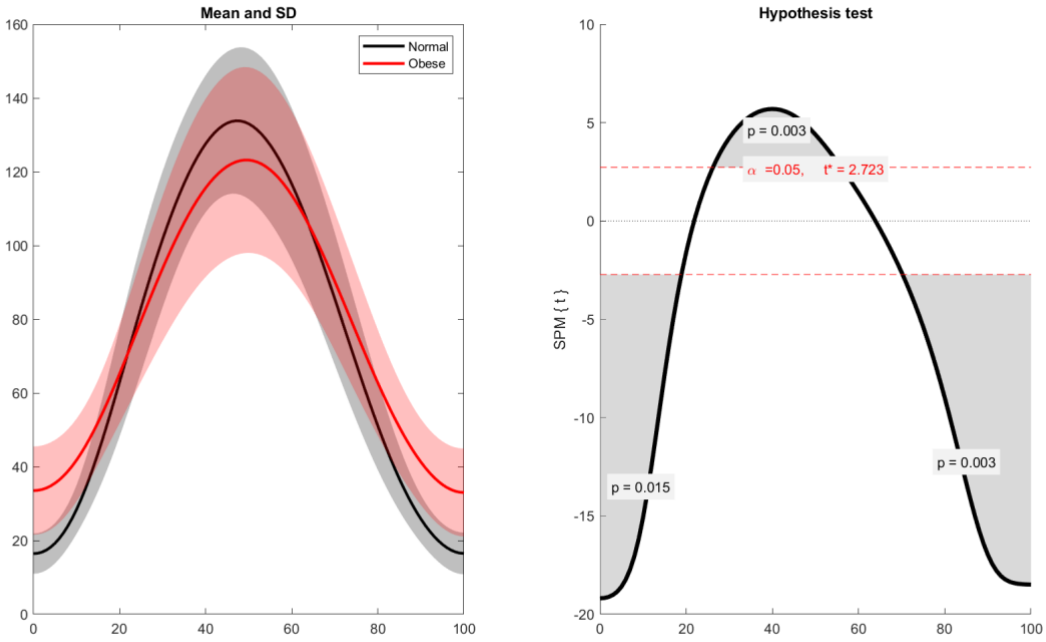

Figure 82: Normality curves representing abduction angles of the shoulder measured with an optoelectronic system during lateral lift of the right arm. The grey curve represents the measures of normal-weight subjects' gestures, the red curve represents the ones of obese subjects' gestures. On the right the correlation indexes.

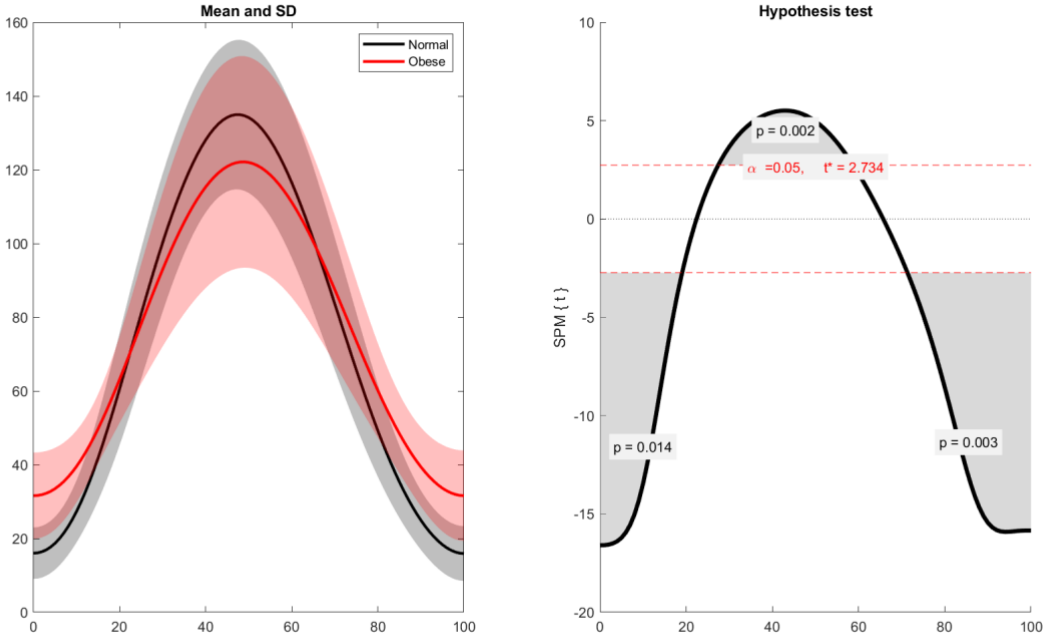

Figure 83: Normality curves representing abduction angles of the shoulder measured with an optoelectronic system during lateral lift of the left arm. The grey curve represents the measures of normal-weight subjects' gestures, the red curve represents the ones of obese subjects' gestures. On the right the correlation indexes.

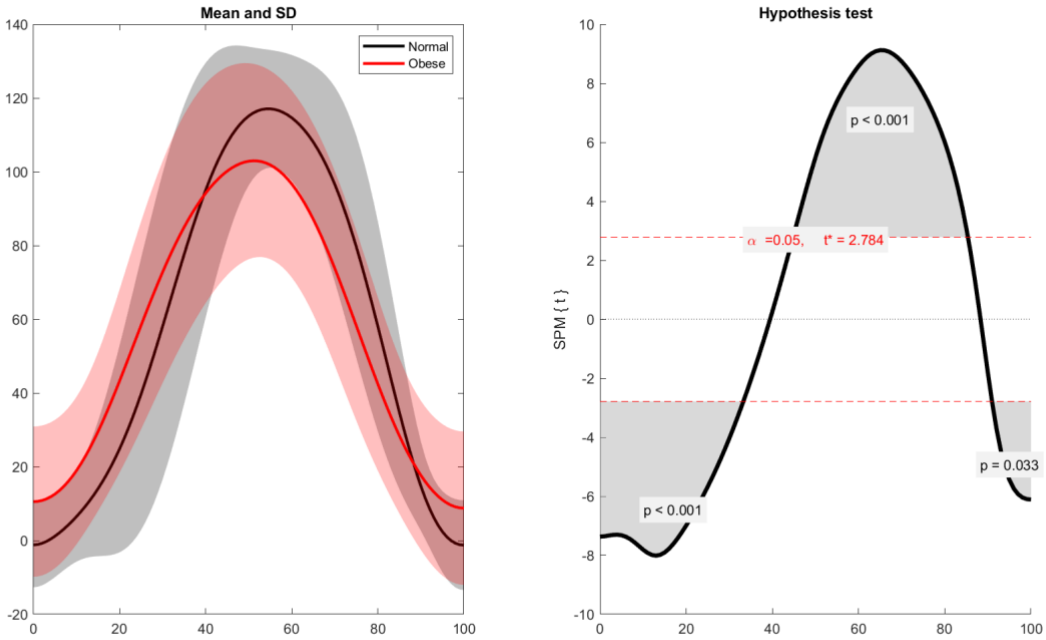

Figure 84: Normality curves representing flexion angles of the shoulder measured with an optoelectronic system during reaching movement. The grey curve represents the measures of normal-weight subjects' gestures, the red curve represents the ones of obese subjects' gestures. On the right the correlation indexes.

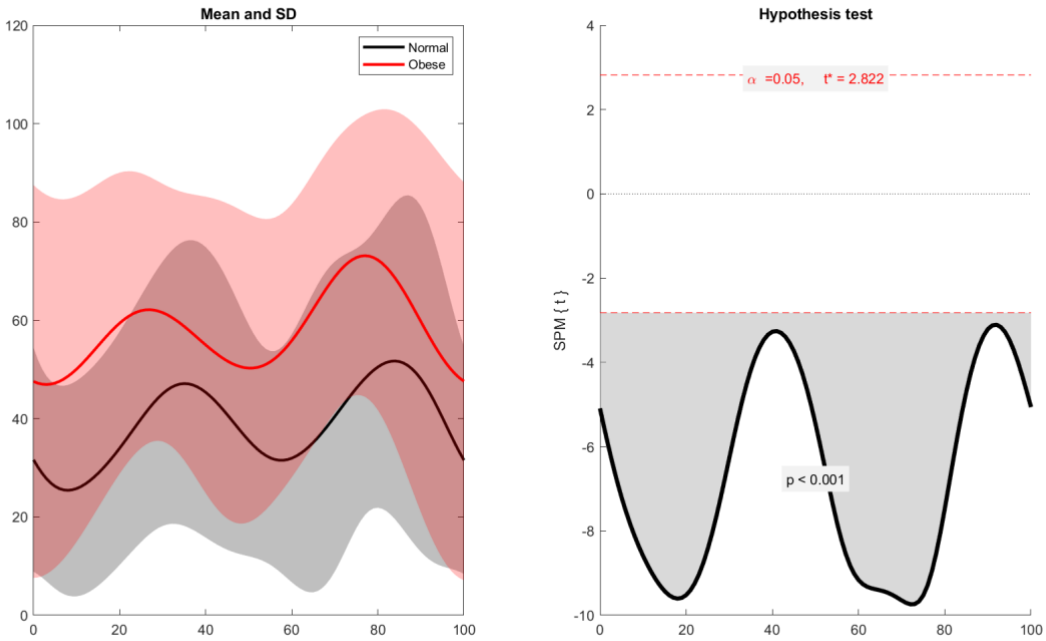

Figure 85: Normality curves representing flexion angles of the elbow measured with an optoelectronic system during reaching movement. The grey curve represents the measures of normal-weight subjects' gestures, the red curve represents the ones of obese subjects' gestures. On the right the correlation indexes

SPM vector field analyses found significance at the beginning, at the apex and at the end of the movements. Coherently with what was reported above, good results in terms of correlation were obtained between the angles measured in the two groups in the plane in which the movement mainly took place with both the systems. The curves which describe normal-weight subjects' gestures have a higher inclination and wider ROMs than the ones associated to obese subjects, which means that the individuals adopted different motion strategies in the two groups.

At the statistical level, the comparison between the IMU-based and the marker-based systems reported some discrepancies; this lack of agreement may be due to the differences between the two motion analysis systems, the implemented protocols and the underlying kinematic models. In fact, the wearable IMU-based system exploited a model with redundancy in measurement and biomechanical constraints regulating the orientation of the axes of the local reference systems. The anatomical reference systems derived from IMU data should have been transformed into the same marker-based systems and adjusted to account for the effect of the mismatch at the start of each trial, when the subject was standing in neutral posture. This issue mainly caused the presence of waveform offsets and slightly different ranges of motion.

In order to estimate the rotation angles different ways were followed in the two cases as far as the shoulder was concerned, the most complex articulation of the human body. Regarding the optoelectronic system, the roto-translation matrix was written starting from the coordinates of the markers, in particular the joint center of the shoulder was derived through the "*chord function*" with the markers on the shoulder, on the clavicle, on the stern, on C7 and on T10 as inputs. The rotation angles were calculated following a different kinematic chain in the case of the inertial system. In fact, two distinct joint angles involving the shoulder were obtained directly as outputs from the system: the former concerns the rotation between T8 and shoulder, the latter between shoulder and upper arm. Since obtaining the same information by means of the optoelectronic system was not possible, the rotation between the segments T8 and upper arm was considered, thus skipping a point of the kinematic chain. According to the protocol, there was not a

sensor applied on T8; the associated data were derived through computations from the ones gathered with the sensors on the shoulders and on the chest. Thus, because of the complexity of the joint and the slightly different kinematic chains, the resulting curves are qualitatively good in both cases, but the statistical analysis evidences some differences.

As for the elbow, the output of the inertial system is more regular even though two markers of the optoelectronic system were placed on the elbow in addition to the ones employed on the arm and forearm in order to find the joint center. With the wearable IMU-based system, the relative positions of the sensors were considered for the evaluation of the elbow joint angles. Despite the use of a lower number of elements, the high sensitivity made it possible to detect even small movements.

With regard to the wrist, the difference between the two outputs is more evident, the range of motion is less pronounced and errors have a grater impact. It should also be taken into account that the articular center of the wrist, in the case of the optoelectronic system, was found by using an anthropometric measure not obtained from the subjects, but found in the literature, which could have negatively affected the accuracy.

Furthermore, the use of non-invasive technological solutions that are externally applied to the skin is highly susceptible to soft tissue artefacts, particularly when considering the obese population.

The comparison between the joint angles of the two groups confirms the thesis explained in the literature (Berrigan et al.): obese participants tend to move their whole body forward while performing the tasks, for this reason the ROMs of their upper limbs resulted smaller.

It would have been interesting to compare the results obtained in this validation with similar studies from the literature. Nonetheless, as stated in the abovementioned systematic review, no other articles concerning validation studies of wearable sensors during obese subjects' upper limb movements were found.

5.1 IMPLICATIONS OF THIS STUDY AND POSSIBLE IMPACT

The scientific value and main novelty of this work consist in demonstrating in which circumstances an IMU-based system results reliable for the movement analysis of obese people's upper limbs. In fact, IMUs are less cumbersome and easier to be used with respect to optoelectronic systems, the gold standard. Very little was found in the literature about this subject.

From a clinical perspective, obese individuals might be less efficient and more at risk of injuries than normal weight individuals in a large number of work tasks and daily activities requiring upper limb movements. This project is consistent with the aim of the "Technology for Health" PhD Program since it provides a technological solution for their assessment, which can be adopted in ecological conditions and allow the identification of dangerous movements for their musculoskeletal apparatus, in a risk prevention perspective. Assessments with optoelectronic systems provide accurate results, but they must be performed in specialized laboratories. Obese individuals' health conditions prevent them from undergoing demanding clinical examinations. For this reason, IMUs, which are non-invasive, ubiquitous and versatile, result useful within obesity context for monitoring their movement strategies during daily activities. The modern artificial intelligence approach could also be applied to efficiently analyze the obtained data and support clinical decisions.

Finally, obesity is recognized as a major public health problem in industrialized countries and it is associated with various musculoskeletal disorders. The introduction of this kind of technology for ecological assessments of working tasks and everyday gestures would have remarkable social impact. It could help people with a high BMI to improve their motion pattern, thus reducing the probability of developing joint pain or injuries. It would cut costs of cares and rehabilitative treatments. Furthermore, the output data of an inertial system do not need long processing. The collected information could be sent in real time to caregivers, a direct communication channel could be provided if necessary.

To sum up, even though further studies are required, the inertial system presents advantages:

- output accuracy,
- ease of use and transport,
- comfortable setup,
- no issues in individuating the landmarks under the soft tissue,
- shorter time required for examination,
- assessment in ecological conditions,
- shorter time required for output data processing.

However, there are some disadvantages with respect to the gold standard:

- difficulty in calibrating the system: several attempts were required for each subject with the inertial system, leading to an excessive waste of time; furthermore, the final result was not always completely satisfying as far as obese volunteers were concerned;
- some errors were noticed in Xsens user manual:
    - inconsistency between the reference systems in T-pose and N-pose;
    - inconsistency in the definition of the sequence of decomposition to compute the Euler angles of the shoulder, in fact, for the frontal flexion of upper limbs, a different sequence was used from the one mentioned in the manual.

5.2 FUTURE DEVELOPMENT

The goal of this project was the validation of an inertial system for obese subjects' movement analysis; therefore, the decisions taken for the definition and implementation of the experimental setup were based on their physiology. For instance, the adoption of rigid clusters and elastic bands reduced the artefacts due to the excessive presence of soft tissue and the use of a probe aimed to a more precise individuation of the anterior iliac crests. This issue of soft tissue artefacts could be further addressed by simultaneously monitoring the movement of skin markers/sensors and the underlying bone by using imaging methods such as biplane radiography and MRI.

It was also realized during the realization of this project, that some convenient changes could be introduced in order to improve the accuracy, such as the addition of a marker on T8 (eighth thoracic vertebra) that would make the kinematic chain of the optoelectronic system more similar to the one of the inertial system.

In addition, the articular center of the wrist was localized by exploiting an average measurement of wrist thickness found in the literature; in order to refine this calculation it would be convenient to acquire the real measurement on the patients.

Since the optoelectronic systems evaluate spatial coordinates, but inertial units mainly consist of gyroscopes and accelerometers, it would be interesting to go into detail by also comparing the respective angular velocity and acceleration values through a similar analysis.

The results of the statistical analysis could become more relevant and the validation more reliable by increasing the number of normal-weight and obese subjects involved into the study.

It is interesting to observe that in future this kind of inertial system could become part of a body area network for a general analysis of obese subjects' health conditions. The information could be sent to hospitals in real time. It would be possible to create accurate databases. The data could be elaborated more efficiently by means of artificial intelligence algorithms, which can learn from experience. The programs would automatically analyze patients' movements and support clinical decisions.

6. CONCLUSIONS

This study demonstrates the usability of a wearable system for motion analysis based on inertial measurement units, not only on normal weight, but also on obese subjects, that are known to be a more critical population. In particular, this work provides a first attempt to evaluate the accuracy of the reconstructed joint kinematics by using an IMU-based system against an optoelectronic reference system. The better results of this validation study were obtained around the principal axis of each movement, which means the Z-axis for the flexion and the X-axis for the abduction of the upper limbs. All the joint angles estimated out of these planes should be carefully interpreted due to the presence of crosstalk.

The curves representing the joint angles acquired with the IMU-based system and the optoelectronic one look similar; their overall values are coherent with the movements under analysis. In the Bland-Altman plots concerning the ROMs, drawn both for normal-weight and obese subjects, the data fall into the acceptability range. The coefficients of multiple correlations reach high levels in both the groups, as regards the shoulder joint in the most representative plane of each movement. Also the R^2 values computed with the linear regression method approach 1 for the most significant angles of each gesture. Furthermore, the SPM vector field analyses are generally satisfying ($p < 0,001$). The results of the comparison between the measures obtained by means of the two different technologies considered in this study show that the IMU-based methodology is a reliable solution not only for normal-weight, but also for obese subjects' upper limb motion analysis in daily scenarios.

Nonetheless, relevant biases affect the measures gathered in the two ways, which indicates some disagreement between the models. Moreover, the correlation coefficients calculated considering the information concerning obese individuals are generally lower. Regarding the comparison of the angles characterizing normal-weight and obese individuals' gestures, SPM vector field analyses found significance at the beginning, at the apex and at the end of the movements. Coherently with what was reported above, good results in terms of correlation were obtained in the plane in which the movement mainly took place with both the systems. The curves which describe normal-weight

subjects' gestures have a higher inclination and wider ROMs than the ones associated to obese subjects.

BIBLIOGRAPHY – chapter 1 and chapter 2

1. Maali Said Mohammed, Sandra Sendra, Jaime Lloret, and Ignacio Bosch, "System and WBAN for controlling obesity", 2018, Hindawi Journal of Healthcare Engineering, Volume 2018
2. Roberto Cattivelli, Gianluca Castelnuovo, Alessandro Musetti, Giorgia Varallo, Chiara A M Spatola, Francesco Vailati Riboni, Anna Guerrini Usubini, Fabio Tosolin, Gian Mauro Manzoni, Paolo Capodaglio, Alessandro Rossi, Giada Pietrabissa, Enrico Molinari "ACTonHEALTH study protocol: promoting psychological flexibility with activity tracker and mHealth tools to foster healthful lifestyle for obesity and other chronic health conditions", 2018, Cattivelli et al. Trials, 19: 659
3. Megan A. Kirk. Mohammad Amiri, Meysam Pirbaglou, Paul Ritvo, "Wearable Technology and Physical Activity Behavior Change in Adults With Chronic Cardiometabolic Disease: A Systematic Review and Meta-Analysis", 2019, American Journal of Health Promotion, 33: 778-791
4. John M.Jakicic, Kelliann K. Davis, Renee J. Rogers, Wendy C. King, Marsha D. Marcus, Diane Helsel, Amy D. Rickman, Abdus S. Wahed, Steven H. Belle, "Effect of Wearable Technology Combined With a Lifestyle Intervention on Long-term Weight Loss - The IDEA Randomized Clinical Trial", 2016, Original Investigation, JAMA 316:1161-1171
5. www.Fitbit.com
6. www.Nike.com
7. Bobak Mortazavi, Suneil Nyamathi, Sunghoon Ivan Lee, Thomas Wilkerson, Hassan Ghasemzadeh, and Majid Sarrafzadeh, "Near-Realistic Mobile Exergames With Wireless Wearable Sensors", 2014, IEEE JOURNAL OF BIOMEDICAL AND HEALTH INFORMATICS, Vol.18, No 2
8. "MVN User Manual", Revision Z 01/04/2021, Xsens
9. Carlo Albino Frigo, "Tecniche per l'analisi del movimento", 2018, "Bioingegneria del sistema motorio", Cap. 6: 177-220
10. "Plug-in gait reference guide", Vicon Motion System, 2018

11. https://www.jmp.com/it_it/statistics-knowledge-portal/t-test.html
12. https://www.mathsly.it/wordpress/plot-di-bland-altman-come-misurare-lagreement/

BIBLIOGRAPHY – chapter 3

1. Rössner, S. Obesity: The disease of the twenty-first century. *Int. J. Obes.* **2002**, *26*, S2–S4. https://doi.org/10.1038/sj.ijo.0802209.
2. Chooi, Y.C.; Ding, C.; Magkos, F. The epidemiology of obesity. *Metabolism* **2019**, *92*, 6–10. https://doi.org/10.1016/j.metabol.2018.09.005.
3. Spyropoulos, P.; Pisciotta, J.C.; Pavlou, K.N.; Cairns, M.A.; Simon, S.R. Biomechanical gait analysis in obese men. *Arch. Phys. Med. Rehabil.* **1991**, *72*, 1065–1070.
4. Messier, S.P.; Davies, A.B.; Moore, D.T.; Davis, S.E.; Pack, R.J.; Kazmar, S.C. Severe Obesity: Effects on Foot Mechanics During Walking. *Foot Ankle Int.* **1994**, *15*, 29–34. https://doi.org/10.1177/107110079401500106.
5. de Souza, S.A.F.; Faintuch, J.; Valezi, A.C.; Sant' Anna, A.F.; Gama-Rodrigues, J.J.; de Batista Fonseca, I.C.; Souza, R.B.; Senhorini, R.C. Gait Cinematic Analysis in Morbidly Obese Patients. *Obes. Surg.* **2005**, *15*, 1238–1242. https://doi.org/10.1381/096089205774512627.
6. Vismara, L.; Romei, M.; Galli, M.; Montesano, A.; Baccalaro, G.; Crivellini, M.; Grugni, G. Clinical implications of gait analysis in the rehabilitation of adult patients with "Prader-Willi" Syndrome: A cross-sectional comparative study ("Prader-Willi" Syndrome vs matched obese patients and healthy subjects). *J. Neuroeng. Rehabil.* **2007**, *4*, 14. https://doi.org/10.1186/1743-0003-4-14.
7. Ghasemi, M.; Arjmand, N. Spinal segment ranges of motion, movement coordination, and three-dimensional kinematics during occupational activities in normal-weight and obese individuals. *J. Biomech.* **2021**, *123*, 110539. https://doi.org/10.1016/j.jbiomech.2021.110539.
8. Galli, M.; Crivellini, M.; Sibella, F.; Montesano, A.; Bertocco, P.; Parisio, C. Sit-to-stand movement analysis in obese subjects. *Int. J. Obes.* **2000**, *24*, 1488–1492. https://doi.org/10.1038/sj.ijo.0801409.
9. Sibella, F.; Galli, M.; Romei, M.; Montesano, A.; Crivellini, M. Biomechanical analysis of sit-to-stand movement in normal and obese subjects. *Clin. Biomech.* **2003**, *18*, 745–750. https://doi.org/10.1016/S0268-0033(03)00144-X.

10. Berrigan, F.; Simoneau, M.; Tremblay, A.; Hue, O.; Teasdale, N. Influence of obesity on accurate and rapid arm movement performed from a standing posture. *Int. J. Obes.* **2006**, *30*, 1750–1757. https://doi.org/10.1038/sj.ijo.0803342.
11. Capodaglio, P.; Castelnuovo, G.; Brunani, A.; Vismara, L.; Villa, V.; Maria Capodaglio, E. Functional Limitations and Occupational Issues in Obesity: A Review. *Int. J. Occup. Saf. Ergon.* **2010**, *16*, 507–523. https://doi.org/10.1080/10803548.2010.11076863.
12. Wearing, S.C.; Hennig, E.M.; Byrne, N.M.; Steele, J.R.; Hills, A.P. Musculoskeletal disorders associated with obesity: A biomechanical perspective. *Obes. Rev.* **2006**, *7*, 239–250. https://doi.org/10.1111/j.1467-789X.2006.00251.x.
13. Lai, P.P.K.; Leung, A.K.L.; Li, A.N.M.; Zhang, M. Three-dimensional gait analysis of obese adults. *Clin. Biomech.* **2008**, *23*, S2–S6. https://doi.org/10.1016/j.clinbiomech.2008.02.004.
14. Cappozzo, A.; Della Croce, U.; Leardini, A.; Chiari, L. Human movement analysis using stereophotogrammetry. Part 1: Theoretical background. *Gait Posture* **2005**, *21*, 186–196. https://doi.org/10.1016/j.gaitpost.2004.01.010.
15. Tao, W.; Liu, T.; Zheng, R.; Feng, H. Gait Analysis Using Wearable Sensors. *Sensors* **2012**, *12*, 2255–2283.
16. Muro-de-la-Herran, A.; Garcia-Zapirain, B.; Mendez-Zorrilla, A. Gait Analysis Methods: An Overview of Wearable and Non-Wearable Systems, Highlighting Clinical Applications. *Sensors* **2014**, *14*, 3362–3394.
17. Shull, P.B.; Jirattigalachote, W.; Hunt, M.A.; Cutkosky, M.R.; Delp, S.L. Quantified self and human movement: A review on the clinical impact of wearable sensing and feedback for gait analysis and intervention. *Gait Posture* **2014**, *40*, 11–19. https://doi.org/10.1016/j.gaitpost.2014.03.189.
18. Picerno, P.; Iosa, M.; D'Souza, C.; Benedetti, M.G.; Paolucci, S.; Morone, G. Wearable inertial sensors for human movement analysis: A five-year update. *Expert Rev. Med. Devices* **2021**, *18*, 79–94. https://doi.org/10.1080/17434440.2021.1988849.
19. Leardini, A.; Chiari, L.; Della Croce, U.; Cappozzo, A. Human movement analysis using stereophotogrammetry. Part 3. Soft tissue artifact assessment and compensation. *Gait Posture* **2005**, *21*, 212–225. https://doi.org/10.1016/j.gaitpost.2004.05.002.

20. Clément, J.; de Guise, J.A.; Fuentes, A.; Hagemeister, N. Comparison of soft tissue artifact and its effects on knee kinematics between non-obese and obese subjects performing a squatting activity recorded using an exoskeleton. *Gait Posture* **2018**, *61*, 197–203. https://doi.org/10.1016/j.gaitpost.2018.01.009.
21. Camomilla, V.; Bonci, T.; Cappozzo, A. Soft tissue displacement over pelvic anatomical landmarks during 3-D hip movements. *J. Biomech.* **2017**, *62*, 14–20. https://doi.org/10.1016/j.jbiomech.2017.01.013.
22. Page, M.J.; Moher, D.; Bossuyt, P.M.; Boutron, I.; Hoffmann, T.C.; Mulrow, C.D.; Shamseer, L.; Tetzlaff, J.M.; Akl, E.A.; Brennan, S.E.; et al. PRISMA 2020 explanation and elaboration: Updated guidance and exemplars for reporting systematic reviews. *BMJ* **2021**, *372*, n160. https://doi.org/10.1136/bmj.n160.
23. Moher, D.; Shamseer, L.; Clarke, M.; Ghersi, D.; Liberati, A.; Petticrew, M.; Shekelle, P.; Stewart, L.A.; Group, P.-P. Preferred reporting items for systematic review and meta-analysis protocols (PRISMA-P) 2015 statement. *Syst. Rev.* **2015**, *4*, 1. https://doi.org/10.1186/2046-4053-4-1.
24. Methley, A.M.; Campbell, S.; Chew-Graham, C.; McNally, R.; Cheraghi-Sohi, S. PICO, PICOS and SPIDER: A comparison study of specificity and sensitivity in three search tools for qualitative systematic reviews. *BMC Health Serv. Res.* **2014**, *14*, 579. https://doi.org/10.1186/s12913-014-0579-0.
25. Ouzzani, M.; Hammady, H.; Fedorowicz, Z.; Elmagarmid, A. Rayyan—A web and mobile app for systematic reviews. *Syst. Rev.* **2016**, *5*, 210. https://doi.org/10.1186/s13643-016-0384-4.
26. Higgins, J.P.D.; Thomas, J.; Chandler, J.; Cumpston, M.; Li, T.; Page, M.J.; Welch, V.A. *Cochrane Handbook for Systematic Reviews of Interventions*; Version 6.3 (updated February 2022); Cochrane: London, UK, 2022.
27. Slim, K.; Nini, E.; Forestier, D.; Kwiatkowski, F.; Panis, Y.; Chipponi, J. Methodological index for non-randomized studies (minors): Development and validation of a new instrument. *ANZ J. Surg.* **2003**, *73*, 712–716. https://doi.org/10.1046/j.1445-2197.2003.02748.x.

28. Kim, D.; Lewis, C.L.; Gill, S.V. The effect of obesity on whole-body angular momentum during steady-state walking. *Gait Posture* **2022**, *94*, 93–101. https://doi.org/10.1016/j.gaitpost.2022.02.029.
29. Kim, D.; Lewis, C.L.; Silverman, A.K.; Gill, S.V. Changes in dynamic balance control in adults with obesity across walking speeds. *J. Biomech.* **2022**, *144*, 111308. https://doi.org/10.1016/j.jbiomech.2022.111308.
30. Vakula, M.N.; Garcia, S.A.; Holmes, S.C.; Pamukoff, D.N. Association between quadriceps function, joint kinetics, and spatiotemporal gait parameters in young adults with and without obesity. *Gait Posture* **2022**, *92*, 421–427. https://doi.org/10.1016/j.gaitpost.2021.12.019.
31. Capodaglio, P.; Gobbi, M.; Donno, L.; Fumagalli, A.; Buratto, C.; Galli, M.; Cimolin, V. Effect of obesity on knee and ankle biomechanics during walking. *Sensors* **2021**, *21*, 7114. https://doi.org/10.3390/s21217114.
32. Davis, R.B.; Õunpuu, S.; Tyburski, D.; Gage, J.R. A gait analysis data collection and reduction technique. *Hum. Mov. Sci.* **1991**, *10*, 575–587. https://doi.org/10.1016/0167-9457(91)90046-Z.
33. Cimolin, V.; Gobbi, M.; Buratto, C.; Ferraro, S.; Fumagalli, A.; Galli, M.; Capodaglio, P. A Comparative Analysis of Shoes Designed for Subjects with Obesity Using a Single Inertial Sensor: Preliminary Results. *Sensors* **2022**, *22*, 782. https://doi.org/10.3390/s22030782.
34. Garcia, S.A.; Vakula, M.N.; Holmes, S.C.; Pamukoff, D.N. The influence of body mass index and sex on frontal and sagittal plane knee mechanics during walking in young adults. *Gait Posture* **2021**, *83*, 217–222. https://doi.org/10.1016/j.gaitpost.2020.10.010.
35. Vakula, M.N.; Fisher, K.L.; Garcia, S.A.; Holmes, S.C.; Post, B.K.; Costa, P.B.; Pamukoff, D.N. Quadriceps Impairment Is Associated with Gait Mechanics in Young Adults with Obesity. *Med. Sci. Sports Exerc.* **2019**, *51*, 951–961. https://doi.org/10.1249/MSS.0000000000001891.

36. Kadaba, M.P.; Ramakrishnan, H.K.; Wootten, M.E. Measurement of lower extremity kinematics during level walking. *J. Orthop. Res.* **1990**, *8*, 383–392. https://doi.org/10.1002/jor.1100080310.
37. Kim, D.; Lewis, C.L.; Gill, S.V. Effects of obesity and foot arch height on gait mechanics: A cross-sectional study. *PLoS ONE* **2021**, *16*, e0260398. https://doi.org/10.1371/journal.pone.0260398.
38. Law, N.-H.; Li, J.X.; Law, N.-Y.; Varin, D.; Lamontagne, M. Effects of body mass and sex on kinematics and kinetics of the lower extremity during stair ascent and descent in older adults. *Sport. Med. Health Sci.* **2021**, *3*, 165–170. https://doi.org/10.1016/j.smhs.2021.06.001.
39. Lamontagne, M.; Beaulieu, M.L.; Varin, D.; Beaulé, P.E. Gait and Motion Analysis of the Lower Extremity After Total Hip Arthroplasty: What the Orthopedic Surgeon Should Know. *Orthop. Clin. N. Am.* **2009**, *40*, 397–405. https://doi.org/10.1016/j.ocl.2009.02.001.
40. Pau, M.; Capodaglio, P.; Leban, B.; Porta, M.; Galli, M.; Cimolin, V. Kinematics Adaptation and Inter-Limb Symmetry during Gait in Obese Adults. *Sensors* **2021**, *21*, 5980. https://doi.org/10.3390/s21175980.
41. Maktouf, W.; Durand, S.; Boyas, S.; Pouliquen, C.; Beaune, B. Interactions among obesity and age-related effects on the gait pattern and muscle activity across the ankle joint. *Exp. Gerontol.* **2020**, *140*, 111054. https://doi.org/10.1016/j.exger.2020.111054.
42. Sample, D.W.; Thorsen, T.A.; Weinhandl, J.T.; Strohacker, K.A.; Zhang, S. Effects of increased step-width on knee biomechanics during inclined and declined walking. *J. Appl. Biomech.* **2020**, *36*, 292–297. https://doi.org/10.1123/JAB.2019-0298.
43. Badawy, M.; Schall, M.C.; Zabala, M.E.; Coker, J.; Sesek, R.F.; Gallagher, S.; Davis, G.A. Effects of age and obesity on trunk kinetics and kinematics during dominant side one-handed carrying. *J. Biomech.* **2019**, *94*, 107–114. https://doi.org/10.1016/j.jbiomech.2019.07.016.

44. Lerner, Z.F.; Board, W.J.; Browning, R.C. Effects of an obesity-specific marker set on estimated muscle and joint forces in walking. *Med. Sci. Sports Exerc.* **2014**, *46*, 1261–1267.
45. Cimolin, V.; Cau, N.; Malchiodi Albedi, G.; Aspesi, V.; Merenda, V.; Galli, M.; Capodaglio, P. Do wearable sensors add meaningful information to the Timed Up and Go test? A study on obese women. *J. Electromyogr. Kinesiol.* **2019**, *44*, 78–85. https://doi.org/10.1016/j.jelekin.2018.12.001.
46. Dames, K.D.; Heise, G.D.; Hydock, D.S.; Smith, J.D. Obese adults walk differently in shoes than while barefoot. *Gait Posture* **2019**, *70*, 79–83. https://doi.org/10.1016/j.gaitpost.2019.02.016.
47. Pamukoff, D.N.; Vakula, M.N.; Holmes, S.C.; Shumski, E.J.; Garcia, S.A. Body mass index moderates the association between gait kinetics, body composition, and femoral knee cartilage characteristics. *J. Orthop. Res.* **2020**, *38*, 2685–2695. https://doi.org/10.1002/jor.24655.
48. Horsak, B.; Schwab, C.; Clemens, C.; Baca, A.; Greber-Platzer, S.; Kreissl, A.; Kranzl, A. Is the reliability of 3D kinematics of young obese participants dependent on the hip joint center localization method used? *Gait Posture* **2018**, *59*, 65–70. https://doi.org/10.1016/j.gaitpost.2017.09.029.
49. Rosso, V.; Agostini, V.; Takeda, R.; Tadano, S.; Gastaldi, L. Influence of BMI on Gait Characteristics of Young Adults: 3D Evaluation Using Inertial Sensors. *Sensors* **2019**, *19*, 4221.
50. Gastaldi, L.; Rosso, V.; Gabola, V.; Agostini, V.; Frutos, M.M.L.; Knaflitz, M.; Takeda, R.; Tadano, S. Technical challenges using magneto-inertial sensors for gait analysis. In Proceedings of the 2016 IEEE International Symposium on Medical Measurements and Applications (MeMeA), Benevento, Italy, 15–18 May 2016; pp. 1–6.
51. Tadano, S.; Takeda, R.; Sasaki, K.; Fujisawa, T.; Tohyama, H. Gait characterization for osteoarthritis patients using wearable gait sensors (H-Gait systems). *J. Biomech.* **2016**, *49*, 684–690. https://doi.org/10.1016/j.jbiomech.2016.01.017.

52. Hagemeister, N.; Parent, G.; Van de Putte, M.; St-Onge, N.; Duval, N.; de Guise, J. A reproducible method for studying three-dimensional knee kinematics. *J. Biomech.* **2005**, *38*, 1926–1931. https://doi.org/10.1016/j.jbiomech.2005.05.013.
53. Milner, C.E.; Meardon, S.A.; Hawkins, J.L.; Willson, J.D. Walking velocity and step length adjustments affect knee joint contact forces in healthy weight and obese adults. *J. Orthop. Res. Off. Publ. Orthop. Res. Soc.* **2018**, *36*, 2679–2686. https://doi.org/10.1002/jor.24031.
54. Yocum, D.; Weinhandl, J.T.; Fairbrother, J.T.; Zhang, S. Wide step width reduces knee abduction moment of obese adults during stair negotiation. *J. Biomech.* **2018**, *75*, 138–146. https://doi.org/10.1016/j.jbiomech.2018.05.002.
55. Agostini, V.; Gastaldi, L.; Rosso, V.; Knaflitz, M.; Tadano, S. A Wearable Magneto-Inertial System for Gait Analysis (H-Gait): Validation on Normal Weight and Overweight/Obese Young Healthy Adults. *Sensors* **2017**, *17*, 2406.
56. Donati, M.; Camomilla, V.; Vannozzi, G.; Cappozzo, A. Anatomical frame identification and reconstruction for repeatable lower limb joint kinematics estimates. *J. Biomech.* **2008**, *41*, 2219–2226. https://doi.org/10.1016/j.jbiomech.2008.04.018.
57. Liu, Z.Q.; Yang, F. Obesity may not induce dynamic stability disadvantage during overground walking among young adults. *PLoS ONE* **2017**, *12*, e0169766. https://doi.org/10.1371/journal.pone.0169766.
58. Meng, H.; O'Connor, D.P.; Lee, B.C.; Layne, C.S.; Gorniak, S.L. Alterations in over-ground walking patterns in obese and overweight adults. *Gait Posture* **2017**, *53*, 145–150. https://doi.org/10.1016/j.gaitpost.2017.01.019.
59. Singh, B.; Vo, H.; Francis, S.L.; Janz, K.F.; Yack, H.J. Changes in Gait over a 30-min Walking Session in Obese Females. *Med. Sci. Sports Exerc.* **2017**, *49*, 555–562. https://doi.org/10.1249/MSS.0000000000001114.
60. Houck, J.; Yack, H.J. Associations of knee angles, moments and function among subjects that are healthy and anterior cruciate ligament deficient (ACLD) during straight ahead and crossover cutting activities. *Gait Posture* **2003**, *18*, 126–138. https://doi.org/10.1016/S0966-6362(02)00188-1.

61. Yang, F.; Kim, J.E.; Yang, F. Effects of obesity on dynamic stability control during recovery from a treadmill-induced slip among young adults. *J. Biomech.* **2017**, *53*, 148–153. https://doi.org/10.1016/j.jbiomech.2017.01.021.
62. Pamukoff, D.N.; Lewek, M.D.; Blackburn, J.T. Greater vertical loading rate in obese compared to normal weight young adults. *Clin. Biomech.* **2016**, *33*, 61–65. https://doi.org/10.1016/j.clinbiomech.2016.02.007.
63. Coren, S.; Porac, C.; Duncan, P. A behaviorally validated self-report inventory to assess four types of lateral preference. *J. Clin. Neuropsychol.* **1979**, *1*, 55–64. https://doi.org/10.1080/01688637908401098.
64. Fu, X.Y.; Zelik, K.E.; Board, W.J.; Browning, R.C.; Kuo, A.D. Soft tissue deformations contribute to the mechanics of walking in obese adults. *Med. Sci. Sports Exerc.* **2015**, *47*, 1435–1443. https://doi.org/10.1249/MSS.0000000000000554.
65. Singh, B.; Yack, H.J.; Francis, S.L.; Janz, K.F. Biomechanical loads during common rehabilitation exercises in obese individuals. *Int. J. Sports Phys. Ther.* **2015**, *10*, 189–96.
66. Houck, J.; Yack, H.J.; Cuddeford, T. Validity and comparisons of tibiofemoral orientations and displacement using a femoral tracking device during early to mid stance of walking. *Gait Posture* **2004**, *19*, 76–84. https://doi.org/10.1016/S0966-6362(03)00033-X.
67. Page Glave, A.; Di Brezzo, R.; Applegate, D.K.; Olson, J.M. The effects of obesity classification method on select kinematic gait variables in adult females. *J. Sports Med. Phys. Fit.* **2014**, *54*, 197–202.
68. Haight, D.J.; Lerner, Z.F.; Board, W.J.; Browning, R.C. A comparison of slow, uphill and fast, level walking on lower extremity biomechanics and tibiofemoral joint loading in obese and nonobese adults. *J. Orthop. Res.* **2014**, *32*, 324–330. https://doi.org/10.1002/jor.22497.
69. Lerner, Z.F.; Board, W.J.; Browning, R.C. Effects of obesity on lower extremity muscle function during walking at two speeds. *Gait Posture* **2014**, *39*, 978–984. https://doi.org/10.1016/j.gaitpost.2013.12.020.

70. Mignardot, J.B.; Olivier, I.; Promayon, E.; Nougier, V. Origins of Balance Disorders during a Daily Living Movement in Obese: Can Biomechanical Factors Explain Everything? *PLoS ONE* **2013**, *8*, e60491. https://doi.org/10.1371/journal.pone.0060491.
71. Ranavolo, A.; Donini, L.M.; Mari, S.; Serrao, M.; Silvetti, A.; Iavicoli, S.; Cava, E.; Asprino, R.; Pinto, A.; Draicchio, F. Lower-limb joint coordination pattern in obese subjects. *Biomed Res. Int.* **2013**, *2013*, 142323. https://doi.org/10.1155/2013/142323.
72. Roemer, K.; Hortobagyi, T.; Richter, C.; Munoz-Maldonado, Y.; Hamilton, S. Effect of BMI on knee joint torques in ergometer rowing. *J. Appl. Biomech.* **2013**, *29*, 763–768. https://doi.org/10.1123/jab.29.6.763.
73. Russell, E.M.; Miller, R.H.; Umberger, B.R.; Hamill, J. Lateral wedges alter mediolateral load distributions at the knee joint in obese individuals. *J. Orthop. Res.* **2013**, *31*, 665–671. https://doi.org/10.1002/jor.22248.
74. Freedman Silvernail, J.; Milner, C.E.; Thompson, D.; Zhang, S.; Zhao, X. The influence of body mass index and velocity on knee biomechanics during walking. *Gait Posture* **2013**, *37*, 575–579. https://doi.org/10.1016/j.gaitpost.2012.09.016.
75. Cappozzo, A.; Cappello, A.; Croce, U.D.; Pensalfini, F. Surface-marker cluster design criteria for 3-D bone movement reconstruction. *IEEE Trans. Biomed. Eng.* **1997**, *44*, 1165–1174. https://doi.org/10.1109/10.649988.
76. Manal, K.; McClay, I.; Stanhope, S.; Richards, J.; Galinat, B. Comparison of surface mounted markers and attachment methods in estimating tibial rotations during walking: An in vivo study. *Gait Posture* **2000**, *11*, 38–45. https://doi.org/10.1016/S0966-6362(99)00042-9.
77. Ehlen, K.A.; Reiser, R.F.; Browning, R.C. Energetics and biomechanics of inclined treadmill walking in obese adults. *Med. Sci. Sports Exerc.* **2011**, *43*, 1251–1259. https://doi.org/10.1249/MSS.0b013e3182098a6c.
78. Russell, E.M.; Braun, B.; Hamill, J. Does stride length influence metabolic cost and biomechanical risk factors for knee osteoarthritis in obese women? *Clin. Biomech.* **2010**, *25*, 438–443. https://doi.org/10.1016/j.clinbiomech.2010.01.016.

79. Vismara, L.; Menegoni, F.; Zaina, F.; Galli, M.; Negrini, S.; Capodaglio, P. Effect of obesity and low back pain on spinal mobility: A cross sectional study in women. *J. Neuroeng. Rehabil.* **2010**, *7*, 3. https://doi.org/10.1186/1743-0003-7-3.
80. Kim, H.K.; Dai, X.; Lu, S.H.; Lu, T.W.; Chou, L.S. Discriminating features of ground reaction forces in overweight old and young adults during walking using functional principal component analysis. *Gait Posture* **2022**, *94*, 166–172. https://doi.org/10.1016/j.gaitpost.2022.03.012.
81. Snider, K.T.; Snider, E.J.; Degenhardt, B.F.; Johnson, J.C.; Kribs, J.W. Palpatory accuracy of lumbar spinous processes using multiple bony landmarks. *J. Manip. Physiol. Ther.* **2011**, *34*, 306–313. https://doi.org/10.1016/j.jmpt.2011.04.006.
82. Nazareth, A.; Mueske, N.M.; Wren, T.A.L. Effect of Tibia Marker Placement on Kinematics in Pathological Gait. *J. Appl. Biomech.* **2016**, *32*, 603–607. https://doi.org/10.1123/jab.2015-0219.
83. Trojaniello, D.; Cereatti, A.; Pelosin, E.; Avanzino, L.; Mirelman, A.; Hausdorff, J.M.; Della Croce, U. Estimation of step-by-step spatio-temporal parameters of normal and impaired gait using shank-mounted magneto-inertial sensors: Application to elderly, hemiparetic, parkinsonian and choreic gait. *J. Neuroeng. Rehabil.* **2014**, *11*, 152. https://doi.org/10.1186/1743-0003-11-152.
84. Bergamini, E.; Ligorio, G.; Summa, A.; Vannozzi, G.; Cappozzo, A.; Sabatini, A.M. Estimating Orientation Using Magnetic and Inertial Sensors and Different Sensor Fusion Approaches: Accuracy Assessment in Manual and Locomotion Tasks. *Sensors* **2014**, *14*, 18625–18649.
85. Scalona, E.; Di Marco, R.; Castelli, E.; Desloovere, K.; Van Der Krogt, M.; Cappa, P.; Rossi, S. Inter-laboratory and inter-operator reproducibility in gait analysis measurements in pediatric subjects. *Int. Biomech.* **2019**, *6*, 19–33. https://doi.org/10.1080/23335432.2019.1621205.
86. Matrangola, S.L.; Madigan, M.L.; Nussbaum, M.A.; Ross, R.; Davy, K.P. Changes in body segment inertial parameters of obese individuals with weight loss. *J. Biomech.* 2008, *41*, 3278–3281. https://doi.org/10.1016/j.jbiomech.2008.08.026.